The Pennsylvania State University

The Graduate School

College of Engineering

PROTOCOL AND INTITIAL SURFACE ANALYSIS OF EXPLANTED BLOOD

SACS FOR THE PENN STATE PEDIATRIC VENTRICULAR ASSIST DEVICE

A Thesis in

Bioengineering

by

Nicholas E. Ceneviva

Submitted in Partial Fulfillment
of the Requirements
for the Degree of

Master of Science

August 2015

The thesis of Nicholas E. Ceneviva was reviewed and approved* by the following:

Keefe Manning
Associate Professor of Biomedical Engineering
Thesis Advisor

William Weiss
Professor of Surgery and Biomedical Engineering

Christopher Siedlecki
Professor of Surgery and Biomedical Engineering

William Hancock
Professor of Biomedical Engineering
Graduate Program Officer

*Signatures are on file in the Graduate School

ABSTRACT

Approximately 2,000 children between the age of 5 and 16 are on the heart transplant list as a result of cardiovascular disease. Only a small portion of these children actually receive a transplant. As a result, there is a need for a pediatric left ventricular assist device (PVAD) as an alternative treatment. Penn State has designed their own PVAD; however, like all ventricular assist devices, thrombus formation is a major concern that may lead to device failure or life-threatening events in the patient. One explanation for the thrombus formation is that it occurs in areas of low shear rate, but the blood contact surface of the polymer sac also plays a role in thrombus formation. The surface of explanted PVAD blood sacs from animal trials carried out at the Penn State Hershey Medical Center is to be analyzed to determine if surface topography plays a role in thrombus formation. To do this, a protocol is developed that allows for the analysis of the same sac sample using multiple microscopy techniques. The samples are first analyzed using confocal microscopy to determine if platelets and/or fibrin, components of thrombi, are present. Then using environmental scanning electron microscopy, the surface of the sample is analyzed. Finally, after degradation of any biological deposits, optical profilometry is used to obtain quantitative data on the surface roughness. In future studies, this protocol will result in surface data than can be correlated with flow data to further understand the cause of the thrombus formation. The correlation can lead to better designed devices and blood sacs that are less likely to induce thrombosis.

TABLE OF CONTENTS

LIST OF FIGURES

LIST OF TABLES

ACKNOWLEDGEMENTS

I first and foremost would like to thank Dr. Keefe Manning for the constant guidance and encouragement that he has provided over the last three years as both my honors and thesis advisor, as well as a mentor. Dr. Manning showed a great deal of patience with me and what seemed like nearly daily emails in order to complete this project. I would also like to thank the rest of the past and current members of the Artificial Heart Lab. Everyone in the group played some sort of role in this project, and not once was I ever not able to get the assistance that I needed. This group showed me what it is truly like to work in a team atmosphere where everyone has each other's best interest in mind. A special thanks to Ashlyn Mueser who has followed me over the past year in order to learn the protocol to continue on the project. She has shown a great deal of flexibility and patience to find time to work alongside of me to perfect this protocol. In addition, this project would not have been possible without my funding source: NIH grant HL108123.

The group in the Division of Artificial Organs at the Penn State Hershey College of Medicine also cannot be thanked enough. Dr. William Weiss gave me the opportunity to start this project through the American Heart Association Summer Undergraduate Research Fellowship over the summer of 2013. Since then, he has provided a great deal of insight and support in order to see this project through to what he had envisioned. I would also like to thank Dr. Weiss and Dr. Chris Siedlecki for serving as my thesis committee. Along with this role, Dr. Siedlecki provided a great deal of insight into the biological side of thrombus formation. Thank you to Eric Yeager for all of the help that

Chapter 1

Introduction

1.1 Clinical Need

Cardiovascular disease (CVD) is a leading medical problem among adults in the United States with an estimated 83.6 million adults in the United States living with one or more forms of CVD according to the American Heart Association. In the past year, nearly 800,000 adults have died from CVD, accounting for nearly 1 out of every 3 deaths in the United States. On average there is a death from CVD every 40 seconds[1]. Although cardiovascular disease is a major problem among adults in the United States, it is not just limited to adults. The number of hospitalizations for heart failure among pediatric patients, a patient younger than 18 years of age, has increased over the past years as shown by an analysis of the Healthcare Cost and Utilization Project Kids' Inpatient Database, which samples pediatric hospitals nationwide[2]. The analysis showed 18 out of every 100,000 children in the United States are hospitalized for heart failure as a result of cardiomyopathy, myocarditis, and congenital heart disease. Cardiomyopathy is the enlargement and weakening of the heart muscle, and myocarditis is the inflammation of the myocardium. Hospitalizations from these heart diseases results in a 7% hospital mortality rate[2]. While the occurrence of cardiovascular disease and deaths is not as severe in pediatric patients as it is in adults, it is a problem considering the number of hospitalizations occurring.

CVD survival has increased with advanced preoperative treatment and operative techniques; however, end-stage heart failure still occurs in many patients, so another treatment option is required. The most established and preferred treatment option for both adults and children is heart transplantation. In the United States, there is a major shortage of donor organs because the ratio of heart transplant recipients to patients on the waitlist is nearly $1:10^3$. As a result, other treatment options, such as mechanical support devices, have been explored for patients with heart failure.

1.2 Mechanical Support Devices

The most widely accepted alternative to heart transplantation is the implantation of a mechanical circulatory support device. The most common circulatory support device is the left ventricular assist device (LVAD)[4]. Left ventricular assist devices are the preferred ventricular assist device because the left ventricle is more susceptible to failure because it experiences a larger stresses and forces. A LVAD does not replace the native heart, but instead it aids the heart in pumping blood throughout the body.

LVADs can be used as bridge-to-transplant, bridge-to-recovery or destination therapy. In bridge-to-transplant, the LVAD is used as a treatment until a donor heart becomes available. For bridge-to-recovery, the LVAD is implanted to reduce the work done by the heart, so the heart can recover. Once the heart has recovered normal function, the LVAD can be explanted. The third treatment option is destination therapy where the LVAD is implanted for the remainder of the patient's life. Over the years, advancement in LVAD technology has resulted in smaller pumps that are more durable

and enhance the survival of the patient, which has led to the wide acceptance of the LVAD as a treatment option for heart failure in adults[5]. However, the technology for pediatric LVADs is significantly lagging behind the technology of adult LVADs.

Advancements in mechanical support devices for pediatric patients have been made over the last decade. Before the advancements, treatment for bridge-to-transplant or bridge-to-recovery was limited to extracorporeal membrane oxygenation (ECMO) for small patients or an adult LVAD for teenagers large enough for the device. ECMO, which uses a modified heart-lung bypass machine to provide cardiac support, is not an ideal treatment option for pediatric patients because it does not provide long-term support[6]. A 2012 study, showed that small children (body surface area less than 0.7 m^2) supported by ECMO survived an average of 13 days, and children with a body surface area between 0.7 m^2 and 1.5 m^2 survived an average of 10 days[7]. Despite the poor survival rate, ECMO was the treatment of choice for small pediatric patients because there was no alternative. The other option was implantation of an adult LVAD into larger patients often in their teenage years. One established LVAD for heart failure treatment in adults that has also been used as treatment for pediatric patients mostly between 11 to 18 years of age is the HeartMate II[8,9]. Based on a review of the Interagency Registry for Mechanically Assisted Circulatory Support (INTERMACS), outcomes of the HeartMate II implanted into pediatric patients were compared to young adults between the ages of 19 and 39 who were implanted with the same device. Comparison of the 6 month follow-up data showed no significant difference between the pediatric and young adult groups. Of the pediatric group, 95.6% of the patients still had the device implanted, received a transplant or had recovered from the cardiovascular disease. This is compared to 96%

survival rate of patients in the young adult group. However, a significant difference was found between the two groups is the length of the hospital stay after the device was implanted. The pediatric group was hospitalized on average of 1.13 months, while the young adult group's average hospitalization was 0.70 months[10].

Another successful case of adult LVAD implantation into a pediatric patient was the implantation of a TandemHeart left ventricular assist device into a nine-year-old girl weighing 23 kilograms. The patient remained on the small centrifugal pump for 10 days until a donor heart became available, which was significant because the girl was much smaller than the patients receiving the HeartMate II[11]. The average pediatric patient receiving the HeartMate II weighed 71 kilograms, which is three times the weight of the nine year old girl. While adult LVAD implantation in teenage patients has shown to be a successful treatment, there is no alternative to ECMO for smaller patients.

The need for an alternative treatment for smaller patients has led to the research and development of pediatric-specific left ventricular assist devices (PVADs). The first ventricular assist device designed specifically for small pediatric patients was a modified adult LVAD. In Germany, the Berlin Heart Group modified their pulsatile adult LVAD to make it smaller for placement in children. The new pediatric LVAD was called the EXCOR Pediatric VAD, and was available in multiple sizes to be implanted in sizes ranging from infants as small as 3 kg to the size for adults. The device was first used in Europe to support pediatric patients in the early 1990s and was first implanted in a patient in the United States in 2000[12]. A study of EXCOR implantation in pediatric patients as part of a clinical trial in the United States showed a 12-month survival rate of 75%[13]. The use of this device in the United States has become more widespread, but the device is not

without its complications[13–16]. The only other PVAD currently approved by the FDA is the HeartAssist 5 also known as the DeBakey VAD Child, which is a continuous flow VAD for use in patients with a body surface area greater than 0.7 m^2, or a child around the age of 5 years[17]. The device has not reached widespread approval due to complications similar to those caused by the EXCOR. Despite the development of pediatric specific ventricular assist devices, the challenge of thrombosis faced in adult VADs still exists.

1.3 Thrombosis

Thrombus formation can become life threatening if the thrombus blocks blood flow where it forms or if it detaches from the area of formation and blocks a blood vessel at another location. The detachment of the thrombus from the formation site is known as thromboembolism. If the thrombus prevents blood flow to the brain or if the thrombus breaks off and flows to the brain, the patient can suffer a stroke. To fully understand thrombosis and to address the problem, an understanding of hemocompatibility is needed. Hemocompatibility is the compatibility of a material when in contact with blood. Thrombosis is caused by activation of the complicated coagulation pathway shown in Figure 1-1[18]. While this process is complex, coagulation can be simplified with an understanding of platelets and fibrin.

Platelets are small, disc-shaped cellular fragments with an average diameter of 2 to 4 microns. Platelets are activated either chemically or mechanically to change shape and form aggregates. The chemical stimuli include thrombin, platelet-activating factor,

von Willebrand factor, and ADP, and the physical stimuli are most commonly shear stress and contact with biomaterials[19]. An activated platelet can activate other platelets and catalyze thrombin production[20]. When fibrinogen comes in contact with thrombin during platelet activation, fibrin, a fibrous protein, is formed. Coagulation as the result of activated platelets and fibrin trapping red blood cells and other cellular components can lead to thrombus formation.
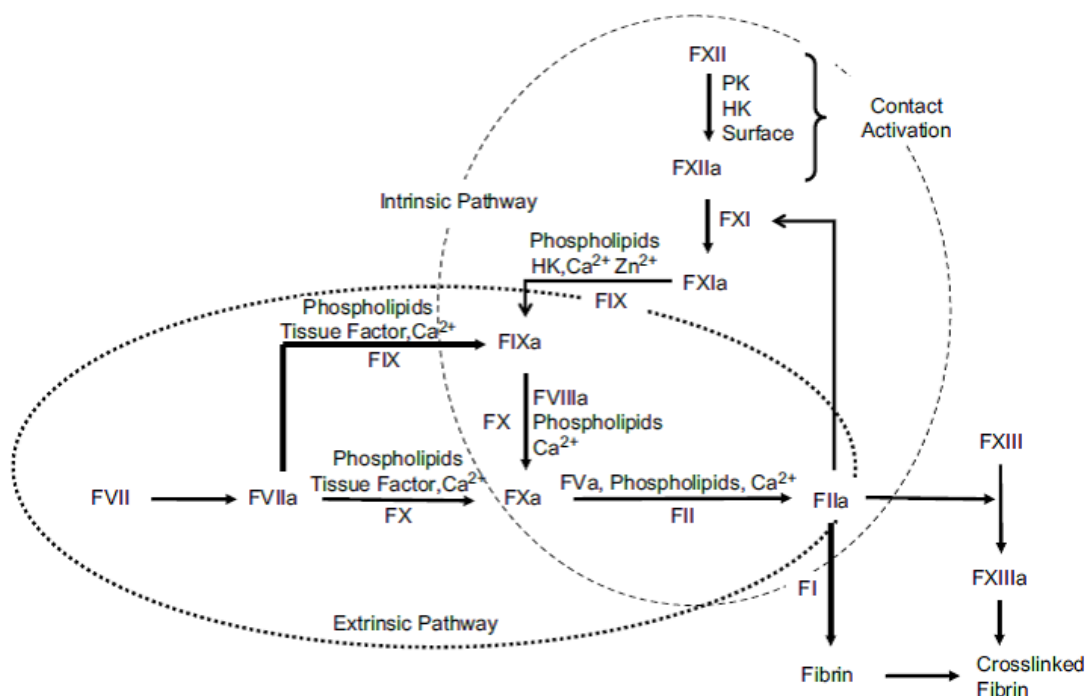
Figure 1-1: The coagulation-plasma cascade[18].

The coagulation pathway is often activated by injury or trauma. An injury that causes a break in a blood vessel will result in the release of the factors responsible for activating platelets and fibrin. The coagulation pathway can also be activated if a foreign material is introduced into the body. The introduction of the LVAD causes the activation of the coagulation pathway and can result in the life-threatening thrombosis that is associated with ventricular device use. As a result, all approved LVADs, both pediatric

and adult, require antithrombotic therapy in the form of anticoagulants and/or antiplatelet medication[21]. Anticoagulants are prescribed because they can prevent the activation of the coagulation pathway. Patients implanted with LVADS often receive heparin after the surgery. For long-term anticoagulation, patients receive low-molecular-weight heparin because prolonged use of heparin can result in low platelet counts, or they receive warfarin sodium (Coumadin®)[22]. Heparin is used as an anticoagulant because it activates antithrombin III, which inactivates thrombin, thus preventing the activation of platelets. Warfarin sodium blocks vitamin K, which will inhibit coagulation factors such as prothrombin and Factor VII. Even with these anticoagulant treatments, thrombosis occurs in some pediatric patients receiving a PVAD. One reason for the thrombosis could be that anticoagulation use has only been studied in adults, but there are differences in the levels of coagulation factors in children compared to the levels in adults. For example, children have a lower level of antithrombin than adults. As a result, children respond to the anticoagulants differently than adults[23].

1.4 Penn State Pediatric Ventricular Assist Device

Taking into account the need for a pediatric ventricular assist device and the complications caused by foreign materials in the body, the Division of Artificial Organs at the Penn State College of Medicine has developed a pediatric ventricular assist device shown in Figure 1-2[24]. The device was developed for use in infants including newborn babies and children. Based on the adult Pierce-Donachy VAD (Thoratec VAD), the Penn State PVAD is a pneumatically driven pulsatile pump. As defined by the National Heart

Lung and Blood Institute, this pump can be used in pediatric patients suffering from ventricular dysfunction of two different classifications of causes. The first classification is congenital heart disease such as single ventricle, transposition of the great arteries, or hypoplastic left heart syndrome. The second classification is ventricular dysfunction caused by sepsis, cardiopulmonary collapse, cardiomyopathy or myocarditis. While these two classifications require different treatment, especially duration of the treatment and therapeutic approaches, the Penn State PVAD could be used for both situations. To reduce thrombus formation, several design features are found in the Penn State PVAD that differentiates it from the other pediatric devices currently available such as the Berlin Heart EXCOR. The major differences are the use of a tilting disc mechanical heart valve and a segmented poly-(ether polyurethane urea) (SPEUU) seamless blood sac. The SPEUU blood sac is used in combination with a diaphragm to pump blood through the PVAD[25]. The valve and the blood sac are the only two components of the device that comes in direct contact with the blood, making them crucial for the biocompatibility of the PVAD.

Figure 1-2: The Penn State Infant VAD[24]**.**

The seamless SPEUU blood sac design change was made to improve the biocompatibility and hemocompatibility of the Penn State PVAD. SPEUU is one of the more biocompatible materials available for use in medical devices; however, no material is perfectly biocompatible, so like every other biomaterial, there is protein adsorption on the polymer surface after coming in contact with the blood. Besides the material, it is important that the blood sac is fabricated without seams, since imperfections in a polymer surface can provide a feature for platelet adhesion, which could lead to thrombus formation. Small topographic irregularities on the surface are part of the manufacturing process that cannot be totally controlled; however, seams would have the same effect as these imperfections. By designing the blood sac without seams, a potential cause of thrombus formation is eliminated.

Thrombosis is also caused by other factors such as fluid flow. The amount of shear induced by the fluid flow can affect the activation of components of the coagulation pathway such as platelets and fibrin. Fibrin deposition can be caused by areas of low

shear, while areas of high shear can cause the activation of platelets[26]. Occurrence of either of these events could lead to thrombus formation in the regions where the shear is too high or too low. Fluid flow is affected by the shape of the sac and by the valve used in the sacs. The previous design of the Penn State ventricular assist device used ball-and-cage valves, which caused disrupted fluid flow. As a result, the Bjork-Shiley Monostrut tilting disk valves and CarboMedics (CM) bileaflet valves were considered for use in the device. To select the valve for the device, flow through the valves was evaluated to determine which valve would best prevent thrombus formation. Hubbell and McIntire had shown on a polyurethane (PU) surface that a wall shear rate greater than 500 s^{-1} markedly reduced platelet adhesion[27]. In addition, thrombus prevention in a LVAD has been shown to occur when there is a strong inlet jet and a late diastolic recirculating flow[28]. Wall washing can also prevent thrombus formation, because it prevents platelets or fibrin from sticking to the walls of the surface. Comparison of the flow of the two valves showed the Bjork-Shiley Monostrut tilting disk valves are the better option for prevention of thrombosis because the major orifice resulted in a stronger jet, better wall washing, and recirculation when compared to the three orifices of the bileaflet valve[29].

While the Penn State pediatric ventricular assist device has yet to reach the clinical stage of testing, the device is undergoing chronic *in vivo* tests in a juvenile ovine model. The device has been implanted into 7 ovine models with a goal of 4 to 6 weeks of survival while being supported by the pump. The animals were split into two groups based on the anticoagulants that the animals would be receiving. Both groups received heparin, but the one group received significantly less heparin than the other. The results showed that a survival range of 4 to 6 weeks was achieved in 5 out of the 7 ovine models

with the mean support duration being 26.1 days. After the study period, the device was explanted from the animal, and a necropsy was performed. During the necropsy, signs of thromboembolism were investigated. Evidence of thromboembolism was seen in only one of the animals, and this animal had a chronic infection and fever. After explanation, the pump was analyzed for thrombi by disassembling the pump and viewing the regions of the device in contact with the blood. Minimal thrombus formation was detected in both groups even though the one group received considerably less anticoagulants[24]. The results of this study show that the design modifications, such as the use of the tilting-disk valve and a seamless SPEUU sac, are beneficial in the prevention of thrombosis.

While thrombus formation was minimal in the *in vivo* animal models, device design and manufacturing can be further improved to reduce thrombus formation. The effects of fluid flow on thrombus formation in the PVAD have been extensively studied. The use of pseudo-3D particle image velocimetry (PIV) to visualize the flow in the Penn State PVAD in a mock circulatory loop provided an understanding of the flow and how the geometry and the small size affect the wall shear rates, which play a crucial role in determining if thrombosis will occur[30]. While the effect of flow on thrombosis in the PVAD has been studied, the effects of surface topography have yet to be investigated.

1.5 Surface Irregularities

As mentioned previously, surface roughness can cause activation of the coagulation pathway especially if the roughness causes the accumulation of platelets in a certain region. While this is known and taken into account in the overall design of the

blood sac, surface specific examination has not been carried out. As a result, one area for potential improvement in the reduction of thrombi is the manufacturing process for the blood sacs. The Division of Artificial Organs at Penn State has been manufacturing polymer blood sacs for LVADs for many years now. Over this time, the ways the sacs are fabricated and the material that is used has evolved. The material has changed from polydimethylsiloxane (PDMS) to PU to the SPEUU that is currently used. These changes were made as advancements in polymers and the understanding of the biocompatibility of polymers resulted in using the best polymer to reduce thrombus formation.

The way the polymers are cast to make the sacs has also changed, which has greatly affected the surface topography. Originally, a wax cast was dipped into the PDMS to fabricate the sac, and then the wax cast was melted and cracked to remove the sac from the mold. Scanning electron microscope (SEM) images of sacs fabricated using this method showed scratch marks from the breaking of the mold, which resulted in a change in the fabrication process to melting out the wax mold instead of breaking it out. SEM images showed that the large scratch marks from the breaking were no longer seen, but pits were now present in the sac surface. Yamanaka suggested that platelet adhesion and thus thrombus formation was encouraged by these pits but proving that was outside of the realm of her study[31]. She was able to show with confocal imaging that fibrin spread around platelets accumulating in regions of a similar size to the pits. While the confocal images did not confirm that pits promote platelet adhesion and thrombus formation, it led Yamanaka to state that further investigation is necessary to determine if surface features in the polymer play a role in thrombosis[31]. The method of fabrication currently used no longer uses a wax mold, but instead a stainless steel mandrel is used to

create the mold. While this method of fabrication is believed to reduce the large pits, the presence of other surface irregularities in the SPEUU blood sacs and their effects on thrombus formation have yet to be investigated.

Surface irregularities such as a pit that are the size of a platelet are believed to induce platelet adhesion. However, sub-micron features on polyurethane have been shown to reduce platelet adhesion. Sub-micron pillars were textured into polyurethane using a replication molding technique. The textured polyurethane was adhered to a rotating disk system that spins the material in platelet rich plasma at physiologically relevant shear stresses to induce platelet activation and adhesion[32]. When compared to smooth samples, the sub-micron textures reduced platelet adhesion at low shear stresses in the range of 0 to 5 dyne/cm^2. As a result, low shear stress is believed to reduce platelet adhesion to surfaces with sub-platelet dimensions because there is a decrease in the area of the material for the platelets to contact[33]. This phenomenon has been seen using other materials[34,35] but has not been studied in a pulsatile LVAD.

While the effects of surface irregularities on the blood sacs of pulsatile LVADs have not been studied, the effects on continuous flow pumps have been. Linneweber *et al.* altered the surface of three metal impellers of rotary pumps to different roughness values (0.05, 0.2 and 0.4 micrometers) that were determined by a stylus profilometer. These three pumps were then placed in a mock circulatory loop with whole blood for one hour. The impellers were then removed from the pump, and the surface was analyzed for platelets and coagulation factors. Platelet adhesion was significantly higher on the roughest surface when compared to the 0.05 micrometer surface as shown by both SEM images and enzyme-linked immunosorbent assays. The SEM images showed that the

platelets were adhering at large scratches in the surface. In addition to the platelet adhesion, higher levels of adsorbed fibrinogen and von Willebrand factor were observed on the rough surfaces[36]. The results of the study clearly showed that surface roughness of metal components in continuous flow LVADs plays a role in the activation of the coagulation pathway. However, a similar study to determine the effects of surface roughness on the coagulation pathway has not been carried out for a pulsatile pump with a polymer sac.

1.6 Current Study

Yamanaka's work[31] and other studies[33,34,36,37] on the effect of topography on platelet adhesion suggest that surface irregularities do play a role in the hemocompatibility of a material. The objective of this study is to develop a protocol to correlate different microscopy techniques to determine if surface roughness in the SPEUU blood sacs of the Penn State PVAD causes thrombosis. This protocol will consist of first viewing sacs explanted from ovine models with confocal microscopy to determine if there are platelets and fibrin on the sac surface and where these are located. To accomplish this, antibodies will first need to be determined to label both platelets and fibrin because despite the ovine model becoming an increasingly more common model for preclinical evaluation of cardiovascular devices such as LVADs, the tools to assess the biocompatibility such as antibodies are limited. The same sample will then be viewed with Environmental-SEM (ESEM) low vacuum mode, which does not require the sample to be coated and allows the actual surface of the sac to be viewed to determine if there

was a surface irregularity causing the adhesion of platelets or fibrin. The final step is to then enzymatically degrade any biological deposition, so the surface can be analyzed with optical profilometry to obtain quantitative surface roughness data. The process for enzymatically degrading the deposition will need to be tested in order to ensure the polymer surface is not altered. Perfecting each of these microscopy techniques with the SPEUU will lead to the development of a protocol to view the same sample with all three techniques.

Chapter 2

Theory

2.1 Environmental Scanning Electron Microscopy

Environmental scanning electron microscopy is a scanning electron microscope that allows for the imaging of wet and insulating samples without prior specimen preparation, which cannot be accomplished using a conventional SEM[38]. To image the wet and insulating samples, a low vacuum chamber is used, as compared to a high vacuum chamber for conventional SEM, which allows for the pressure and temperature to be varied. Also, a gas is present in the sample chamber, often water vapor, to obtain high resolution images[39].

All SEMs consist of an electron column that creates a beam of electrons that are accelerated and focused onto the sample. Signals from the interactions between the sample and the electron beam are monitored by detectors and are reconstructed into a virtual image that is displayed on a monitor[40]. The signal is one of two categories of emitted electrons: low-energy secondary electrons and backscattered electrons. The secondary electrons, which are more commonly used for constructing images, are the result of inelastic collisions with the sample, and the backscattered electrons are produced from elastic collisions with the sample[38].

As previously mentioned a high vacuum chamber is required for conventional SEM because the presence of gas molecules can scatter the electrons and degrade the

beam. However, in ESEM a gaseous environment is maintained around the sample in a low vacuum chamber, which allows the samples to be imaged in their native state even if it is a hydrated sample. In order to achieve the low vacuum environment, a differential pumping system is used down the column as shown in Figure 2-1. The electron gun is kept at a high vacuum state and the pressure gradually increases through a series of pressure zones, which minimize the presence of gas molecules to interfere with the electron beam. Another benefit of having gas in the sample chamber is that the buildup of charge that would occur on an insulating surface can be dissipated, so insulating surfaces do not need to be coated[38]. As a result, the true polymer surface can be imaged with ESEM without needing to sputter coat the surface.
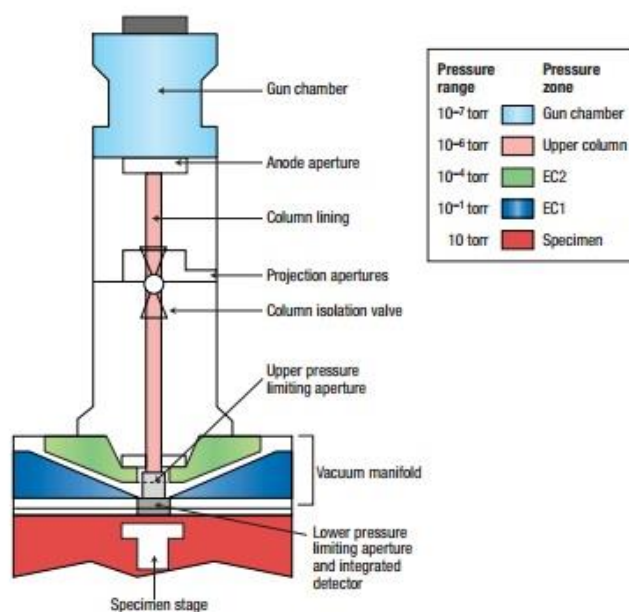
Figure 2-1. Schematic of ESEM showing the different pressure zones[38].

2.2 Optical Profilometry

Optical profilometry is a non-contact method of characterizing surface topography by utilizing the interference of light to measure height variations. Compared to contact profilometers such as atomic force microscopy, optical profilometry has no risk of harming the surface in any way because no contact is made with the sample. Also optical profilometry allows for more rapid data collection which saves both time and money[41]. The wave properties of light are used to compare the difference in the optical path between the test surface and a reference surface. This is done through the use of a beam splitter that reflects half of the light beam from the test reference, and the other half of the light beam is reflected from the reference mirror as shown in Figure 2-2.
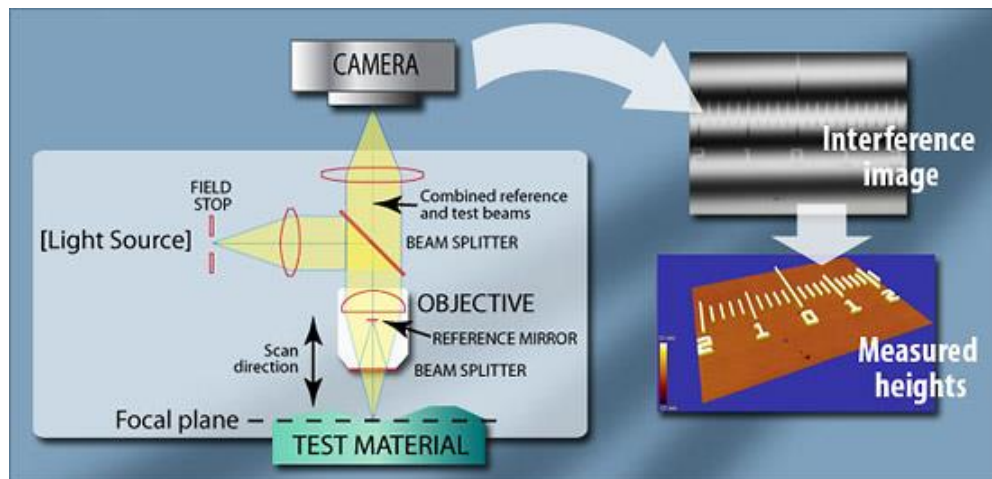
Figure 2-2: Optical profilometry light path[42].

When the reference mirror and the test material are at an equal distance from the beam splitter, the split light beams recombine, and constructive and destructive light interference occurs wherever the length of the light beams differ. The difference in the length of the light beam is caused by height variances in the test surfaces as compared to

the perfectly flat reference mirror, which creates interference fringes that are characterized by light and dark bands and can be seen Figure 2-2. The lighter bands are areas of constructive interference, while the darker bands are destructive interference when focused onto a digital camera. Knowing the wavelength of the light allows for the difference in the height to be calculated across the surface to obtain a 3D surface map[42].

From the surface map a variety of roughness parameters exist that can be used to quantitatively analyze the surface. The two most commonly used parameters are the roughness average, R_a, and the root-mean-square roughness, rms or R_q. The roughness average is the arithmetic average deviation of all points in the surface profile and is calculated according to Equation 1 where L is the length of the sample and z(x) is the surface profile. R_a is commonly used because it is statistically very stable and can be easily repeated for surfaces that are fabricated using a controlled process.

$$R_a = \frac{1}{L} \int_0^L |z(x)| dx \qquad (1)$$

R_q is the root-mean-square average of the roughness profile, so the amplitudes are squared as shown in Equation 2. As a result of the amplitudes being squared, R_q is more sensitive to peaks and valleys than R_a. A comparison of R_a and R_q for the same profile is shown in Figure 2-3 where the R_q is slightly larger than R_a due to the sensitivity to the

$$R_q = \sqrt{\frac{1}{L} \int_0^L z^2(x) dx} \qquad (2)$$

peaks[43].
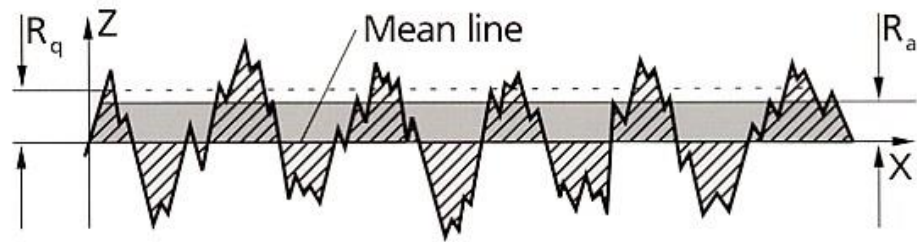
Figure 2-3: Comparison of R$_a$ and R$_q$ [43]

While there are many other surface parameters that can be used, the ten-point height, R$_z$, and the Swedish height, H, will also be used for the analysis of the blood sac surface. R$_z$ is the average absolute value of the five highest peaks and five lowest peaks over the evaluation area and is calculated according to Equation 3 with a visual representation given in Figure 2-4. The ten-point height is used because it is a good indicator of the height of the peaks and valleys, which cannot be obtained from the average roughness.

$$R_z = \frac{(P1 + P2 + \cdots + P5) - (V1 + V2 + \cdots + V5)}{5} \tag{3}$$
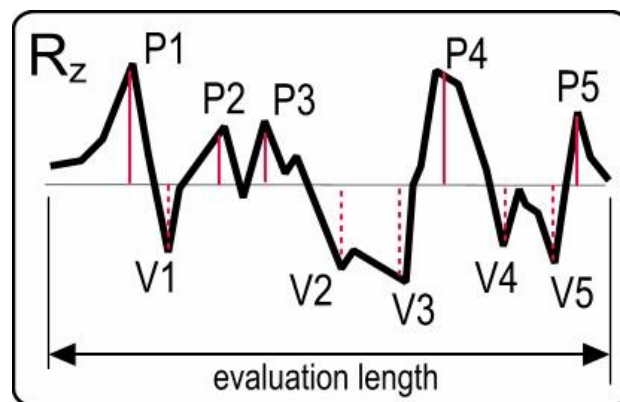
Figure 2-4: Ten-point height, R$_z$ [44].

While the ten-point height only takes the peaks and valleys into account, the Swedish height does the opposite and is less sensitive to data spikes as it only takes into account the middle 90% of the data. The Swedish height, is the height between two reference lines that removes the upper and lower 5% of the data as shown in Figure 2-5[44].
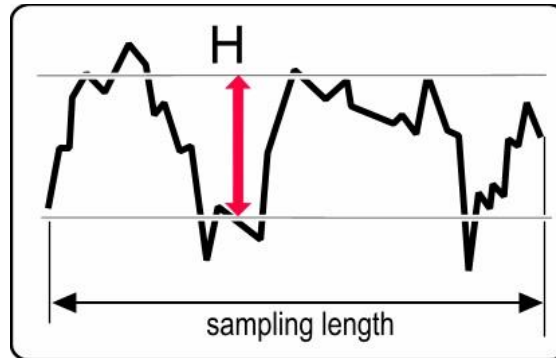
Figure 2-5: Swedish height, H[44].

Chapter 3

Methods

3.1 Blood Sac Fabrication

All of the blood sacs were manufactured by the Division of Artificial Organs at the Penn State College of Medicine (Hershey, Pennsylvania) using SPEUU and a successive dip-casting and curing protocol. The SPEUU is validated before every sac is fabricated to ensure proper composition and percent solids of the polymer. After validation of the polymer, a steel mandrel shown in Figure 3-1 of the desired shape is dipped in the polymer. Once the desired thickness of the sac is achieved, the sac is stretched over the mandrel to remove the sac from the mandrel. Final post processing and measurements are made to select sacs to be used in the PVAD. Sacs that are not selected are kept in inventory for future use or studying the manufacturing process. Following the selection process, the sacs that are selected for animal trials need to have the ports grinded to proper specification, and they are then heat-formed to create a mate with the valve of the PVAD.

Figure 3-1: The steel mandrel is shown to the left, the sac used in the PVAD with the heat-formed ports is shown in the middle and the sac after removal from the mandrel is shown on the right.

3.2 Smooth vs Rough Sac Analysis

The purpose behind developing the protocol to analyze the sac surface is to determine if surface irregularities play a role in thrombus formation. The surface irregularities present in the sacs needed to first be identified before determining what affect they have on thrombosis. To identify any irregularities, sacs that were not selected for implantation were first examined at 40x using an Olympus SZ61 light microscope (Olympus America Inc., Center Valley, Pennsylvania) with a PixeLINK camera interface (PixeLink, Ottawa, Ontario) to identify any visible surface irregularities. Any visible surface irregularities were imaged and marked on the sac surface for future analysis. Next, samples approximately 1 cm^2 in size were cut from regions of the sac with and without visible irregularities and mounted onto a microscope slide with double-sided tape. The samples that had visible surface irregularities were classified as a rough

sample, while samples without any visible surface irregularities were classified as "smooth" samples. These samples were then examined with ESEM to obtain higher magnification images of the surface and optical profilometry to compare the surface roughness. For the optical profilometry data, statistical significance was determined using a Student's t-test (α=0.05).

3.3 *In Vitro* Controls

In order to evaluate the surface of the blood sacs, several methods were used to produce positive and negative *in vitro* controls of fibrin and platelets to identify any biological deposition that may be present on the sac surface. The negative controls were approximately 0.5 cm^2 samples cut from the polymer blood sacs that were not used in the animal trials. Because these sacs have never come in contact with blood, they are free of any biological deposition such as platelets and fibrin, the requirement for a negative control.

Positive ovine platelet controls were prepared using two different methods: platelet rich plasma (PRP) clots and activation of platelets on polyurethane urea (PUU) using a rotating disk system (RDS). Positive fibrin and platelet controls were prepared from clots developed by a backward facing step model in a blood flow loop. All three of these methods used ovine blood obtained from the Penn State College of Medicine. Approximately 450 mL of whole blood was drawn from the jugular vein of a healthy ovine into a blood bag containing citrate phosphate dextrose adenine. The blood bag was

then transported to the laboratory in University Park in an insulated container with ice packs.

To obtain PRP, the blood was centrifuged according to a protocol used by Lauren Grunenwald, a previous member of the Artificial Heart Lab[45]. The blood was transferred in 45 mL whole blood aliquots into 50 mL centrifuge tubes, and the samples were centrifuged at 600 g for 12 minutes using a Jouan CR3i centrifuge (Thermo-Fisher Scientific, Waltham, MA) at 25°C with acceleration and deceleration settings of 1%. Following completion of the centrifugation, a 25 mL serological autopipette was used to carefully remove the top PRP layer, making sure to not remove any of the buffy white layer or the packed red blood cells. The PRP was then transferred to clean 50 mL centrifuge tubes.

The PRP clots were prepared according to a protocol used by Hanako Yamanaka, a former graduate student[31]. In a 24-well tissue culture polystyrene plate, 1 mL of PRP was added to the wells of the plate. To induce clotting, 15 μL of 1 M $CaCl_2$ was added to each well, and the samples were incubated for 2 hours at 37°C. Following incubation, the samples were rinsed three times with phosphate buffered saline (PBS), fixed with 1% paraformaldehyde (PFA) solution for 1 hour at 4°C, and then rinsed three times with PBS. The clots were then thinly sliced with a scalpel for imaging.

The second method for obtaining positive platelet controls was using a RDS as shown in Figure 3-2. For this method, 50 mL of PRP was placed into a 100 mL polytetrafluoroethylene beaker, which was placed on a hot plate underneath the RDS to keep the temperature of the PRP constant at 30° C. The RDS (Pine Instrument Company, Grove City, Pennsylvania) consists of a motor connected to a threaded shaft. Using a

stamp, PUU was cut into 20 mm diameter circular samples that were adhered to a metal disk using double-sided tape. This disk was then fastened onto the threaded shaft and lowered approximately 3 mm into the PRP. The RDS was turned on, and the rotation rate was set to 283 rpm and was allowed to rotate for two hours. Upon completion of the two hours, the RDS motor was turned off, and an autopipette was used to carefully replace the PRP with PBS by adding and removing 35 mL aliquots six times. The PBS was then replaced by 1% PFA solution in the same manner that the PRP was replaced. The PUU remained in the PFA solution for 1 hour at 30°C. Finally, the PFA solution was replaced with PBS, and the metal disk was removed from the RDS[46].
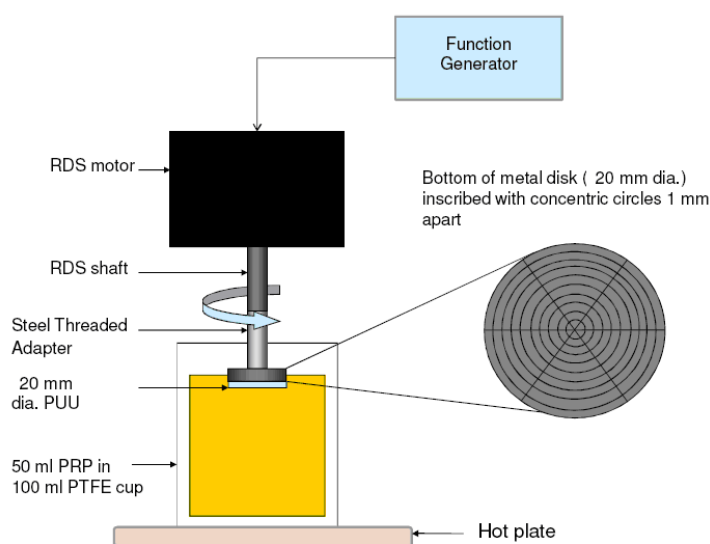
Figure 3-2: Rotating disk system used for positive platelet controls[46]**.**

Positive controls for fibrin were created using purified ovine fibrinogen (Molecular Innovations, Novi, Michigan). Fibrinogen as opposed to fibrin could be used as a positive control because the primary antibody used labels an epitope present in both

fibrinogen and fibrin. The fibrinogen solution was plated on a glass coverslip. The fibrinogen was fixed with 1% PFA for 1 hour at 4°C, and then rinsed with PBS.

The final *in vitro* control was clots from a backward facing step model in a blood flow loop. These clots were created with whole ovine blood that was obtained using the same procedure for the PRP clots and RDS. To reverse the effects of the CPDA anticoagulant used to prevent clotting in the blood bag, 4 mL of 6.45% $CaCl_2$ was added for every 250 mL of blood that was used. The backward facing step geometry shown in Figure 3-3 creates a region of stagnant, low shear flow that leads to thrombosis. To construct the flow loop shown in Figure 3-4, the two acrylic segments of the backward facing step model shown in Figure 3-3B were fastened together with four nylon nuts and bolts and a rubber O-ring to create a tight a seal to avoid fluid loss. To both ends of the model, a short segment of Tygon® tubing with an inner diameter of 5/8" was fastened using plastic c-clamps. To each of these pieces of tubing, a 1/4"- 5/8" adapter was attached and fastened using a plastic c-clamp to provide a transition for the use of 1/4" tubing throughout the rest of the flow loop. The remaining tubing consisted of five pieces of the 1/4" tubing and 2 Y adapters connected as shown in Figure 3-4. Two of the tubing pieces were placed in 1 L beakers to serve as inlet and outlet for filling and draining. The final piece of tubing was connected between the Y adapters to create a continuous loop. The last component of loop is a peristaltic pump (Cole-Palmer Instrument Company, Vernon Hills, Illinois). Due to the peristaltic nature of the pump, a slightly sinusoidal pressure gradient is created, but at the speed used in the loop, the flow was considered to be continuous.
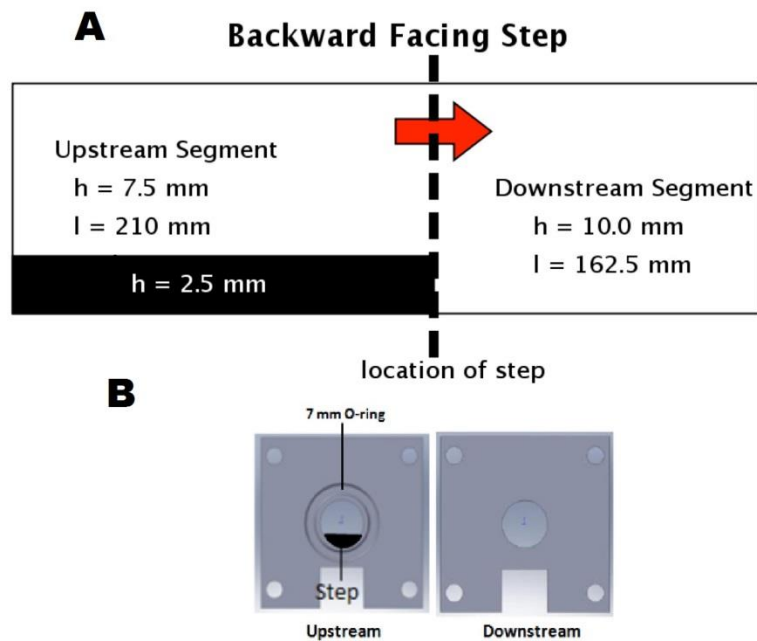
Figure 3-3: Diagram of acrylic backward facing step model is shown in A. The cross-sectional area of the acrylic pieces at the step is shown in B[47].
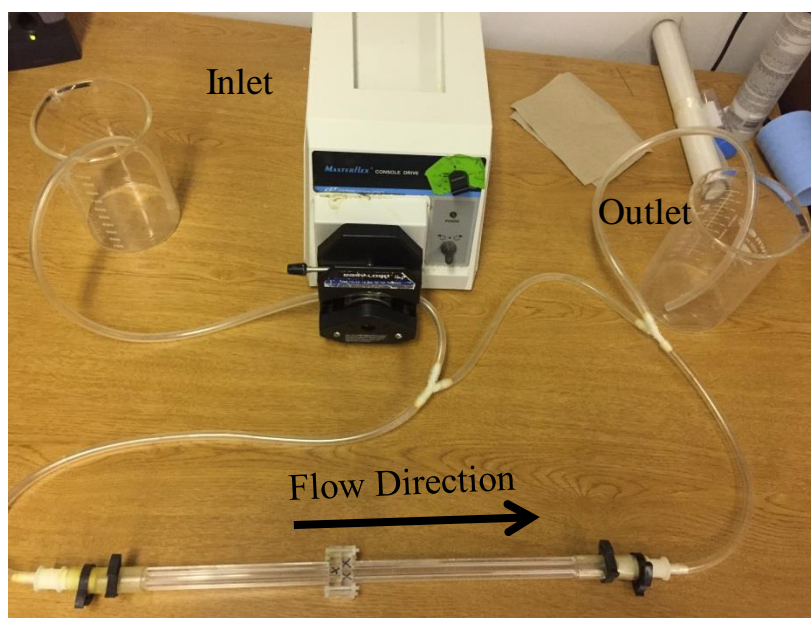
Figure 3-4: Flow loop construction for filling the loop with fluid. Fluid is placed in the inlet beaker and any waste is created in the outlet. The direction of the flow is shown.

Before the loop could be filled with whole ovine blood, the tubing and model was filled with PBS to create a biologically relevant environment with a pH of approximately 6.80 within the loop. The PBS also removed any air that was contained in the loop. To fill the loop, the inlet tubing was placed in the beaker containing PBS, and the tubing was placed in the pump as shown in Figure 3-4. The pump was turned on until all of the tubing contained PBS at which point it was stopped. Once the loop was filled with PBS, whole ovine blood was pumped at 0.20 L/min through the loop to replace the PBS. With the loop filled with blood, the inlet and outlet tubing were clamped with hemostats, and the tubing section connected between the two Y adapters was placed in the pump as shown in Figure 3-5. With the pump calibrated for a flow rate of 0.76 L/min, blood was pumped through the loop for 30 minutes. Once the 30 minute time period was completed, the loop was again filled with PBS at 0.20 L/min to purge the loop of the blood. The pump was stopped, and the loop was then disassembled. The blood clot contained within the backward facing step was carefully removed using a metal spatula and placed in PFA for 48 hours to fix the cells.
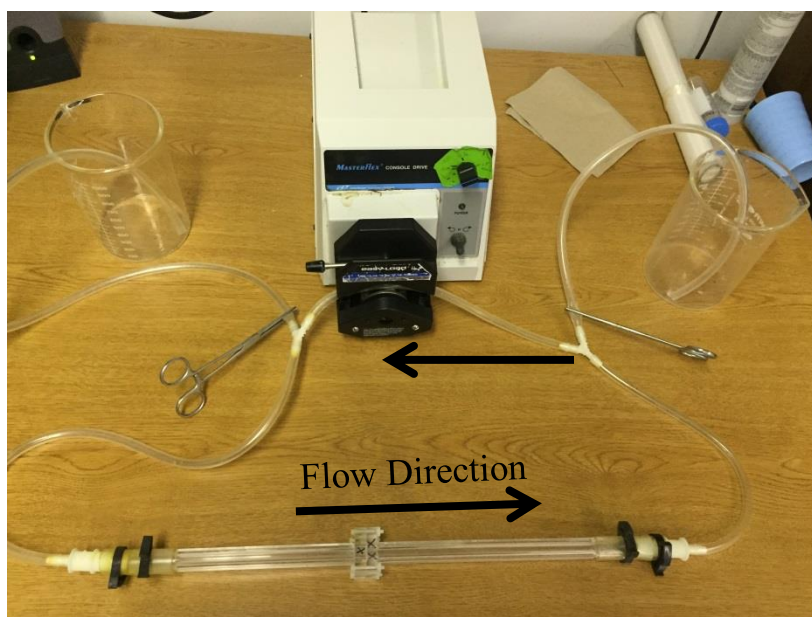
Figure 3-5. Flow loop setup for operating the loop after it is filled with fluid. Hemostats are used to clamp the inlet and outlet tubing. The direction of the flow is shown.

After fixation in the PFA, the clot was placed in a fine mesh histology cassette and placed in the Leica TP1020 – Automatic Tissue Processor (Leica Microsystems GmbH, Wetzlar, Germany), a paraffin embedder at the Huck Institutes for the Life Sciences. Using the animal tissue program, the embedder replaced the water molecules of the thrombus with wax through an 8-hour series of emulsions. After the cycle of emulsions was completed, the thrombus was sectioned in 5 µm slices using a Thermo Scientific Shandon Finesse Microtome, (ThermoFisher Scientific, Waltham, Massachusetts) under a soft tissue blade (ThermoFisher Scientific, Waltham, Massachusetts). The sections were placed on a glass microscope slide and left overnight on a slide warmer (ThermoFisher Scientific, Waltham, Massachusetts) to melt the paraffin onto the glass slides. The final step in preparing the slides for imaging was

dewaxing the samples using the Shandon Gemini Varistainer (ThermoFisher Scientific, Waltham, Massachusetts)[48].

3.4 *In Vivo* Studies

The PVADs were tested in animal trials performed at the Hershey College of Medicine as approved by the Institutional Animal Care and Use Committee (IACUC #2012-032). The animals used in these studies are Dorset-Finn crossbreed sheep. After baseline assessment and monitor of the sheep, the PVADs were surgically implanted, and the driver maintained the pump at a beat rate ranging from 50 to 110 beats per minute for 75 +/- 2 days post operation. Following completion of the trials, the device was explanted, and the blood sac was flushed with saline. During the pump teardown, the sacs were examined for any potential thrombi or biological deposits, and pictures of the front, back, top, bottom, inlet side, and outlet side of the sac were taken using a digital camera. In addition, the biological deposits are photographed and the size, location and color of each deposit were noted. The location was mapped according to the blood sac region diagram shown in Figure 3-6.

The saline contained within the sac was then replaced with 1% PFA, and the inlet and outlet of the sac were clamped. After 1 hour, the PFA was rinsed out by pouring 1 L of saline through the inlet. Finally, the saline was replaced with PBS and the inlet and outlet were again clamped. The sacs were stored in an 8 oz. plastic container in a refrigerator at approximately 4°C until the sacs were transported to University Park for evaluation.
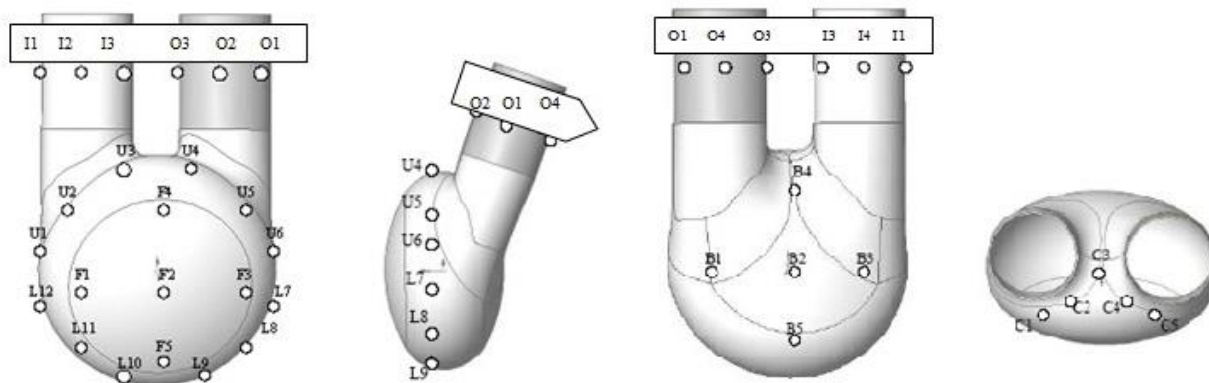
Figure 3-6: Schematic of locations on the blood sac. These regions are used to describe locations of deposits and regions for sampling[49].

3.5 Immunofluorescent Labeling and Confocal Microscopy

Indirect immunofluorescent labeling can be used to demonstrate the presence of platelets and fibrin and to distinguish between the two biological components. Indirect immunofluorescent labeling involves a primary antibody binding to an antigen of interest. A secondary polyclonal antibody that is tagged with fluorophores is then used to bind to the primary antibody as shown in Figure 3-7. The binding of the secondary antibody to the primary antibody indirectly labels the antigen of interest. A blocking agent, most commonly a serum, is commonly used in this method to adsorb to the sample surface to prevent nonspecific adsorption of the antibodies to the sample. Indirect labeling has a superior fluorescent signal over direct labeling using fluorescently labeled primary antibodies because multiple secondary antibodies can bind to one primary antibody, thus amplifying the fluorescent signal[50].
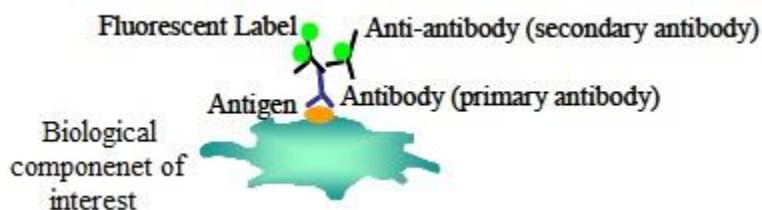
Figure 3-7: Schematic of indirect immunofluorescent labeling[50].

To study the explanted sacs, two different primary antibodies will be needed, one that binds to an antigen present in platelets, and one that binds to an antigen present in fibrinogen. In order to distinguish between platelets and fibrin, two secondary antibodies of different color labels are also needed. Because the secondary antibody is polyclonal and recognizes a class of antibody, the primary antibodies cannot be from the same host species and the same class of antibody. For example, two antibodies that are both mouse IgG will be fluorescently labeled by the same secondary antibody. To avoid this limitation, labeling kits are available that allow for the labeling of the primary antibody with the secondary antibody to occur before labeling the antigen.

To fluorescently label ovine platelets, two primary antibodies were identified as having species reactivity with sheep. The first antibody was anti-phospho-ITGB3 antibody produced in rabbit (Sigma-Aldrich, St. Louis, Missouri), which identifies platelets by labeling the phosphorylation site of tyrosine 773 on the $\alpha_{IIb}\beta_3$ integrin on the platelet membrane. The secondary antibody used with this primary antibody was anti-rabbit CF™ 555 antibody produced in goat (Sigma-Aldrich, St. Louis, Missouri) to dye the platelets red. Because the secondary antibody was produced in goat, the blocking agent used was 1% goat serum (Sigma-Aldrich, St. Louis, Missouri).

The second antibody was CAPP2A IgG1 (Monoclonal Antibody Center, Pullman, Washington), a mouse antibody that labels the CD41 antigen that encodes for the α_{IIb} integrin on the platelet membrane. This antibody has been used in the Artificial Heart Lab in the past, and Alexa Fluor® 488 chicken anti-mouse IgG (Life Technologies, Grand Island, New York) was used as the secondary antibody to dye the platelets green. The blocking agent used was 1% donkey serum (Sigma-Aldrich, St. Louis, Missouri).

Only one primary antibody could be identified that labels ovine fibrin, monoclonal anti-fibrinogen antibody produced in mouse (Sigma-Aldrich, St. Louis, Missouri), which recognizes a conformational epitope that is found in both fibrinogen and fibrin. When used with the anti-phospho-ITGB3 antibody, the secondary antibody used was anti-chicken CF™ 488 antibody produced in goat (Sigma-Aldrich, St. Louis, Missouri) to dye the fibrin green, and the blocking agent used was 1% chicken serum (Sigma-Aldrich, St. Louis, Missouri). Because the fibrin antibody and the CAPP2A are both produced in mouse, antibody labeling kits were needed to use these antibodies together. A mix-n-stain™ CF™ 555 antibody labeling kit (Sigma-Aldrich, St. Louis, Missouri) was used to label the anti-fibrinogen antibody, and a mix-n-stain™ CF™ 488 antibody labeling kit (Sigma-Aldrich, St. Louis, Missouri) was used to label the CAPP2A. The blocking agent used with the labeling kits was 6% goat serum. The primary and secondary antibodies along with the blocking agents tested are summarized in Table 3-1.

Table 3-1: Summary of primary antibodies, secondary antibodies and blocking agents.

Biological Component	Primary Antibody	Secondary Antibody	Blocking Agent
Platelets	Anti-phospho-ITGB3	Anti-rabbit CF™ 555	1% goat serum
Platelets	CAPP2A IgG1	Alexa Fluor® 488	1% donkey serum
Fibrin	Monoclonal anti-fibrinogen	anti-chicken CF™ 488	1% chicken serum
Platelet and Fibrin	CAPP2A IgG1 and Monoclonal anti-fibrinogen	Mix-n-stain™ CF™ 488 and mix-n-stain™ CF™ 555 labeling kits	6% goat serum

The different platelet and fibrin controls were labeled using the following procedure for all of the antibodies except for the labeling kits. When both platelets and fibrinogen were labeled, both blocking agents are used in the antibody solutions. Controls that were not previously fixed with 1% PFA were placed in PFA for 1 hour and incubated at 4°C. The samples were then rinsed with PBS, which was replaced with a primary antibody solution containing the primary antibody and the blocking agent, and the samples were incubated overnight at 4°C. After incubation, the samples were rinsed with PBS. The PBS was then replaced with a secondary antibody solution that contained the secondary antibody and the blocking agent, and the samples incubated in the dark for 1 hour at room temperature. Finally, the samples were gently washed with PBS to remove non-specifically bound antibodies. For the primary antibody solutions, 1.5 μL of anti-phospho-ITGB3, 1.5 μL of CAPP2A, and 1 μL of anti-fibrinogen per milliliter of

blocking agent were used. For the secondary antibody solutions, 1.25 μL of anti-rabbit CF™ 555, 1.5 μL of Alexa Fluor® 488, and 1.25 μL of anti-chicken CF™ 488 per milliliter of blocking agent were used.

To label both platelets and fibrin using CAPP2A and the anti-fibrinogen antibody, the antibody labeling kits were used, which changed the labeling procedure. The primary antibodies were labeled with the secondary antibodies using the labeling kits according to the following protocol provided by Sigma Aldrich. In a microcentrifuge tube, the primary antibody is mixed with the 10x mix-n-stain reaction buffer at a ratio of 1:10 or 9 μL of antibody for every 1 μL of 10x reaction buffer. The entire solution in the microcentrifuge tube is then transferred to the vial containing the CF dye, and the vial is mixed for a few seconds. Following incubation of the vial in the dark for 30 minutes, the solution is now ready to be used as a fluorescently labeled primary antibody.

After fixing samples in PFA for 1 hour and rinsing with PBS, the samples were placed in a solution containing 10 μL of the mix-n-stain labeled CAPP2A and 10 μL of the mix-n-stain labeled anti-fibrinogen for every milliliter of 6% goat serum. The samples were incubated overnight at 4°C and then rinsed with PBS to remove any unbound primary antibody. The samples were imaged using the 488-nm and 543-nm lasers on an Olympus Fluoview 1000 confocal microscope (Olympus America Inc., Center Valley, Pennsylvania) at the Huck Institute of the Life Sciences. A 10x dry objective (Olympus America Inc., Center Valley, Pennsylvania) was used to focus onto the sample and to identify regions of interest. Then, higher magnification images were captured using both a 60x oil objective (Olympus America Inc., Center Valley,

Pennsylvania) and a 100x dry objective (Olympus America Inc., Center Valley, Pennsylvania).

3.6 Environmental Scanning Electron Microscopy

ESEM was used because the samples did not have to be sputter coated, thus the true surface of the samples can be viewed. Samples were mounted onto aluminum SEM stubs with carbon tape as shown in Figure 3-8 before being imaged with a Quanta 200 Environmental SEM (FEI, Hillsboro, Oregon) in the Materials Characterization Lab of the Materials Research Institute. The images were captured using the low vacuum mode at a pressure of 30 Pa to dissipate the charge of the uncoated samples, and an accelerating voltage of 20 kV was used. The images were first captured at 100x, and additional images were taken at higher magnifications as needed to examine specific features.
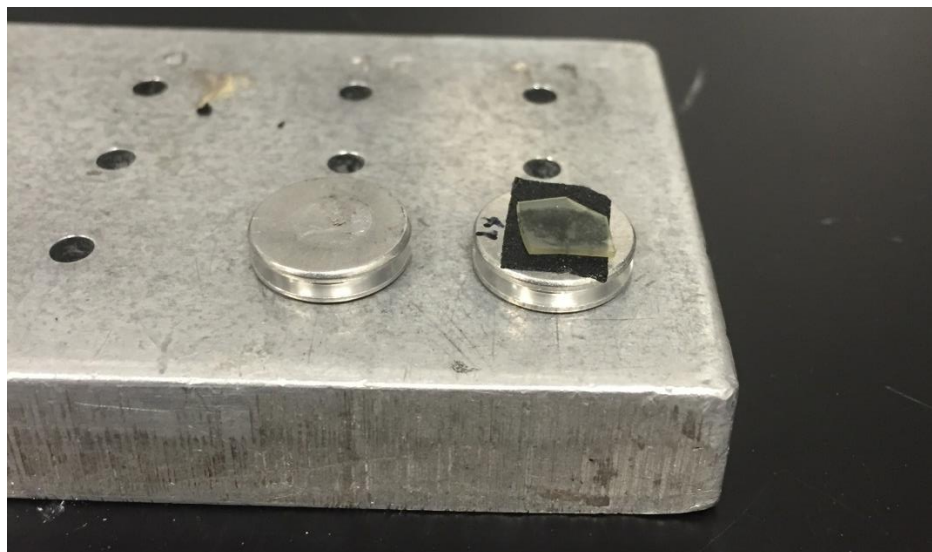
Figure 3-8. Aluminum SEM stubs with and without sac samples mounted by carbon tape.

Because the true surface is being exposed to the accelerating voltage, it is possible that the polymer surface could be affected in some way. In order to test this, three samples were taken from an unused sac and mounted onto a microscope slide for analysis with optical profilometry as described below to gather baseline data. The samples were then mounted onto SEM stubs and exposed to the accelerating voltage for several seconds at the locations where optical profilometry data was taken. The samples were then again imaged with optical profilometry data, and the before and after data were compared to determine if the accelerating voltage is altering the surface. For the comparison, a paired t-test ($\alpha=0.05$) was used to determine statistical significance.

3.7 Optical Profilometry

Optical profilometry was used to obtain quantitative data to describe the surface roughness of the samples. Samples approximately 0.5 cm^2 in size were taken from unused sacs using a sterilized scalpel, and then fixed to a microscope slide using either carbon tape or double-sided poster tape. Surface data was obtained using the Zygo NewView 7300 optical profilometer (Zygo Corporation, Middlefield, Connecticut) in the Materials Characterization Lab of the Materials Research Institute. The 50x objective and 0.5 zoom lens (Zygo Corporation, Middlefield, Connecticut) were used to image the surface. The data was obtained using the CSI measure mode and a high z resolution. Data were taken at random spots on the sample using a scanning length of 40 microns. If a large number of data points were missing due to the curvature of the sample resulting in

data points following outside of the scanning length, then a scanning length of 65 microns was used.

The data were processed using a developed application with the MetroPro® 8.3.5 software (Zygo Corporation, Middlefield, Connecticut) that provides continuity between the scaling of the surface profile plots. An example of the MetroPro® interface is given in Figure 3-9. This application uses the 4-th order remove function, which removes a best fit, 4-th order polynomial to remove the overall shape of the sac surface to focus on the surface roughness during the analysis. From the software, the R_a, rms, R_z and H values were obtained and recorded in a Microsoft Excel spreadsheet (Microsoft Corporation, Redmond, Washington).
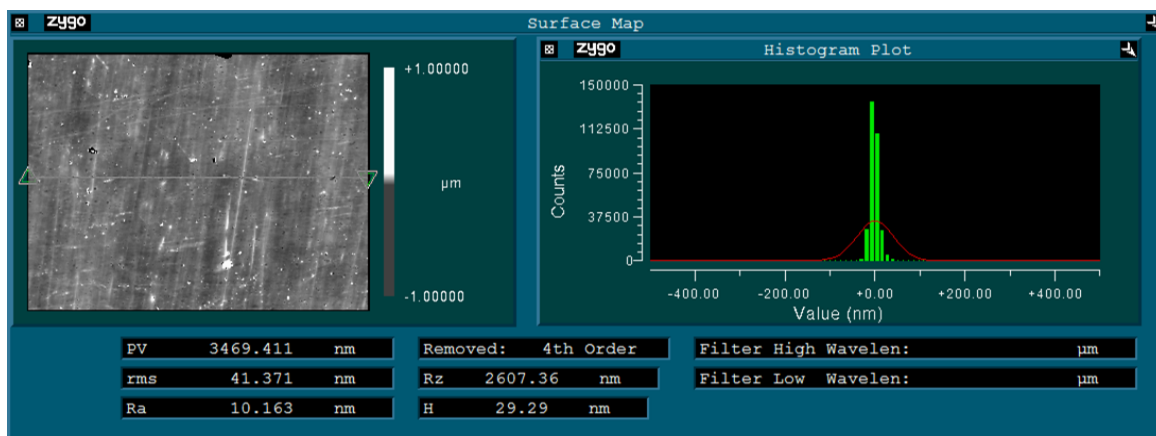
Figure 3-9: A representative image of the MetroPro interface.

3.8 Degradation of Biological Depositions

To determine if surface roughness played a role in thrombosis, optical profilometry data needed to be obtained for the samples. The roughness of just the surface and not the surface combined with the deposition needs to be characterized to

provide the most meaningful data, so the biological deposition will need to be degraded from the surface of the blood sac without affecting the surface of the sac in any way. Pepsin (Sigma-Aldrich, St. Louis, Missouri) was identified as an enzyme that would be capable of degrading any biological deposition, but its effect on the SPEUU sac surface was unknown[51].

To determine if both platelets and fibrin are indeed being degraded from the surface without altering the surface in any way, 15 samples approximately 0.5 cm by 0.3 cm were taken from an unused blood sac. When sectioning the sample, the upper right-hand corner was removed to serve as a landmark to correlate imaging as illustrated in Figure 3-10. Because the sac samples are unused, they had never been through the fixing protocol that is used after the sacs are explanted. To account for any affects this fixing protocol might have on the surface, the samples were placed in PFA for 1 hour and then rinsed with PBS before being placed on glass microscope slides with double sided tape to be imaged. These samples were imaged with optical profilometry according to the procedure given previously with measurements taken at 6 spots starting in the upper right-hand corner of each sample to obtain reference data of the surface roughness. Figure 3-10 shows the 6 spots where the optical profilometry was obtained.
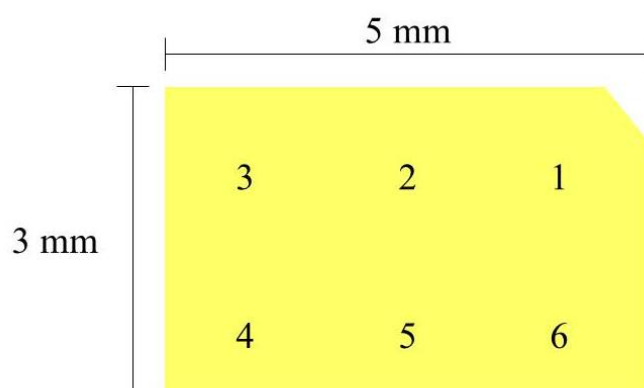
Figure 3-10: Sac sample diagram and the 6 spots where optical profilometry data was obtained.

These samples were then exposed to varying concentrations of pepsin to test if the pepsin had an effect on the polymer surface. The pepsin needed to be placed in an environment that activated the pepsin. Because pepsin normally functions in the stomach, a temperature similar to body temp (37°C) and similar acidic conditions (pH=1) were required. The acidic conditions were created by combining the pepsin solution with hydrochloric acid (HCl). However, the exposure time and concentration of the pepsin solution needed to completely degrade the deposition was unknown, so each of the different times and concentrations shown in Table 3-2 were tested on 3 samples. Following incubation at 37°C for the specified time, the samples were rinsed 3 times with PBS.

Table 3-2. The different conditions used to test the pepsin degradation.

Condition	Amount of pepsin in DI water	Amount of 1 M HCl	Incubation time
1	1 mL	1 mL	2 hours
2	1.5 mL	0.5 mL	2 hours
3	1.67 mL	0.33 mL	2 hours
4	1.5 mL	0.5 mL	3 hours
5	1.67 mL	0.33 mL	3 hours

Then, the samples were imaged with optical profilometry in the same regions of each sample to obtain surface data. The optical profilometry data from before and after the pepsin degradation were compared using a paired t-test ($\alpha=0.05$) to determine if the pepsin is altering the surface in a significant manner.

The next step was to determine the best concentration of pepsin and exposure time for degradation of the biological deposits by degrading clots created on polyurethane urea using the backward facing step model during two separate runs. The same procedure for the backward facing step model that was used in Section 3.3 to create controls was used but strips about 3 cm by 1 cm of PUU were taped down at the base of the step as shown in Figure 3-11 so that the clot was created on the polymer. The strips of PUU were then removed, and any large clot was scraped from the surface of the polymer. The two strips were then sectioned into 0.5 cm by 1 cm samples, so 6 samples were obtained from each run of the model. These samples were then mounted to SEM stubs and imaged using the ESEM at 100x at 6 regions of the sac in a similar manner as described for imaging with optical profilometry.
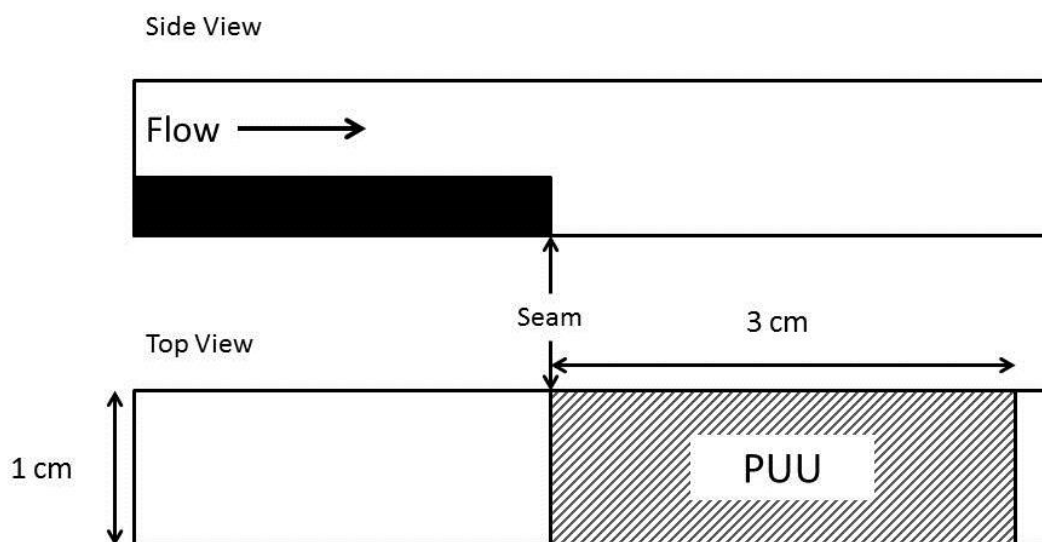
Figure 3-11. Diagram of how PUU was taped down at the base of backward facing step.

The samples mounted onto the SEM stubs were then exposed to varying pepsin conditions to determine the best concentration and exposure time. All of the samples were incubated at 37°C. The samples from the first run were incubated for 2 hours, with three of the samples in 2 mL of 1:1 pepsin to HCl and the other three samples in 2 mL of 3:1 pepsin to HCl. The samples from the second run were incubated for 3 hours, with three of the samples in 2 mL of 1:1 pepsin to HCl and the other three samples in 2 mL of 3:1 pepsin to HCl. Following the incubation, the samples were gently rinsed with PBS three times and imaged with ESEM. To correlate the imaging, the same regions or features were observed to provide comparison from before and after the pepsin degradation.

3.9 Protocol Development

Upon identification of antibodies for immunofluorescent labeling and a method for degrading biological depositions from the sac surface, a protocol was developed that allows all three microscopy techniques to be used on the same samples taken from the explanted sacs of the animal trials. To allow for correlation between images obtained using the different microscopy techniques, the field of view for each technique was determined using the measure feature of ImageJ (National Institutes of Health, Bethesda, Maryland) where the length of the scale bar in pixels was determined by tracing the provided scale bars from the images and then selecting the measure feature. With this known length of the scale bar, the "set scale" function was used to set the scale of the image in microns. With this scale, the length of the image in the x and y direction was measured using a line that traced the outer edge of the image. The field of view was used to decide upon the magnification that should be used for each sample along with the size of each sample. The number of images that should be obtained from each image was also determined using the field of view measurements. In addition to mapping how to obtain the images, observations made during each technique were used to optimize the protocol for using all three microscopy techniques.

Chapter 4

Results and Discussions

4.1 Surface Irregularities

The purpose behind developing the protocol to analyze the sac surface is to determine if there are surface irregularities present that could play a role in thrombus formation. The surface irregularities present in the sacs first needed to be identified to determine whether or not the visible irregularities are at the surface and not in the bulk material. Samples of sacs that were not implanted and were classified as rough because they contained visible irregularities when viewed with a 40x microscope are shown below in Figure 4-1. These irregularities have been classified as scuffs that arise during the fabrication process as a result of the stretching of the sac to remove it from the steel mandrel. While this process is carried out with great care, the irregularities are seen in many sacs, which lead to rejection of the sac from use in the animal trials. Compared to the rough samples, Figure 4-2 shows a representative image of a "smooth" sac. In all of the images, dark circles can be seen in the background; however, the circles are not a surface irregularity but instead just the background that was used to view the samples in order to provide sufficient contrast to view the clear samples.
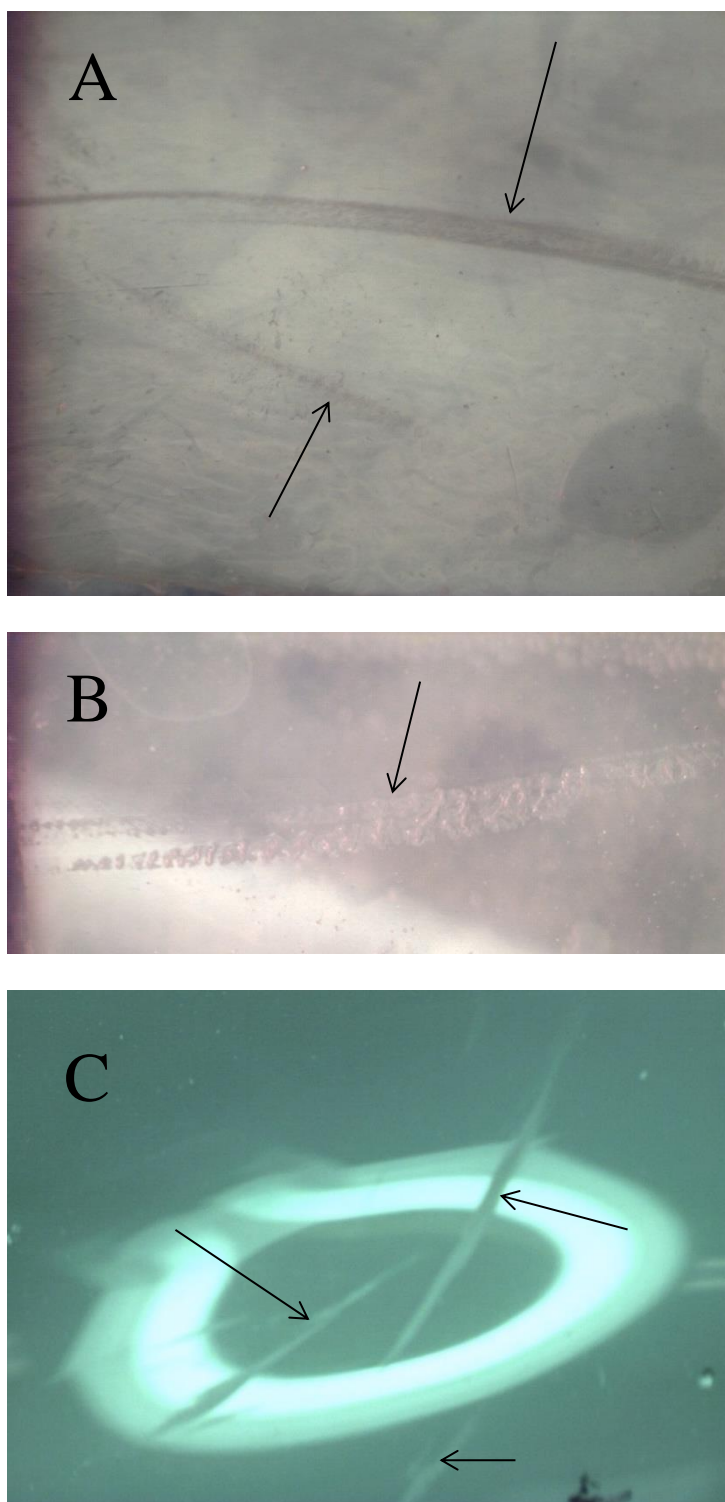
Figure 4-1. Representative images of surface irregularities are shown in (A), (B), and (C). All of the irregularities, or scuffs, are identified with an arrow.

Figure 4-2. Representative image of a "smooth" sac sample or a sample containing no visible irregularities when imaged at a magnification of 40x.

Figure 4-1B appears to contain a surface irregularity that is on the surface of the sac sample, but it is difficult to determine if the irregularities in Figure 4-1A and 4-1C are indeed on the surface and not in the bulk material. To better determine if the irregularities are on the surface, the samples were analyzed with optical profilometry to obtain quantitative data of surface roughness that could be compared between the "smooth" and the rough surfaces.

The optical profilometry data for 15 smooth samples and 4 different rough samples was obtained and analyzed in MetroPro. Despite the samples being mounted onto microscope slides in a clean room, dust particles appeared to be present on the surface of a few of the samples. These dust particles had a large effect on all of the values but especially the rms value because this value is sensitive to peaks. To try and limit the effect of dust particles and other debris that is not truly part of the surface profile

but is just noise, MetroPro has a mask feature that can be used to exclude certain regions of the data in the analysis. The mask feature was used, when necessary, to best reflect the true surface profile. For example, Figure 4-3 shows the MetroPro data for a "smooth" surface that does not contain any masking. As the circle in the upper left hand corner of the image shows, there is a region that is all black. The surface profile in the bottom left shows a major drop in the height of the sample and an area where no data was collected. The surface roughness values are summarized in Table 4-1.
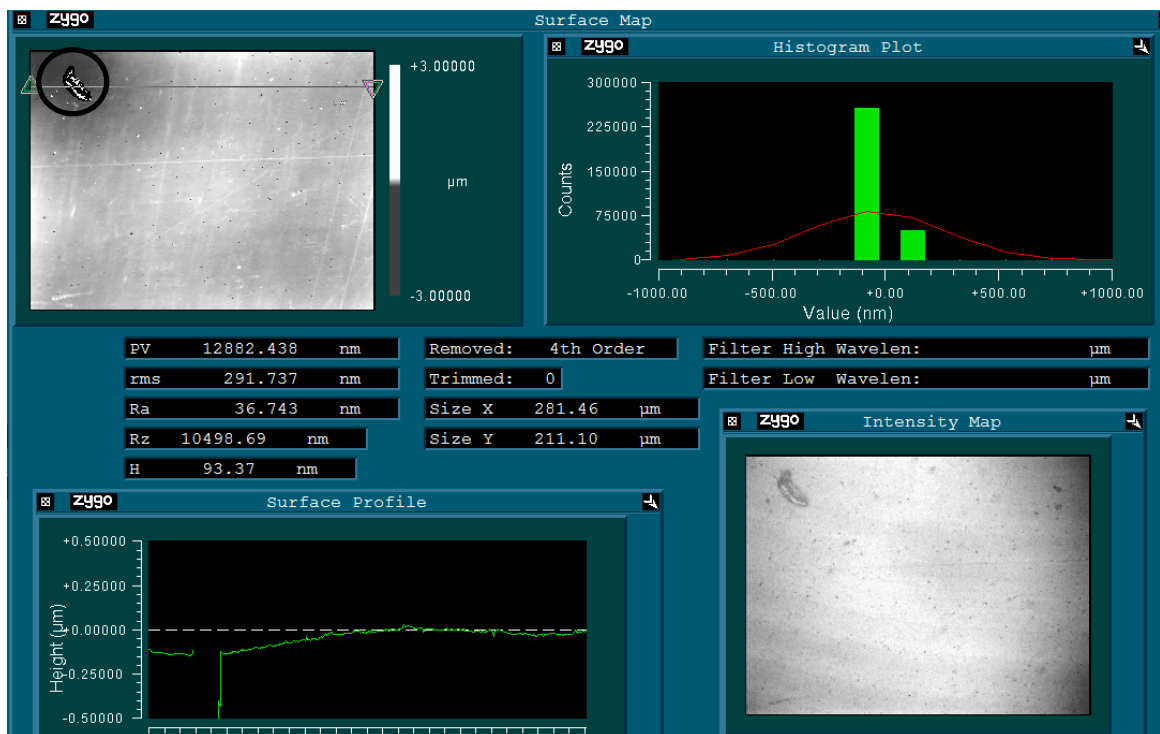

Figure 4-3. MetroPro output for a "smooth" sample that contains debris that has a major effect on the data. The debris is circled in the upper right-hand corner.

Figure 4-4 shows the MetroPro output if a mask is applied to the region circled in Figure 4-3 to exclude the foreign particle. With that region of data removed, the new surface roughness values are provided in Table 4-1.
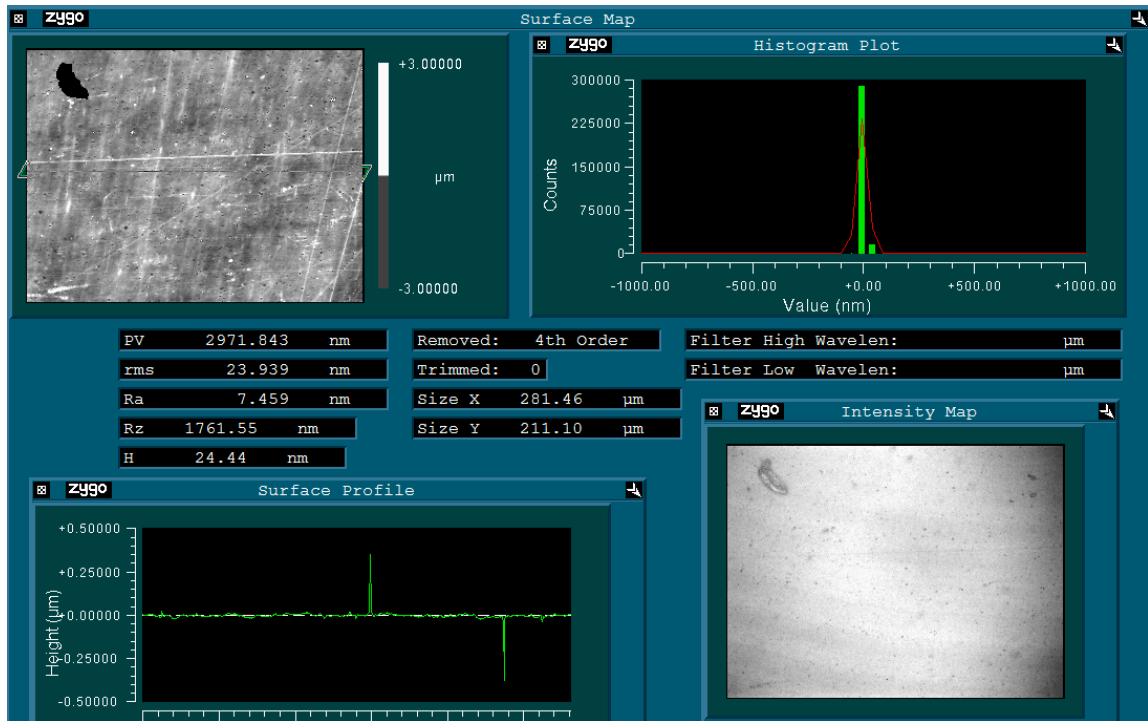
Figure 4-4. MetroPro output for the same "smooth" sample in Figure 4-3 that contains debris. For this output, a mask was used to exclude the debris for the data analysis.

Table 4-1. Surface roughness values for the same sample with and without including debris in the analysis. The without mask sample includes the debris, while the with mask sample does not include the debris.

Sample	RMS (nm)	Ra (nm)	Rz (nm)	H (nm)
Without Mask	291.737	36.743	10498.69	93.37
With Mask	23.939	7.459	1761.55	24.44

This table clearly shows that all four of the surface roughness values decrease as a result of the debris. As expected, the debris appears to have the smallest effect on the Swedish Height because the height values of the debris would fall outside of middle 90% of the data. For this reason, the Swedish height is used in all of the analyses to compare surface roughness as it is least affected by the unavoidable debris that is not a part of the

surface profile. The rms and Rz values on the other hand are very sensitive to the debris, as shown by the decrease in the values by a magnitude as a result of including the mask. Because the Rz is a measure of the peaks and valleys and the rms is more sensitive to peaks, the major decrease in the values is expected. These results show the importance of analyzing the true surface when comparing samples, as one small piece of debris can have a major effect on the outputted surface roughness data. Going forward in the MetroPro analysis, masks were used when necessary to remove any debris from the surface and to ensure that the true surface was being analyzed.

Representative MetroPro output for a "smooth" sample is provided in Figure 4-5, and representative output for a rough sample is provided in Figure 4-6. The plot in the upper left-hand region of the image is a surface topography plot. The line between the two triangles is used to determine where to obtain the surface profile that is provided in the lower left-hand corner of the image. Comparison of the smooth and the rough sample surface topography plots shows many differences, which can also be seen in the surface profiles. The "smooth" sample appears to be very smooth beyond a few pits and scratches, and the surface profile contains no major peaks or valleys suggesting that the pits and scratches are not major changes in the topography. However, the rough sample clearly has a wavy nature to the surface, which is shown in the surface profile by random peaks and valleys.
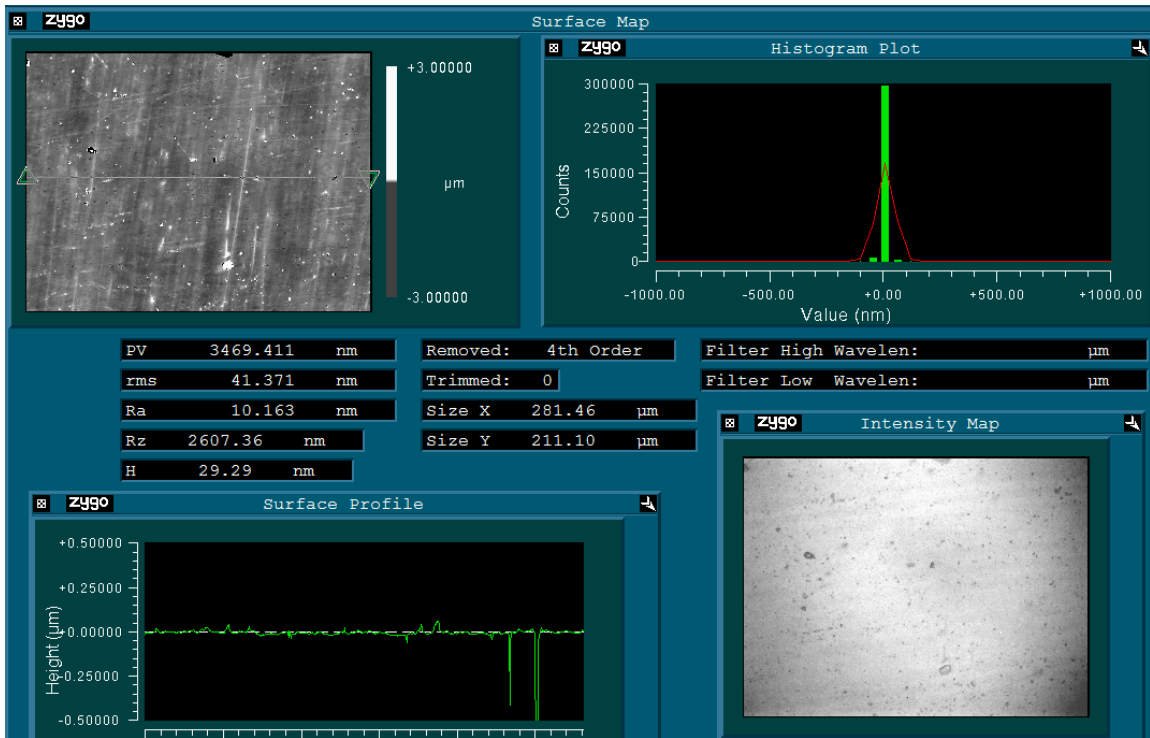
Figure 4-5. Representative MetroPro output for a "smooth" sample.
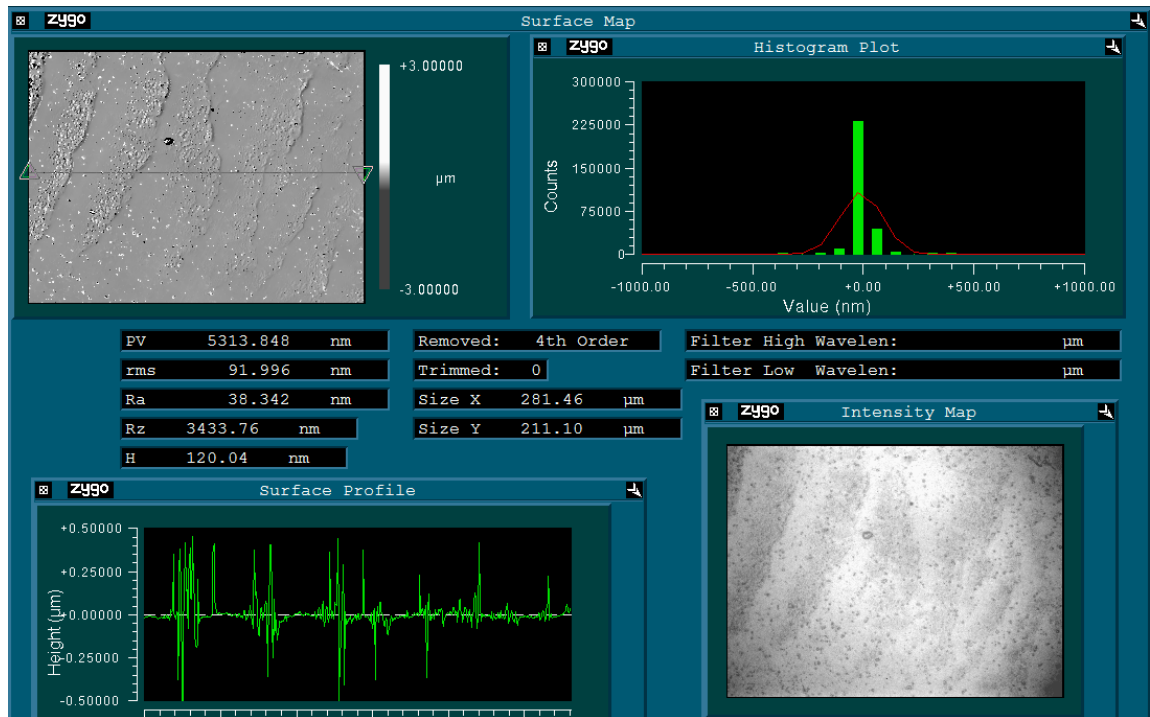
Figure 4-6. Representative MetroPro output for a rough sample.

The optical profilometry data was analyzed for both the "smooth" and the rough samples, and the results were compared. Figures 4-7 through 4-10 show the comparison between the average of the rms, Ra, Rz, and H for the smooth and rough samples.
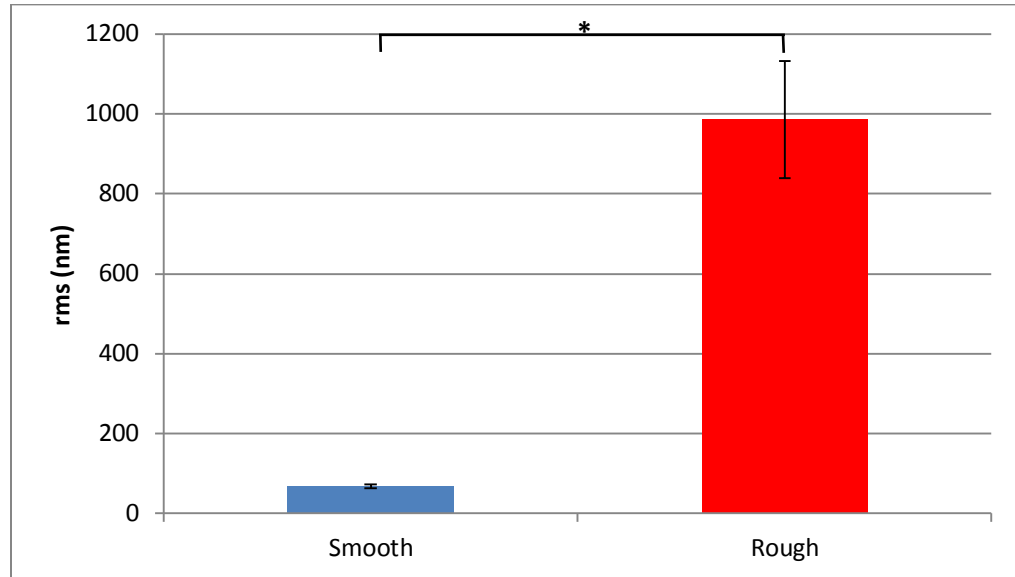
Figure 4-7. Smooth vs rough comparison of the average rms.
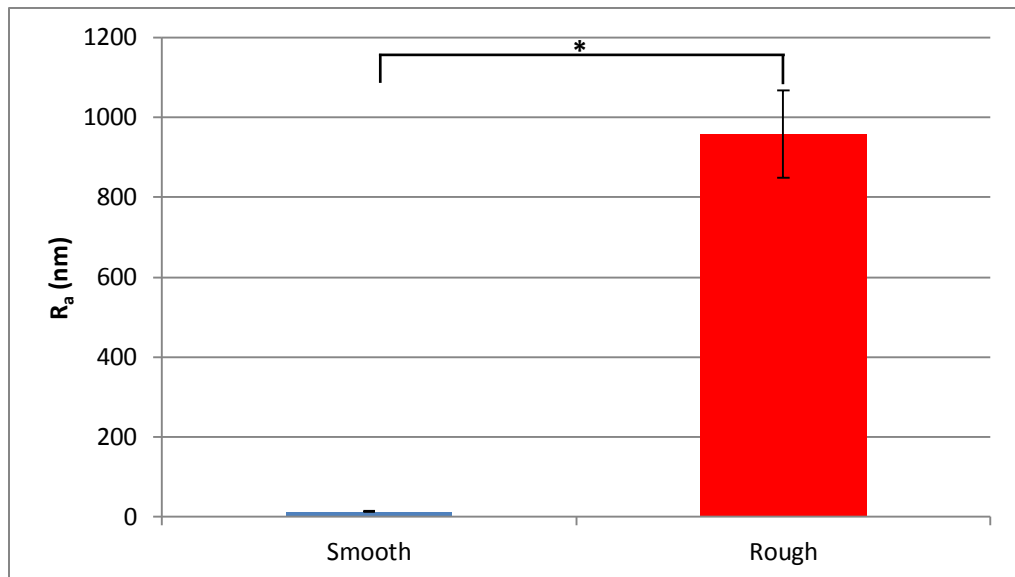
Figure 4-8. Smooth vs rough comparison of the average Ra.
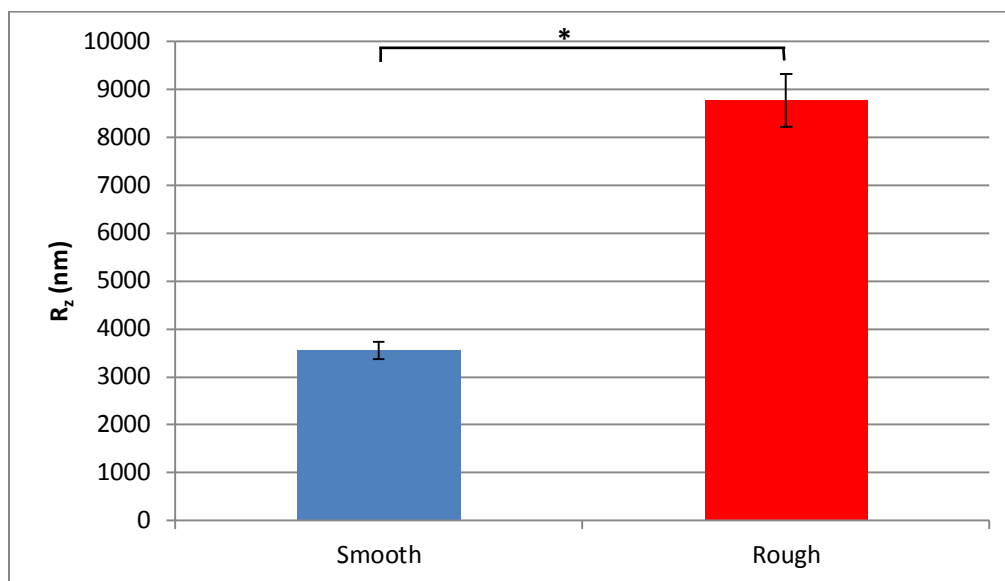
Figure 4-9. Smooth vs rough comparison of the average Rz.
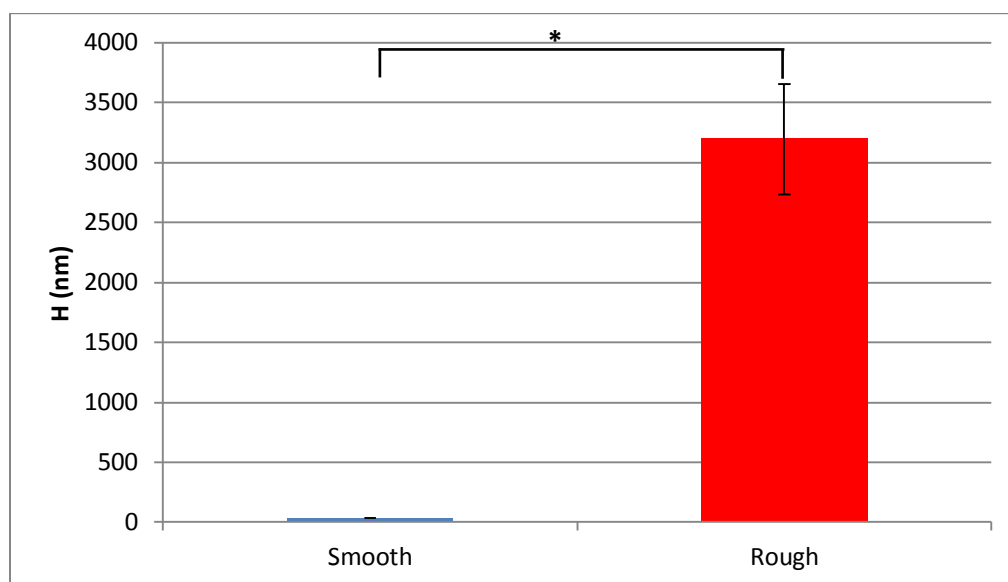
Figure 4-10. Smooth vs rough comparison of the average Swedish Height (H).

For each surface roughness parameter, the smooth and rough samples are significantly different showing that the visible irregularities were indeed occurring at the surface of the samples and not in the bulk material. Smooth and rough samples were also viewed with ESEM to determine if any microscopic features are present at the surface.

The smooth samples do include microscopic surface features as shown by the scratches in Figure 4-11 and the pits in Figure 4-12. These scratch marks are similar to what was seen in the MetroPro data in Figure 4-5 and are the result of the steel mandrel, which contains scratches from the polishing process. The rough sample that had the scuffs on the surface is shown in Figure 4-13.
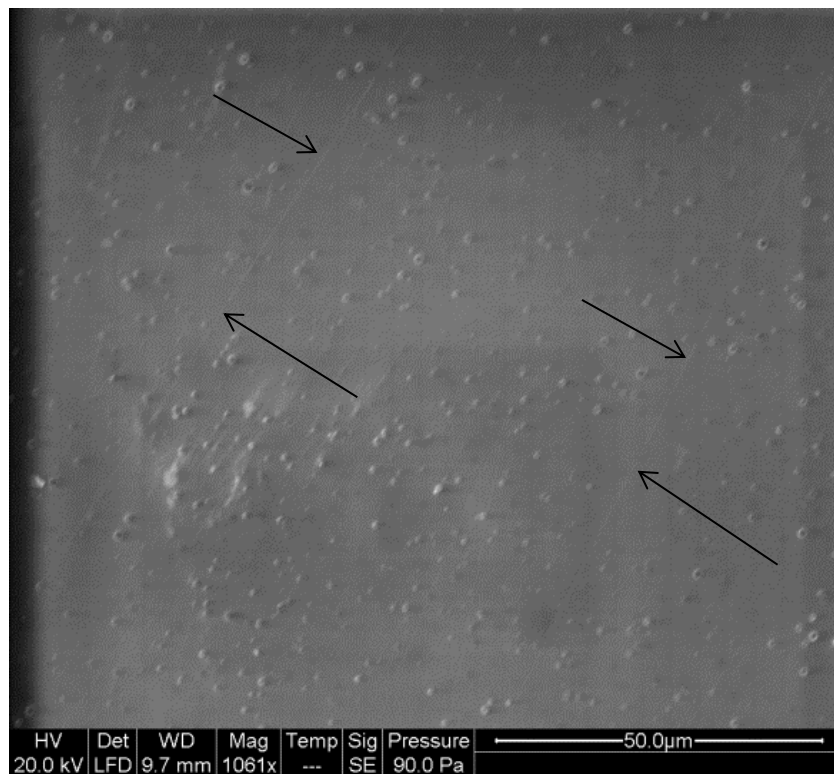
Figure 4-11. ESEM image of a smooth sac sample that has scratch marks as shown by the arrows.

Figure 4-12. ESEM of a smooth sac sample that contains pits in the surface.
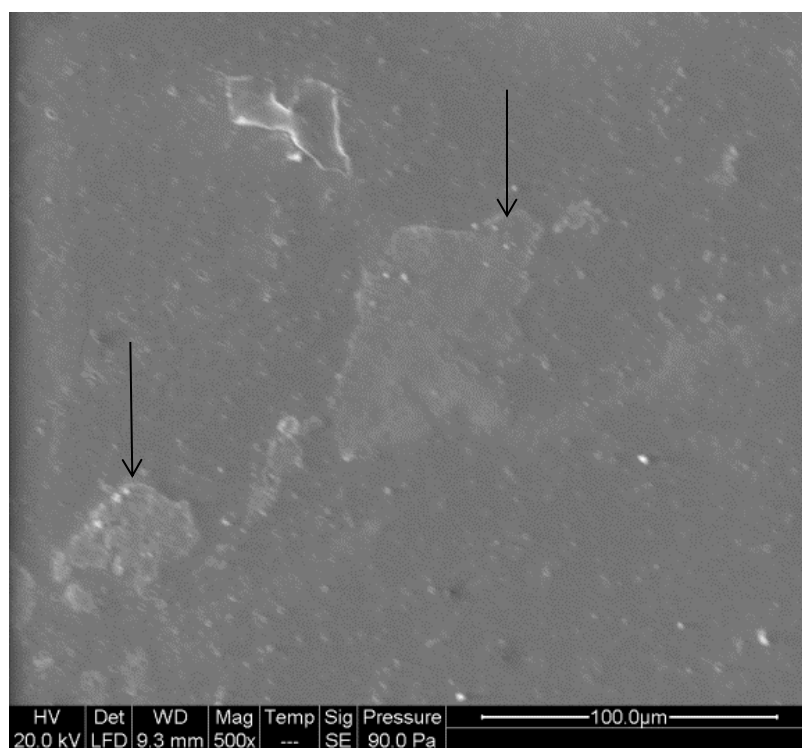
Figure 4-13. ESEM of a rough sample with arrows showing the scuff.

4.2 Confocal Microscopy

Confocal microscopy is used along with indirect immunofluorescence to identify both platelets and fibrin because they are the two major components of a thrombus. Polyurethane can be difficult to fluorescently image because it autofluoresces when excited by the lasers. For this reason, confocal microscopy is used as it reduces the effect of the autofluorescence by creating a 2-D image of maximu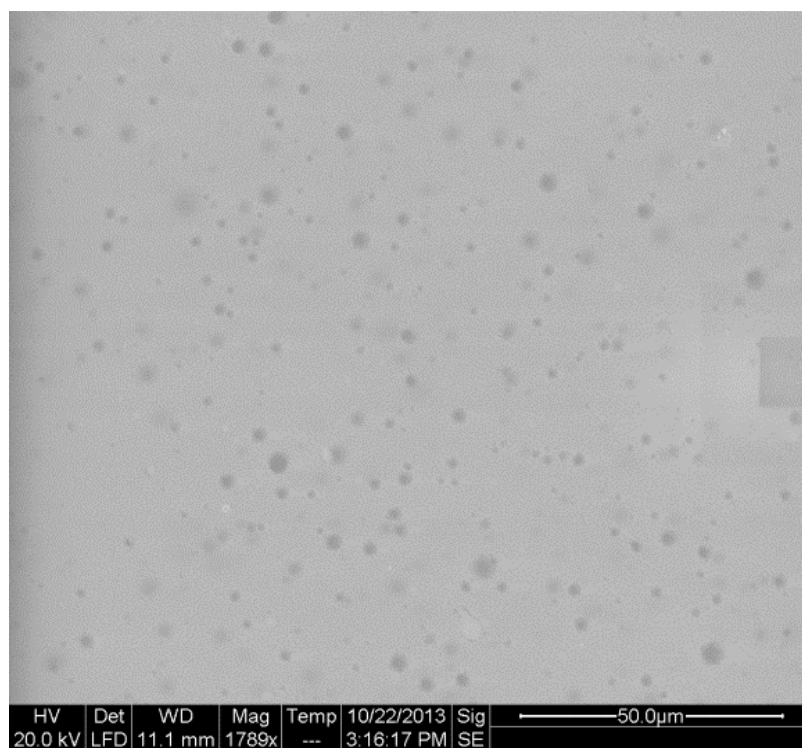m pixel intensities for each location from a stack of images where only the z-position is changed. The stack of images allows for the platelets and fibrin to be observed because the fluorescent signal transmitted at the pixels where they are located is stronger compared to the autofluorescence for multiple slices within the stack.

Despite only one fibrin antibody being identified, it was still tested using purchased fibrinogen plated onto a microscope slide and shaved clots from the backward facing step model. Figure 4-14 shows a representative image from the purchased fibrinogen. While the desired structure to be labeled is fibrin, the antibody labels an epitope present on both fibrin and fibrinogen allowing fibrinogen to be used as control. A backward facing step model was also used to create clots that would contain fibrin, but the presence of fibrin in the clots was not guaranteed in a similar manner as the plated fibrinogen. Figure 4-15 shows a representative image from the backward facing step model clot. Fibrin is being labeled green in the representative images, and the intensity of the fluorescence in contrast to the background provides strong assurance that fibrin is being labeled. In these images the fibrin appears as microclots about 2-4 microns in

sized. While not seen in either of these representative images, fibrin can also appear in a
web-like structure.
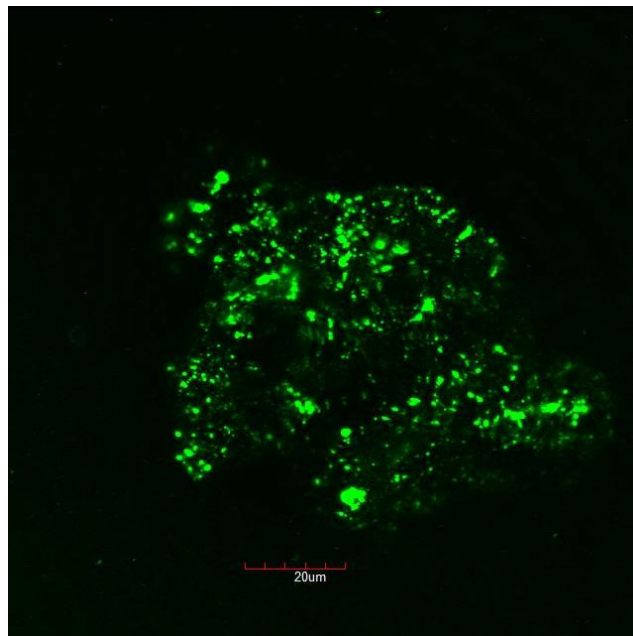
Figure 4-14. Representative confocal image of the plated fibrinogen control.
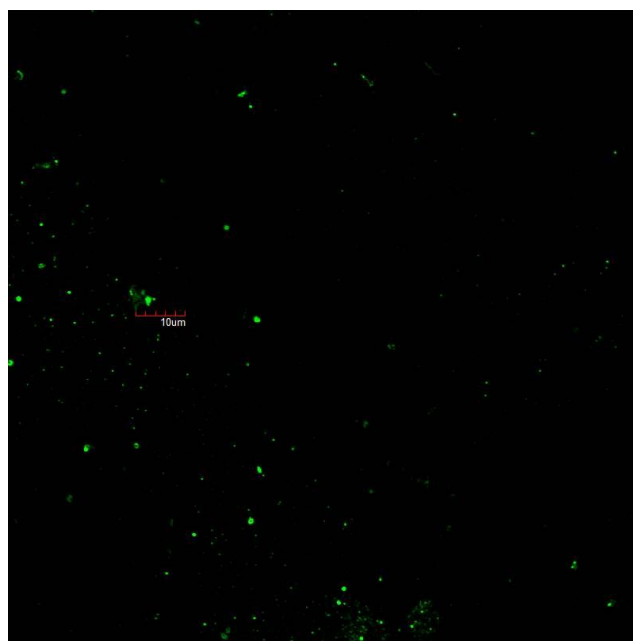
**Figure 4-15. Representative confocal image of fibrinogen from a clot produced in
the backward facing step model.**

Two different platelet antibodies were identified and tested with *in vitro* controls. A representative image of a PRP clot labeled with the anti-phospho-ITGB3 antibody is shown in Figure 4-16 where the red fluorescence is the platelets. The fluorescence is on the order of 1 to 3 microns, which is the typical size of platelets. Again the intensity of the fluorescence in contrast to the background provides a strong assurance that platelets are being labeled. However, when clots from the backward facing step model or samples from RDS were labeled with this antibody, no fluorescence could be found despite multiple attempts to refocus the microscope and adjust the laser intensity. The lack of fluorescence in the RDS was especially concerning as this is a very common method of activating platelets and therefore, surface adhesion. Past studies have showed that upwards of 500 platelets can be identified in one frame.
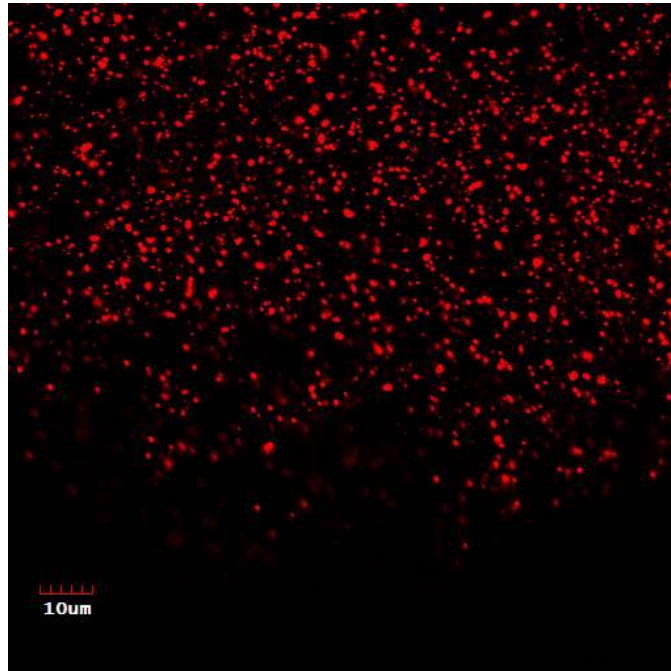
Figure 4-16. Representative image of platelets from a PRP clot labeled with anti-phospho-ITGB3.

The lack of fluorescence of platelets in samples generated using the backward facing step model or the RDS led to CAPP2A being tested. Platelets were labeled in both the backward facing step model as shown in Figure 4-17 and for the RDS as shown in Figure 4-18. For the backward facing step model, the individual platelets are best seen near the scale bar. The large regions of green fluorescence that are not in focus are platelet aggregates. The presence of fluorescence for both controls was a much more promising result than the anti-phospho-ITGB3, so the experiments continued on with CAPP2A as the antibody for labeling platelets.
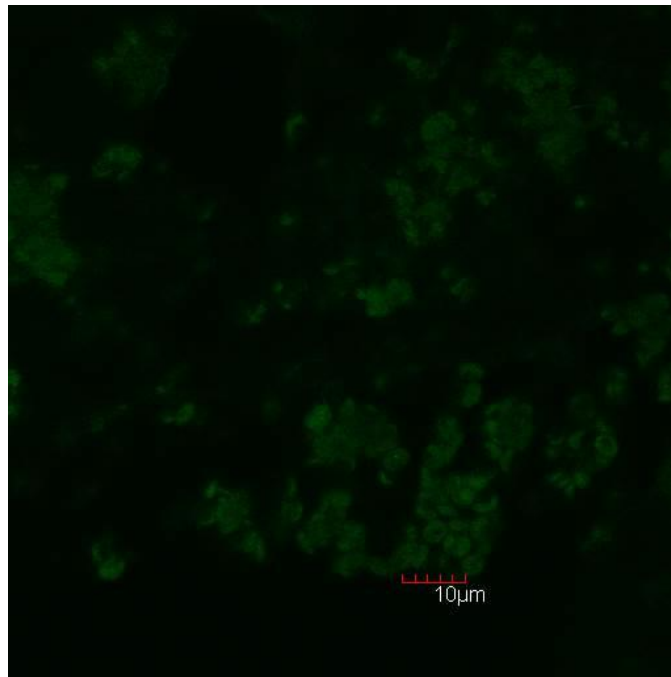
Figure 4-17. Representative image of platelets from a backward facing step clot labeled with CAPP2A.
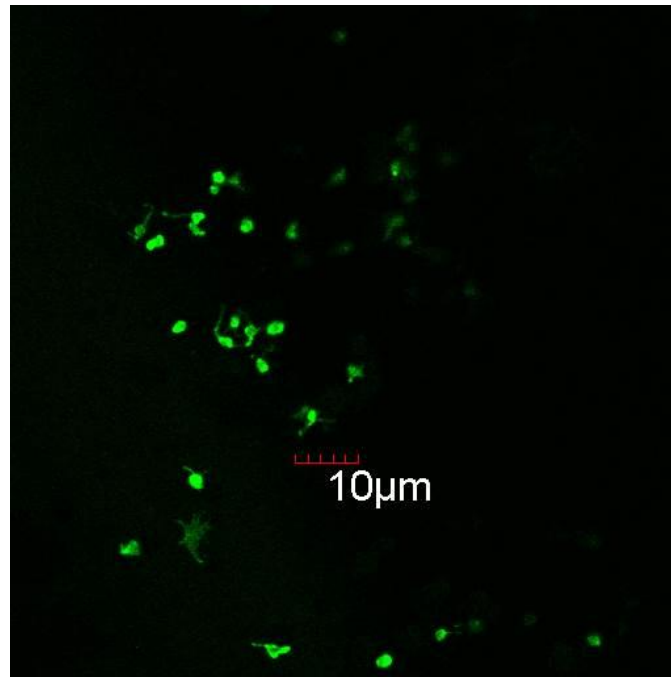
Figure 4-18. Representative image of platelets from RDS labeled with CAPP2A.

Both CAPP2A and the anti-fibrinogen antibody are mouse derived antibodies, so a secondary antibody would label both of the antibodies. As a result, multi-color imaging would not be possible to label the platelets one color and fibrin another with secondary antibodies. This is an important requirement for the protocol as fibrin and platelets have been found to be located at different regions of the sac, so being able to differentiate between the two is a necessity. Antibody labeling kits were identified as a possible method for allowing multi-color imaging because the kits label the primary antibody before the primary antibody label is applied to the samples. The use of both CAPP2A and the anti-fibrinogen antibody simultaneously using antibody labeling kits was tested using sac samples from an explanted sac. Representative images are shown in Figures 4-19 and 4-20 where the platelets are labeled green and the fibrin is red. These images show that the multi-color imaging is possible through the use of the antibody labeling kit.
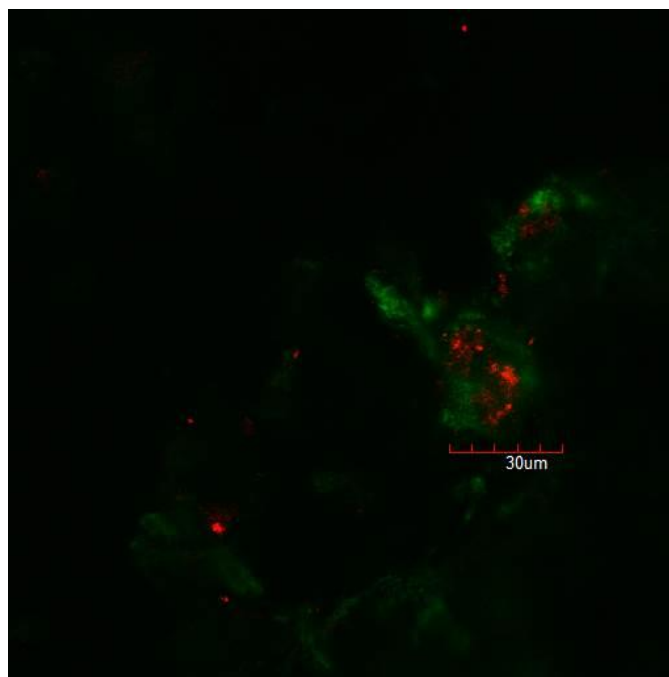
Figure 4-19. Representative image of an explanted sac. Platelets are labeled green and fibrin is labeled red.
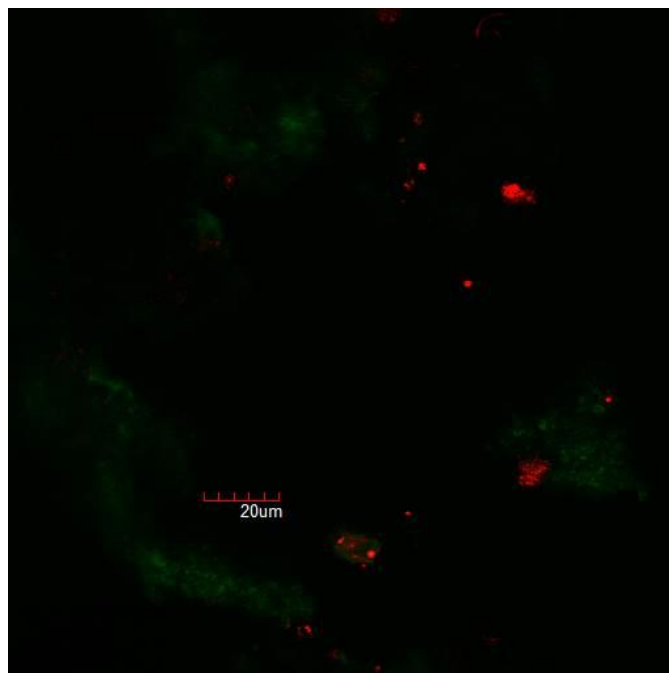
Figure 4-20. Representative confocal image of an explanted sac. Platelets are labeled green and fibrin is labeled red.

Despite controls being used that were expected to have either platelets or fibrinogen, it is inherently difficult to focus the microscope in the correct region and on the correct plane. Because controls are being used no fluorescence implies that either the microscope is out of focus or the antibody is not labeling the desired structure. In the case of no fluorescence such as with the anti-phospho-ITCB3 antibody labeling the RDS controls, the laser intensity is increased to bring any structure present into focus. However, increasing the intensity runs the risk of structures that are neither platelets nor fibrin become visible as a result of autofluorescence.

A labeling protocol to label ovine platelets and fibrin had not been previously established by the lab group because an ovine model had never been used before because previous studies had been carried out using a bovine model. No labeling could be found in the literature due to antibodies for an ovine model being not as commonly used as the bovine model. Only the one antibody was identified to label fibrin, mouse anti-fibrinogen, and two antibodies, CAPP2A and anti-phospho-ITGB3 were identified to label platelets. Since there was no proof in the literature of any of these antibodies being used for fluorescently labeling platelets and fibrin, the antibodies needed to be tested to confirm that the structures are being properly labeled and that platelets and fibrin could be simultaneously imaged.

4.3 Environmental Scanning Electron Microscopy

While confocal microscopy was used to identify platelets or fibrin on the sac surface, ESEM was used to confirm the structures and to provide insight into the surface

topography. Because ESEM allows the true surface of the sample to be imaged without the need to sputter coat the samples, the same samples were able to be examined with both ESEM and confocal providing a useful comparison for the confirmation of the structures found on the surface and what the surface topography is at the location of the deposition. ESEM is easier to bring the samples into focus when compared to confocal microscopy, but the difficulty lies in the ability to achieve optimal contrast. For the polymer samples it is especially difficult to achieve optimal contrast because the samples are not conductive and have the potential to show charging depending on the accelerating voltage used.

To test the effect of viewing the uncoated surface, sac samples that had never been implanted were imaged with ESEM. As Figure 4-21 shows, sufficient contrast to view structures on the surface while still being able to recognize any surface features is possible to obtain. The structure in Figure 4-21 is just debris, as the sample had never been implanted, but it showed the achieving contrast is possible.
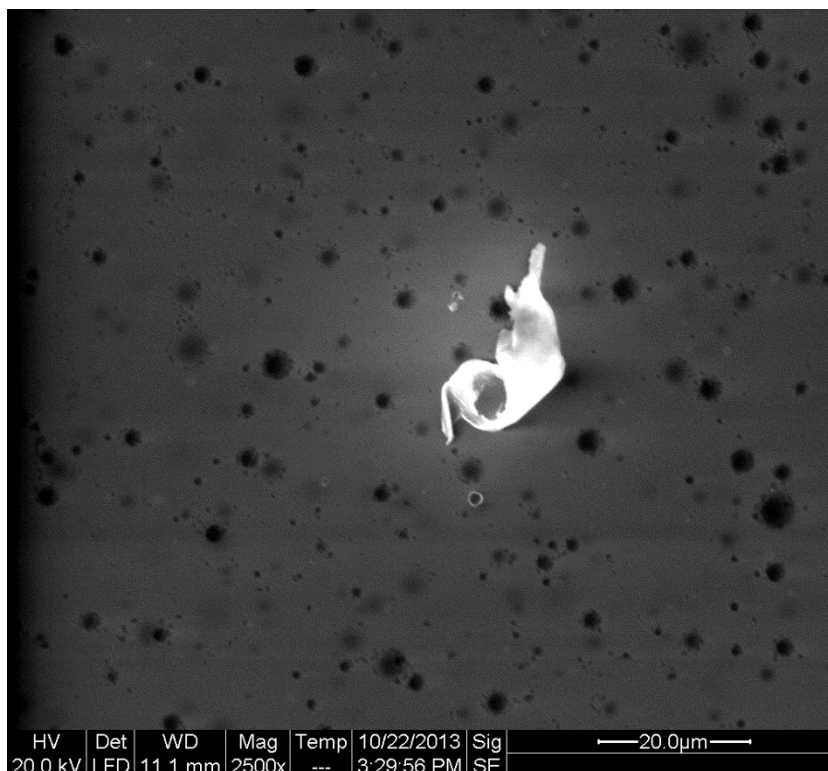
Figure 4-21. ESEM image of uncoated polymer surface with some debris. The debris showed that it is possible to obtain images with sufficient contrast.

After obtaining a high magnification image such as the one shown in Figure 4-21, and then returning to a lower magnification, the location where the high magnification image was obtained is visible on the sac surface. This darker square region is shown in Figure 4-22 and is the result of beam damage to the polymer surface from the accelerating voltage. In order to test if this beam damage is altering the surface of the polymer samples in any way, optical profilometry was carried out on the same samples before and after ESEM, and the surface roughness data were compared.
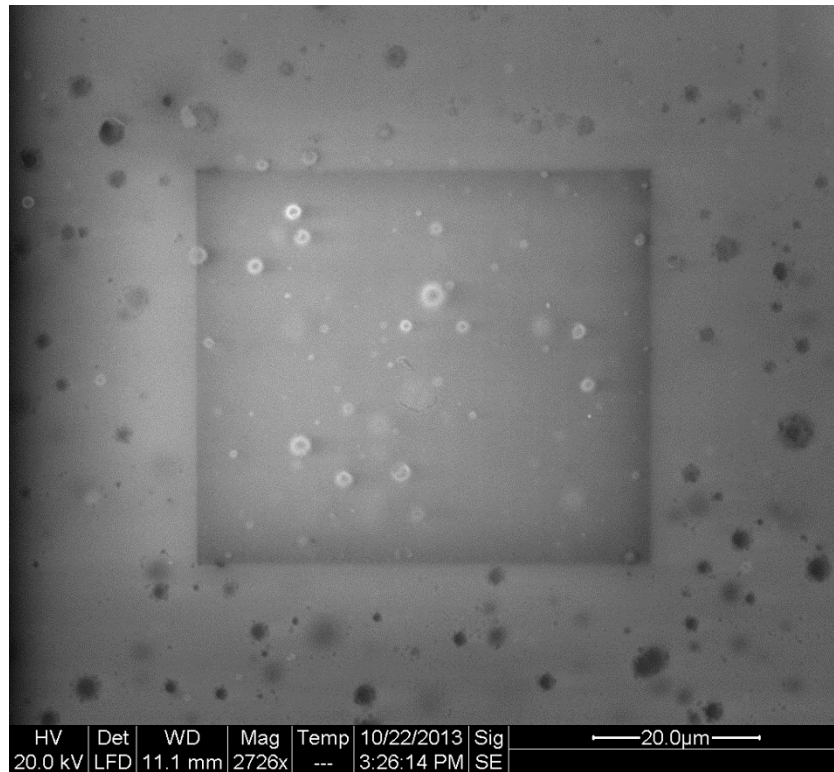
Figure 4-22. Beam damage on the polymer surface as the result of capturing a higher magnification image in the darker square region.

The optical profilometry data were analyzed for three different samples before and after being imaged with ESEM. For each sample, rms, Ra, Rz and H values were obtained at 6 different locations, and then each parameter was averaged. Figures 4-23 through 4-26 show the comparison between the average of the four different surface roughness parameters for the before and after data.
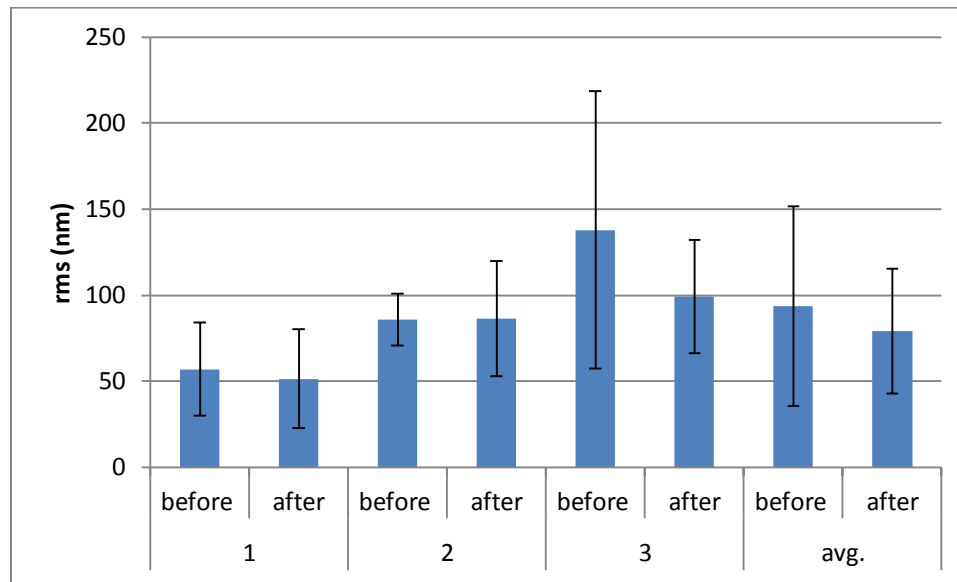
Figure 4-23. Before and after ESEM average rms values for 3 different samples and the average of the 3 samples.
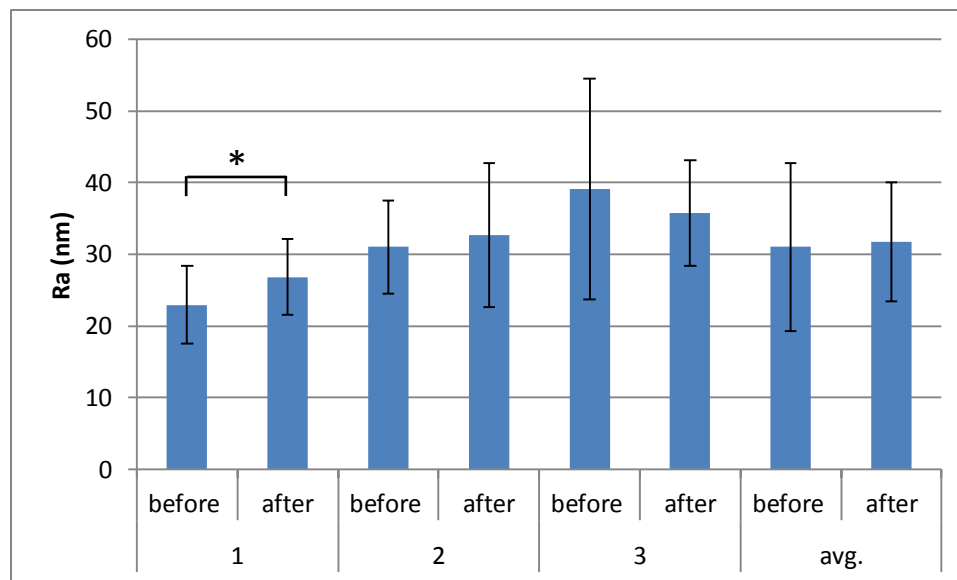
Figure 4-24. Before and after ESEM average Ra values for 3 different samples and the average of the 3 samples.
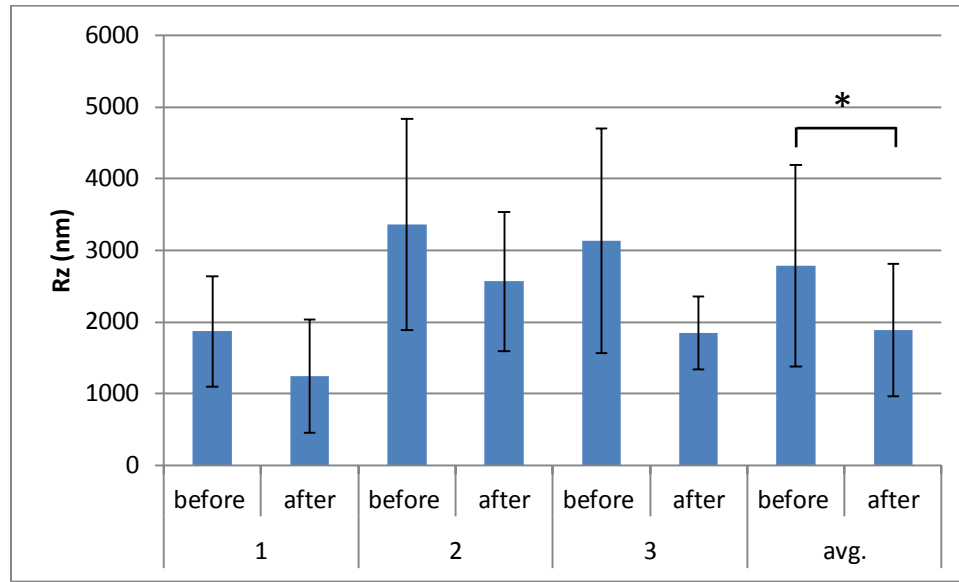
Figure 4-25. Before and after ESEM average Rz values for 3 different samples and the average of the 3 samples.
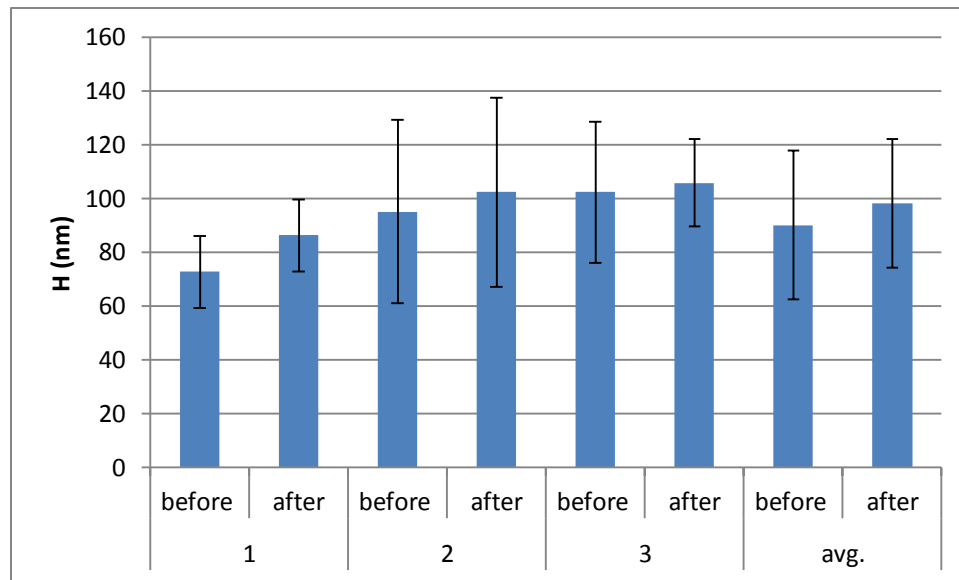
Figure 4-26. Before and after ESEM average H values for 3 different samples and the average of the 3 samples.

The only significant difference between any of the samples or the averages is sample 1 for Ra and the average of all three samples for Rz. For Ra, only sample 1 is significantly different, and neither the other two samples nor the overall average is

significantly different, so the significant difference is most likely the result of background noise affecting the data for sample 1. While for all three samples the Rz values decrease from the before and after, the only significant difference is seen in the overall averages. The evident decrease in the Rz can be attributed to the samples being rinsed with DI water to wash away any debris that may have been present on the surface. Closer observation and comparison of the before and after MetroPro outputs, provided in Figures 4-27 and 4-28 respectively, shows that there appears to be some minor changes in the surface. Comparing the surface profiles shows that the surface has more high frequency peaks and valleys. While the surface profile is from only one x-z plane, this pattern can be seen throughout the sample at multiple x-z planes. Comparing the histogram plots, the overall range of the height values is nearly identical for the before and after, which would explain why there is no significant difference between the averages. However, the after data has a more widespread distribution of height values, which can be seen by comparing the peaks of the plots. This further explains how the surface profile is wavier in Figure 4-28 when compared to the surface profile in Figure 4-27. Although the ESEM accelerating voltage may be altering the surface slightly, it can be considered noise as the variations are only on the order of 0.1 microns.
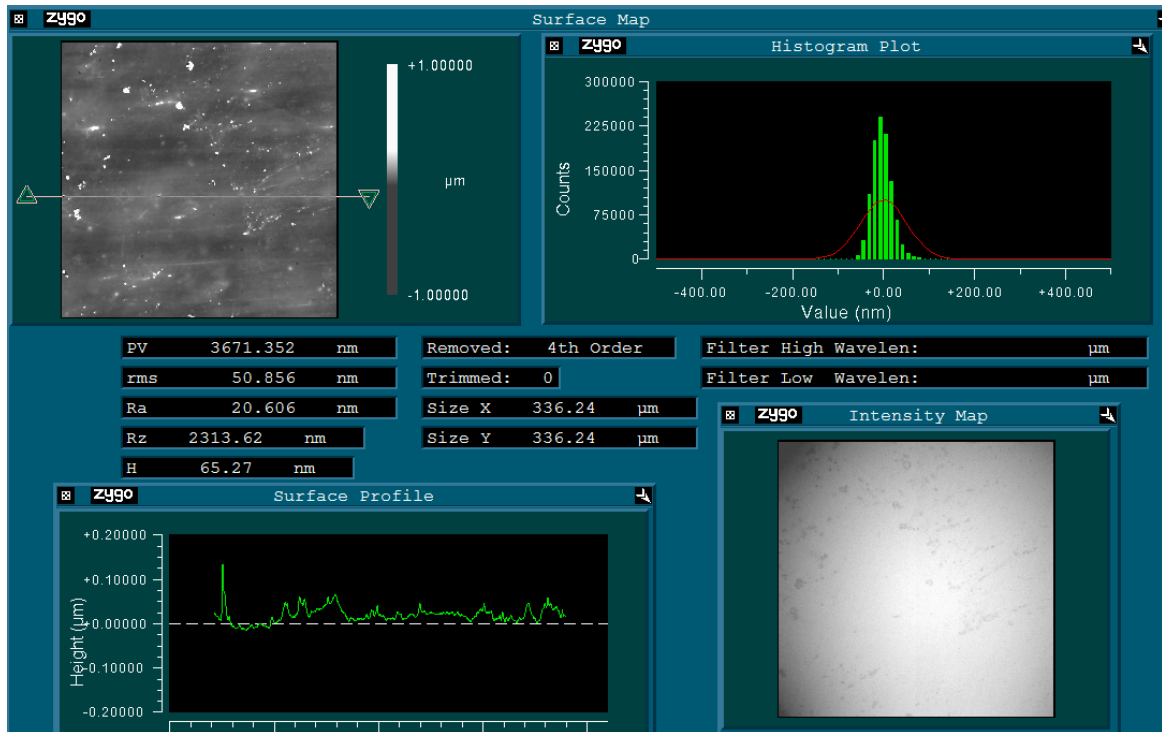
Figure 4-27. MetroPro output for before the sample was imaged with ESEM.
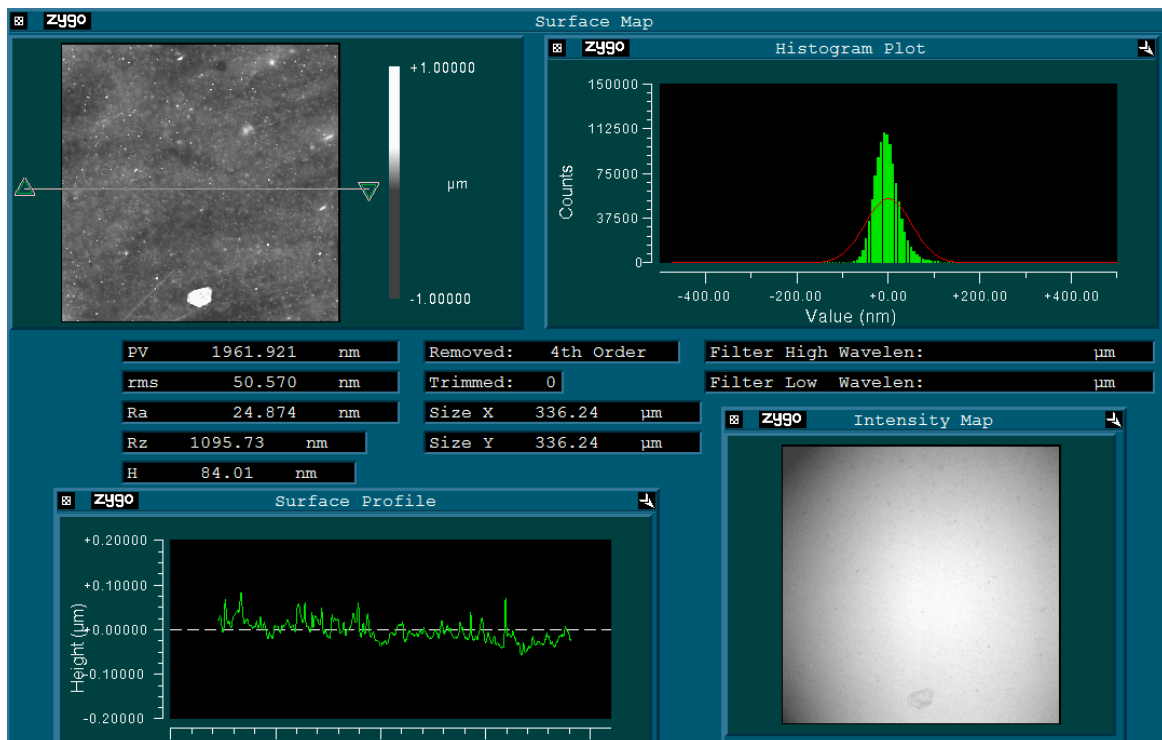
Figure 4-28. MetroPro output for after the sample was imaged with ESEM.

As previously mentioned, ESEM is used to further confirm the identity of platelets and fibrin on the sac surface. In order to be able to recognize the structures, controls were created and imaged with ESEM. Figure 4-29 shows platelet adhesion from RDS onto the polymer surface. The RDS trial is the same sample that was labeled with the anti-phospho-ITGB3, which further proved that this antibody was not labeling the platelets. Figure 4-30 shows a positive fibrinogen control created by plating the purchased fibrinogen on a SEM stub.
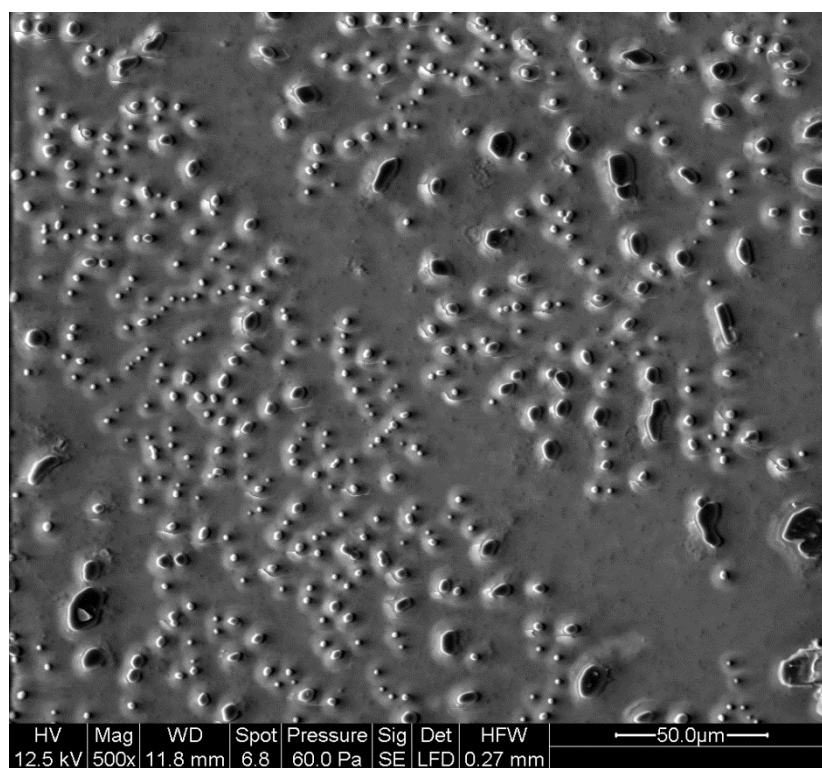
Figure 4-29. Positive platelet control from RDS.

HV | Det | Mag | WD | Sig | Spot | Pressure | 500.0μm
20.0 kV | LFD | 100x | 10.6 mm | SE | 7.0 | 100.0 Pa |
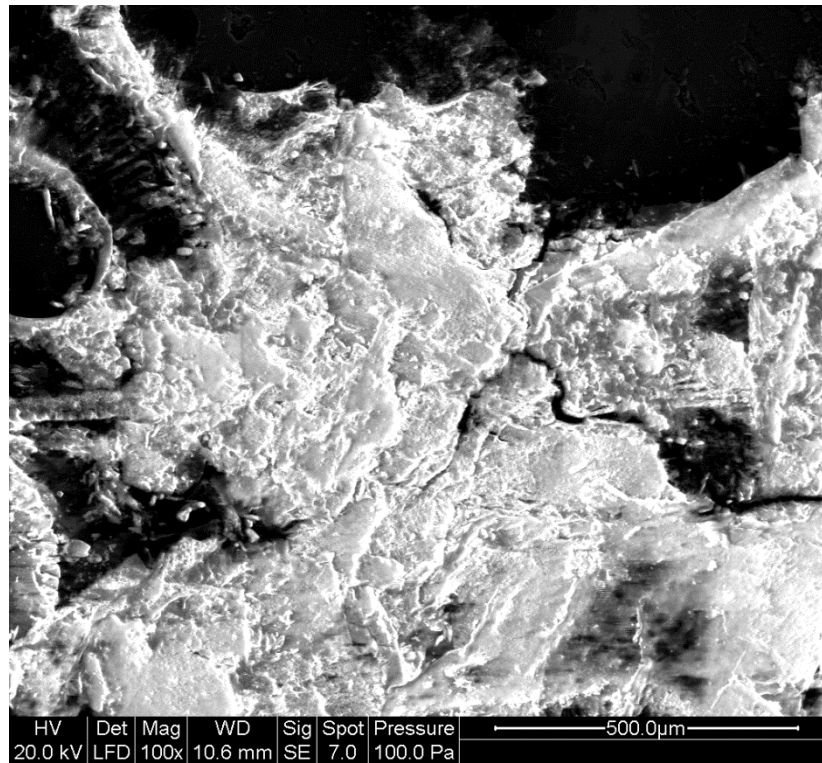
Figure 4-30. Positive fibrinogen control of purchased fibrinogen.

While the features in Figure 4-29 are the same size of a platelet, 1 to 3 microns, the activated platelets appear different from previous images taken with a conventional SEM. Activated platelets are characterized by pseudopodia and a more spread out appearance, which cannot be seen. There also are larger features that could be platelet aggregates; however, the aggregates appear as one large feature instead of multiple platelets. A comparison of platelet controls imaged with SEM and ESEM should be carried out in the future as it is possible that the imaging capabilities of the ESEM prevent significant contrast to view the pseudopodia.

4.4 Pepsin Degradation

Pepsin was identified as an enzyme capable of degrading the biological deposition that is found on the sac surface, which is a necessary step in the surface analysis as it will allow for the true surface of the sample to be identified without the biological deposition altering the surface roughness data. The obtained roughness data can be correlated to both the confocal microscopy and ESEM results to determine if there were any surface irregularities in the region of the deposition that could have played a role in the thrombus formation. Similarly to other experiments, the effects of the pepsin degradation protocol on the SPEUU needed to be tested to ensure that the pepsin was not altering the surface of the samples. The protocol discovered in the literature was vague with regards to what concentration of pepsin to use and the length of the pepsin exposure.

Optical profilometry was used to determine if the surface was being altered by the pepsin exposure by collecting data before and after the pepsin degradation protocol. The optical profilometry data were analyzed for varying pepsin concentrations and exposure durations. All of the pepsin concentrations tested are denoted as the ratio of pepsin dissolved in DI water to 1 M HCl (pepsin:HCl). For each degradation condition, rms, Ra, Rz and H values were obtained at six different locations from three samples and then averaged. Figures 4-31 through 4-35 show the comparison between the average of the four different surface roughness values for the before and after data for each pepsin condition that was tested.
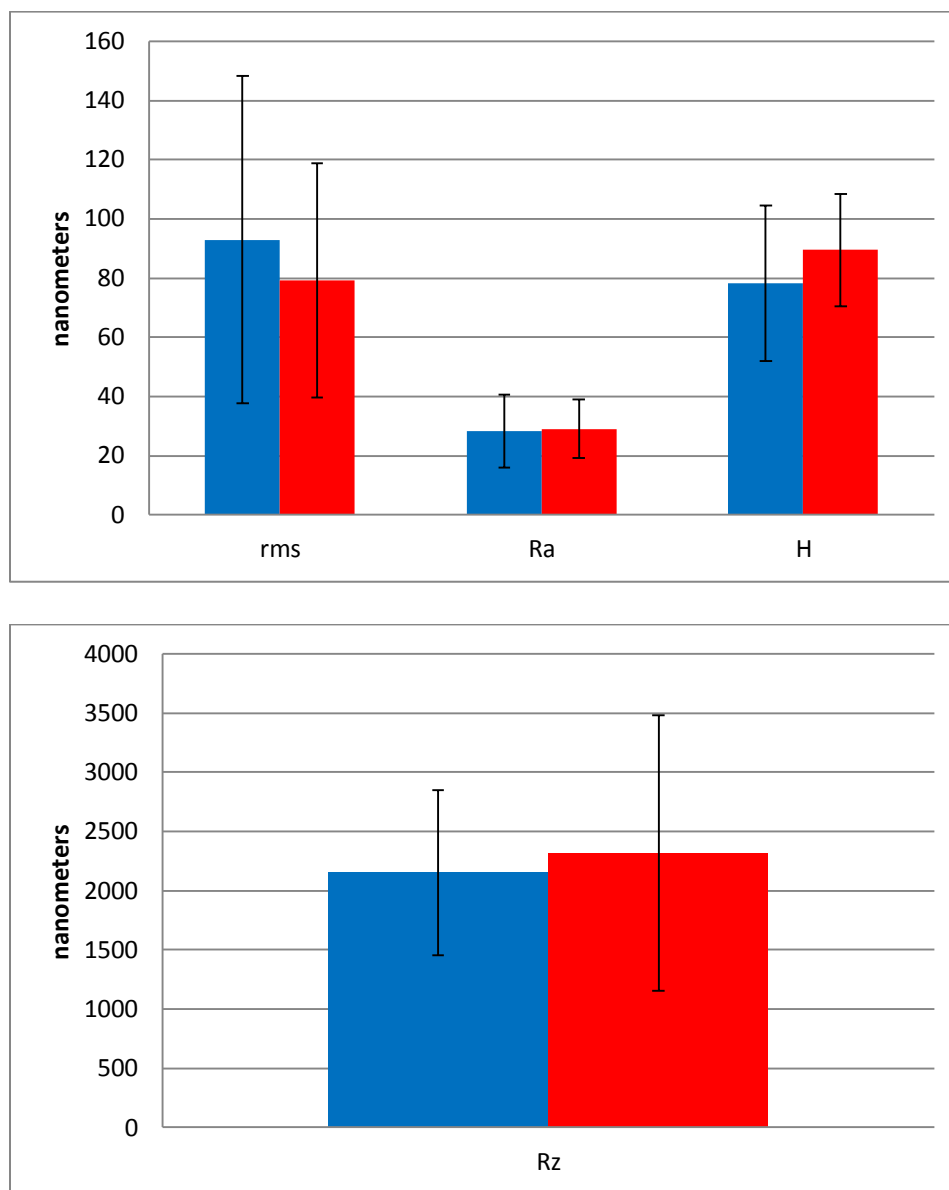
Figure 4-31. Surface roughness values for before (blue) and after (after) pepsin exposure of a 1:1 pepsin:HCl for 2 hours.
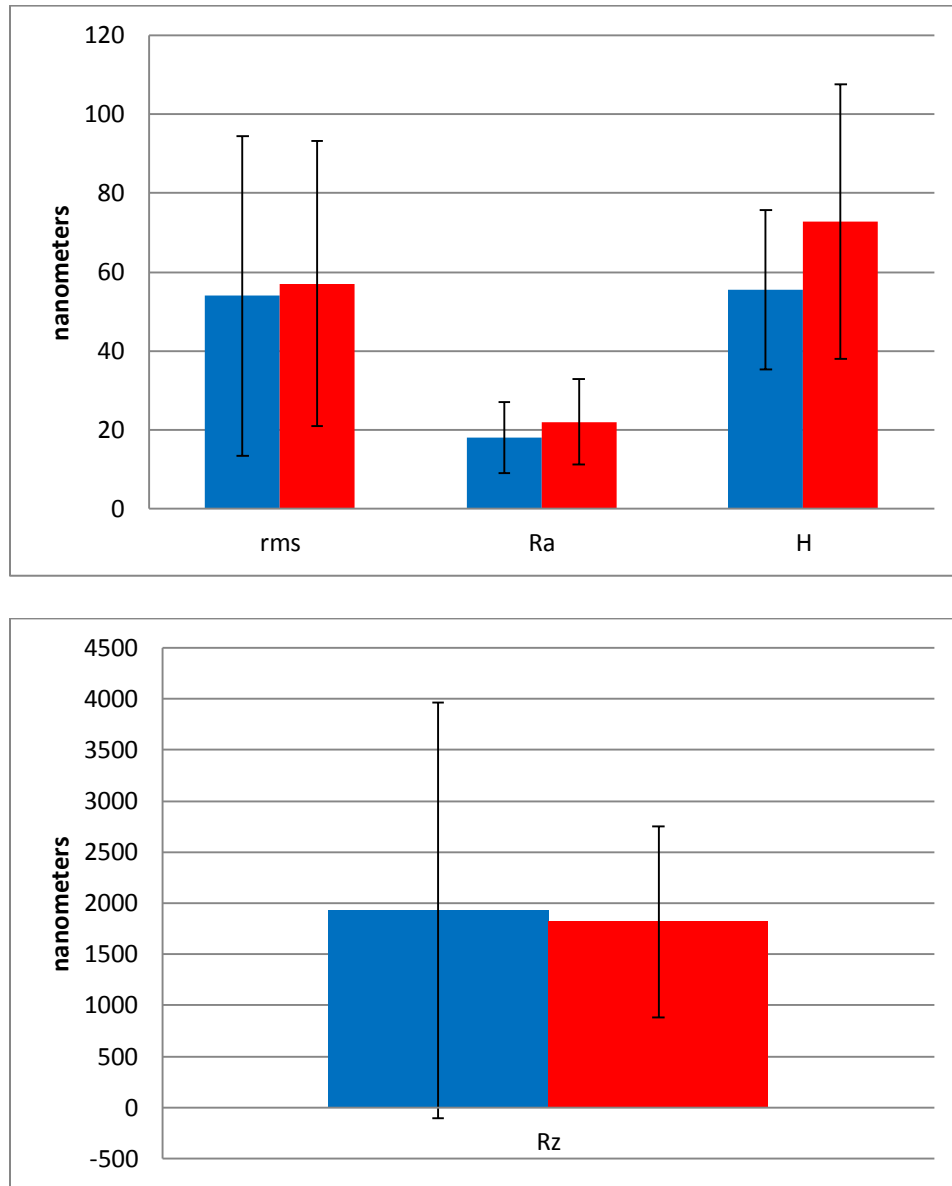
Figure 4-32. Surface roughness values for before (blue) and after (after) pepsin exposure of a 3:1 pepsin:HCl for 2 hours.
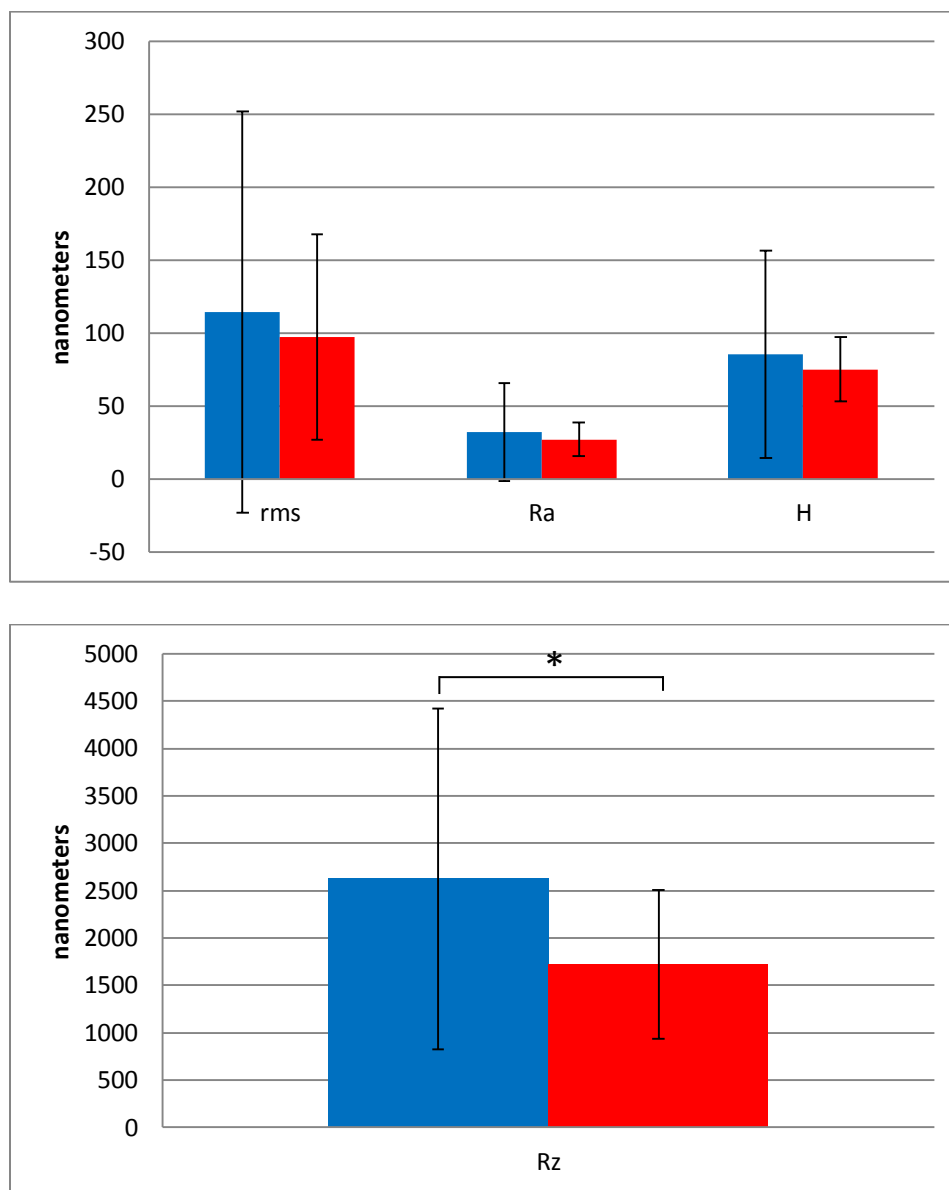
Figure 4-33. Surface roughness values for before (before) and after (after) pepsin exposure of a 5:1 pepsin:HCl for 2 hours.
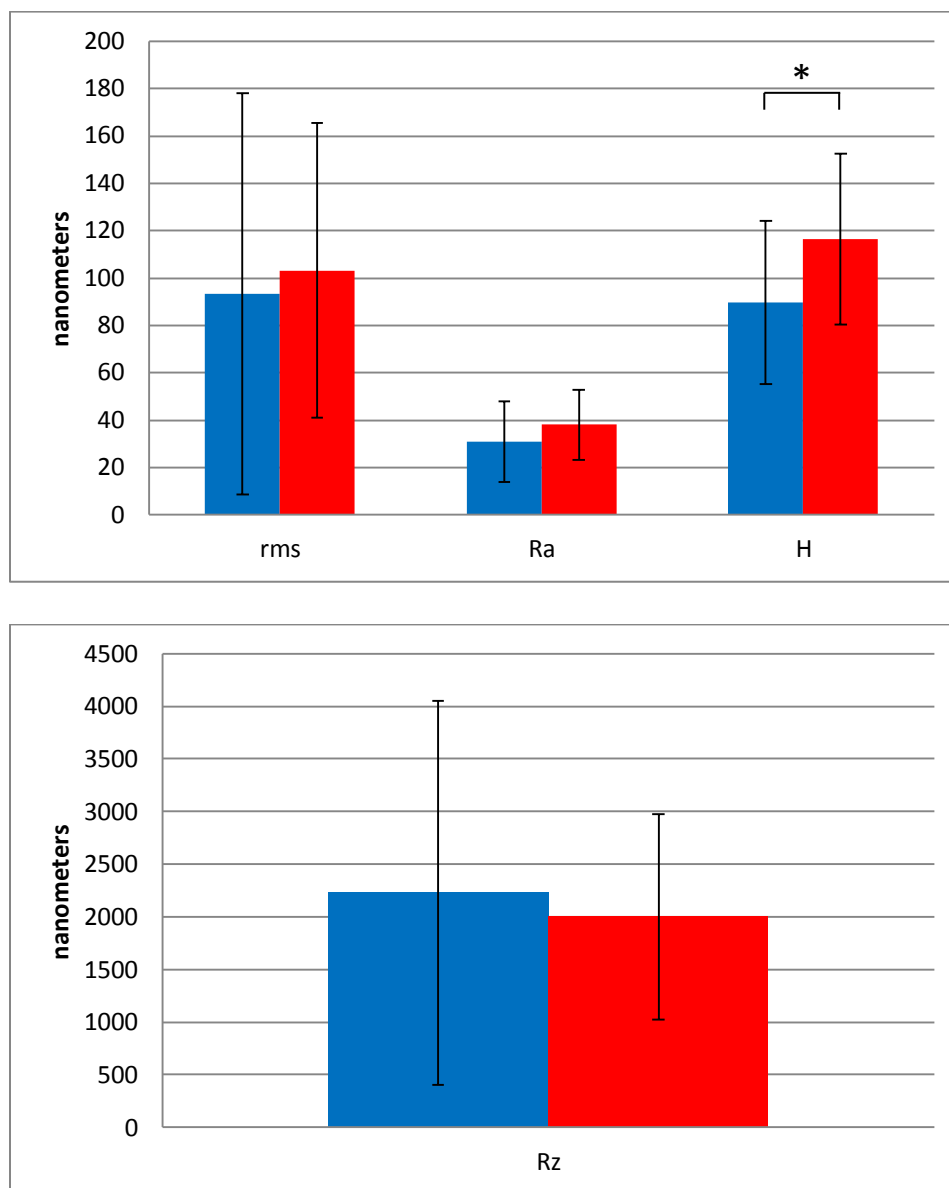
Figure 4-34. Surface roughness values for before (blue) and after (red) pepsin exposure of a 3:1 pepsin:HCl for 3 hours.
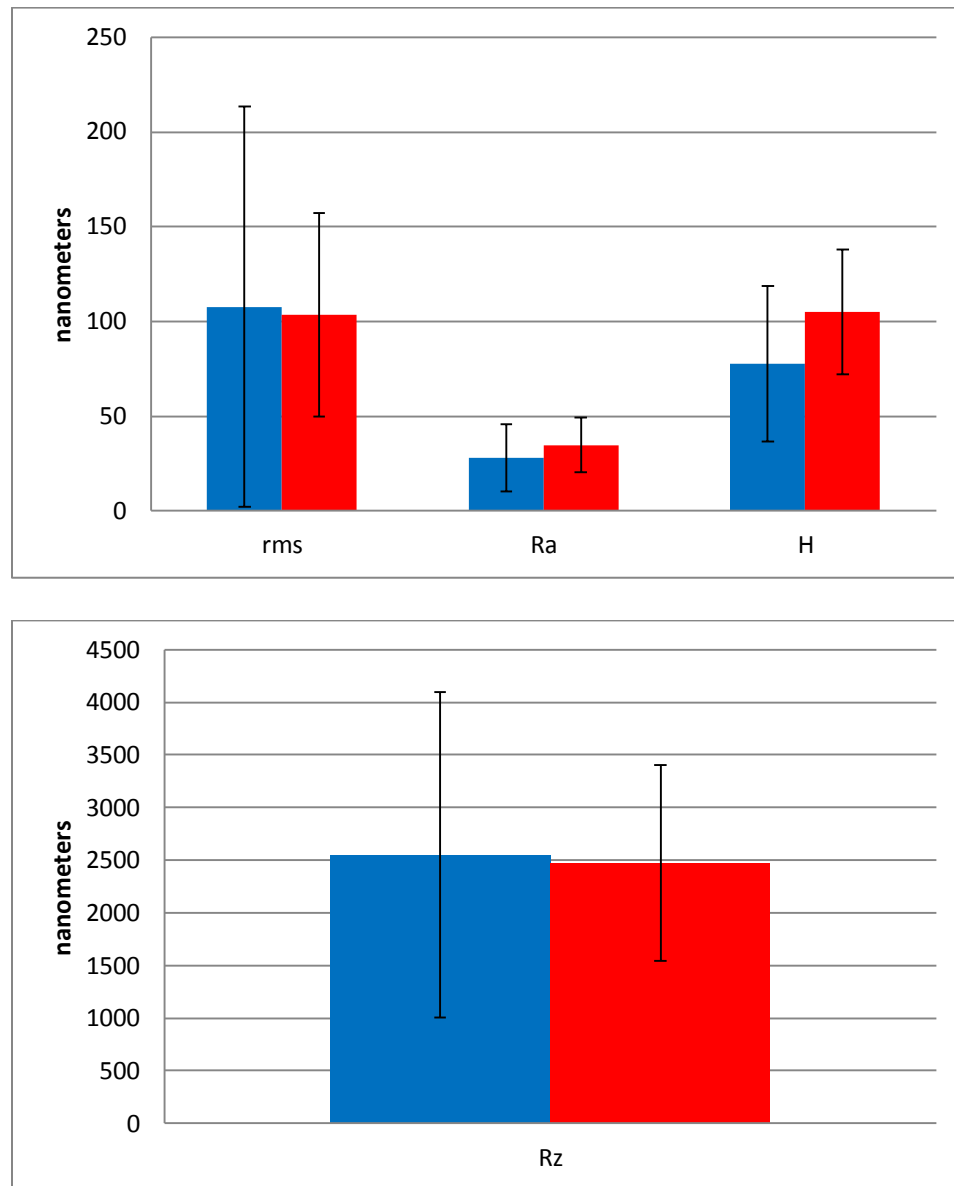
Figure 4-35. Surface roughness values for before (blue) and after (red) pepsin exposure of a 5:1 pepsin:HCl for 3 hours.

The results show that there is no significant difference between the majority of the values as a result of the pepsin exposure, but there is a significant difference for the Rz value for 5:1 pepsin:HCl for 2 hours and the H value for 3:1 pepsin:HCl for 3 hours. The majority of the values do not change, but the ones that do are not in any particular pattern. For some conditions the value will decrease and for others increase, so the

difference is most likely not a result of the pepsin exposure. The lack of a clear pattern when comparing the before and after data is further shown in Figures 4-36 to 4-39, which shows a comparison between the pepsin exposure conditions for each of the four roughness values.
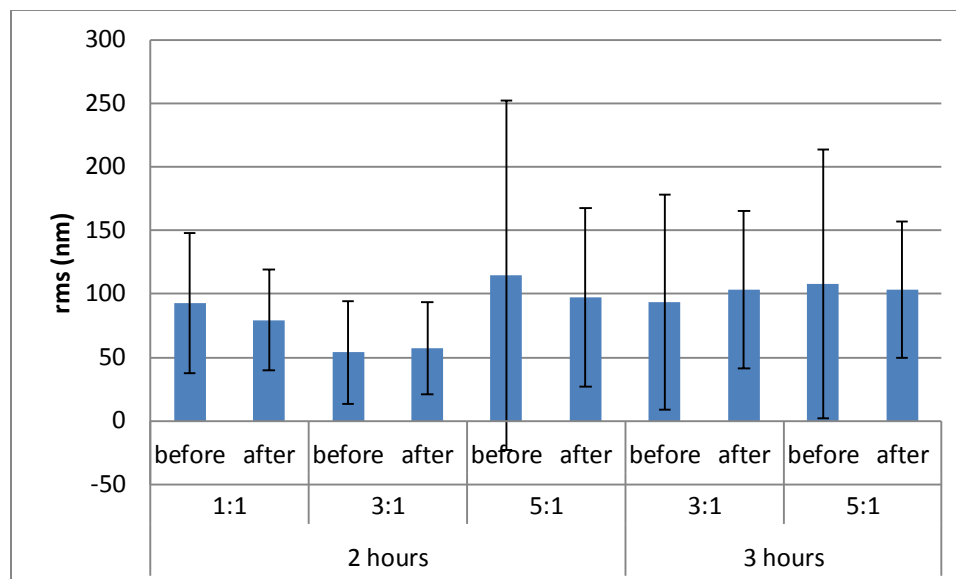
Figure 4-36. Average rms values for before and after pepsin degradation of varying pepsin concentrations and exposure times.
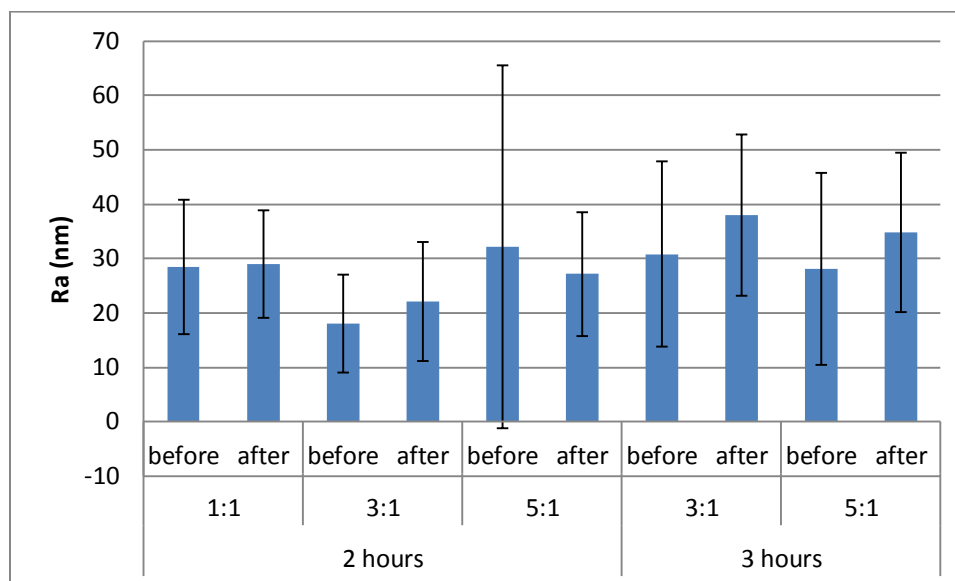
Figure 4-37. Average Ra values for before and after pepsin degradation of varying pepsin concentrations and exposure times.
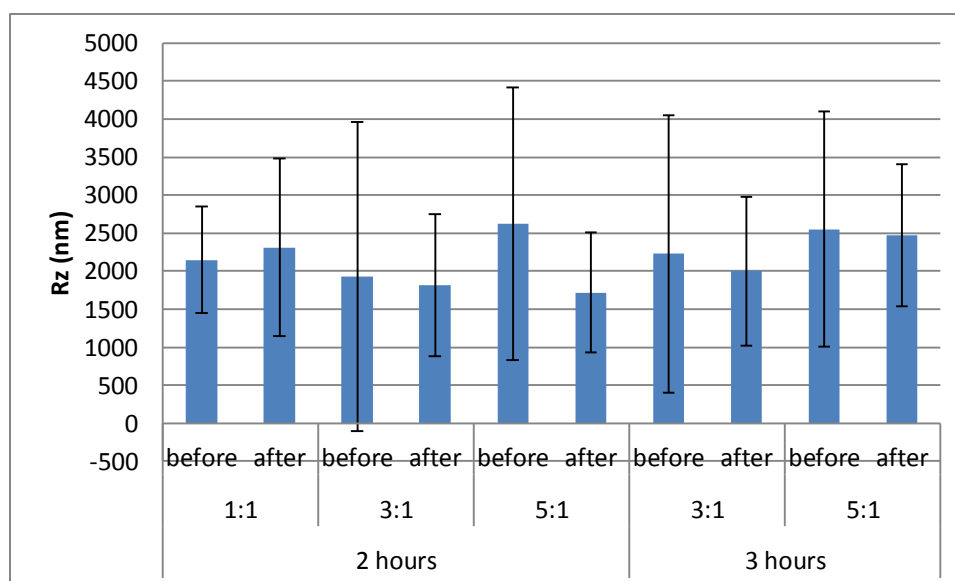
Figure 4-38. Average Rz values for before and after pepsin degradation of varying pepsin concentrations and exposure times.
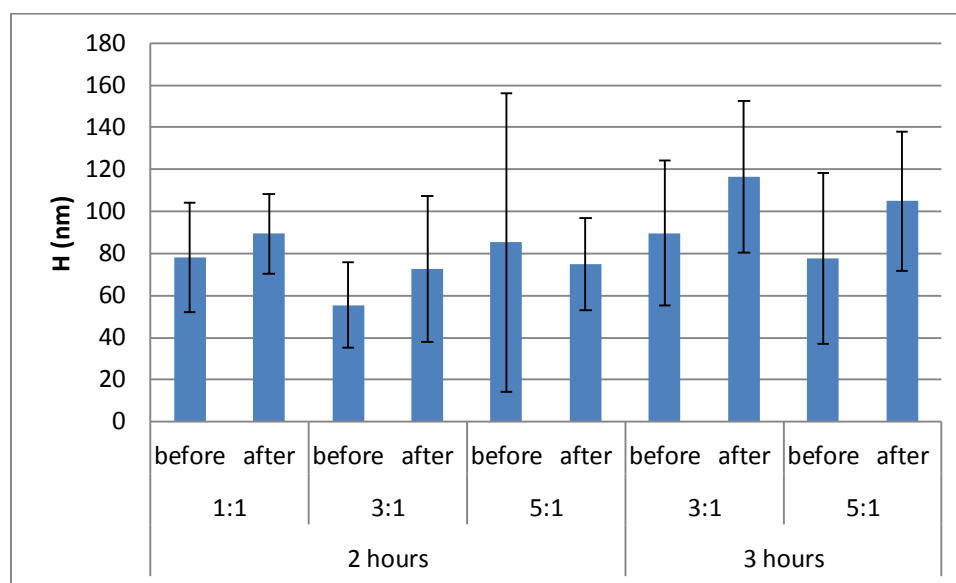
Figure 4-39. Average H values for before and after pepsin degradation of varying pepsin concentrations and exposure times.

These figures further show that the pepsin is not altering the surface in a significant manner. Because the before measurements are dependent on the samples, but the after measurements are a result of the pepsin degradation, and there is no pattern of a value always increasing or decreasing after pepsin exposure, the change in the surface roughness value is not a result of the pepsin degradation, but is either the result of debris on the surface or is a result of the same region not being analyzed before and after. To further examine if the pepsin is altering the surface the surface profiles provided by MetroPro can be compared. The comparison is similar to the results of the before and after ESEM results that showed there are more high frequency waves in the surface profile after pepsin exposure. However, these waves are on the order of 0.1 microns, so they will not have a significant effect on thrombosis and can be considered noise.

With it determined that the surface is not being significantly altered as a result of the pepsin degradation, the different concentrations and exposure times were then tested

on positive controls to ensure that the pepsin is indeed degrading any surface depositions so that the true surface can be analyzed with optical profilometry. ESEM images taken before and after the varying pepsin concentrations and length of exposure are provided in Figures 4-40 to 4-43.
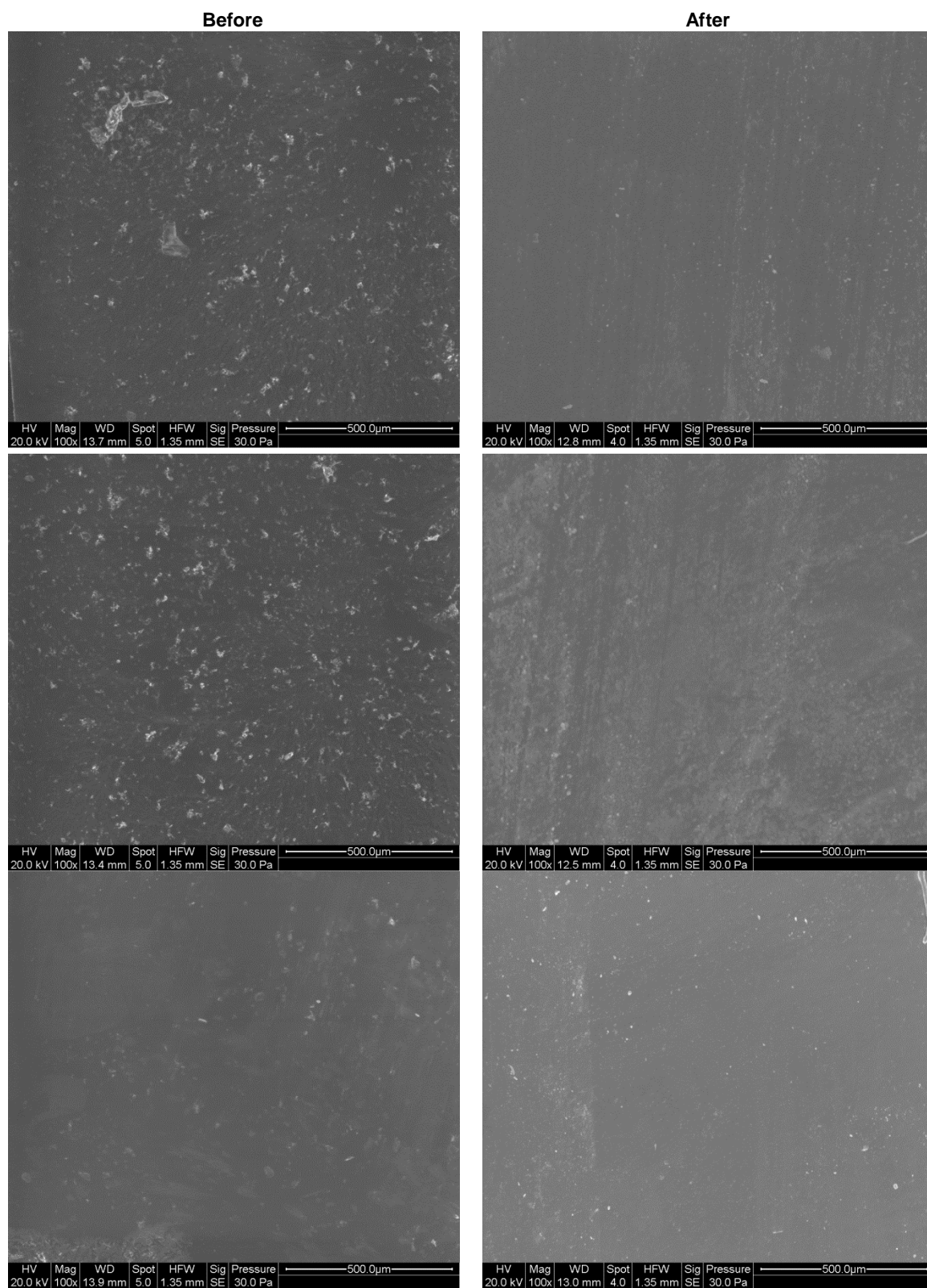
Before   **After**

Figure 4-40. Before and after pepsin degradation images for samples exposed to 3:1
pepsin:HCl for 2 hours.
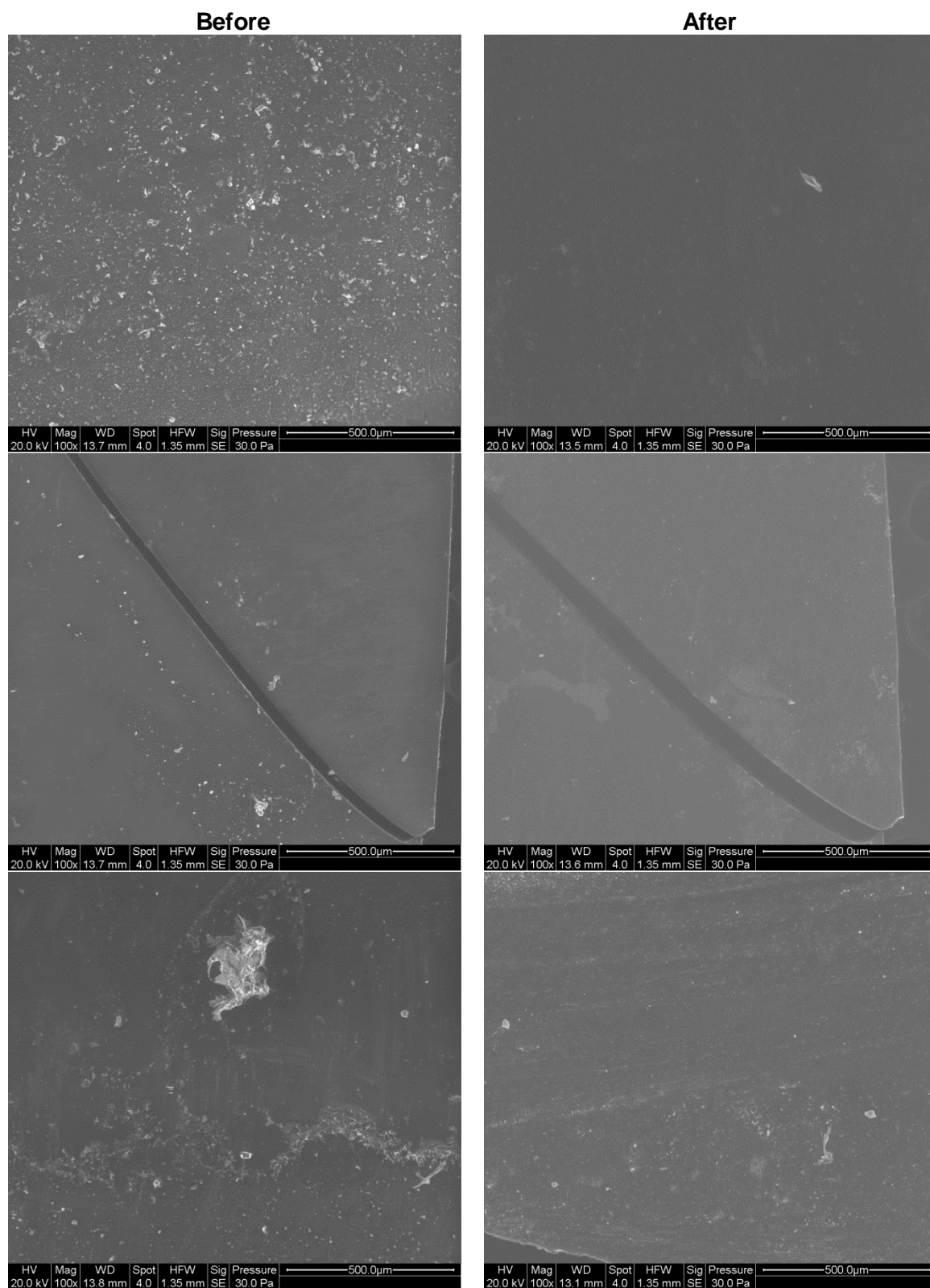
Before

After

Figure 4-41. Before and after pepsin degradation images for samples exposed to 5:1 pepsin:HCl for 2 hours.
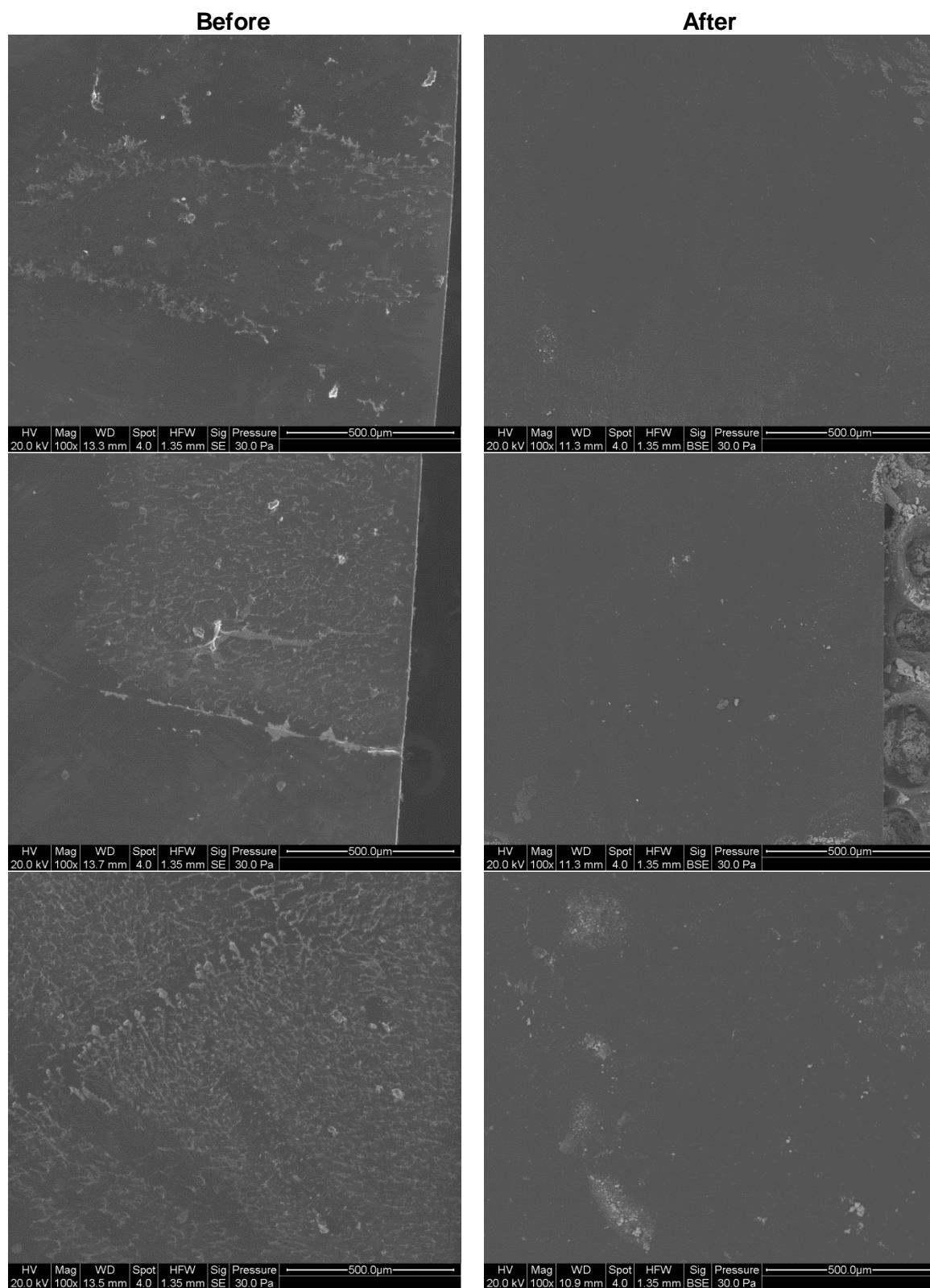
Before **After**

Figure 4-42. Before and after pepsin degradation images for samples exposed to 3:1 pepsin:HCl for 3 hours.
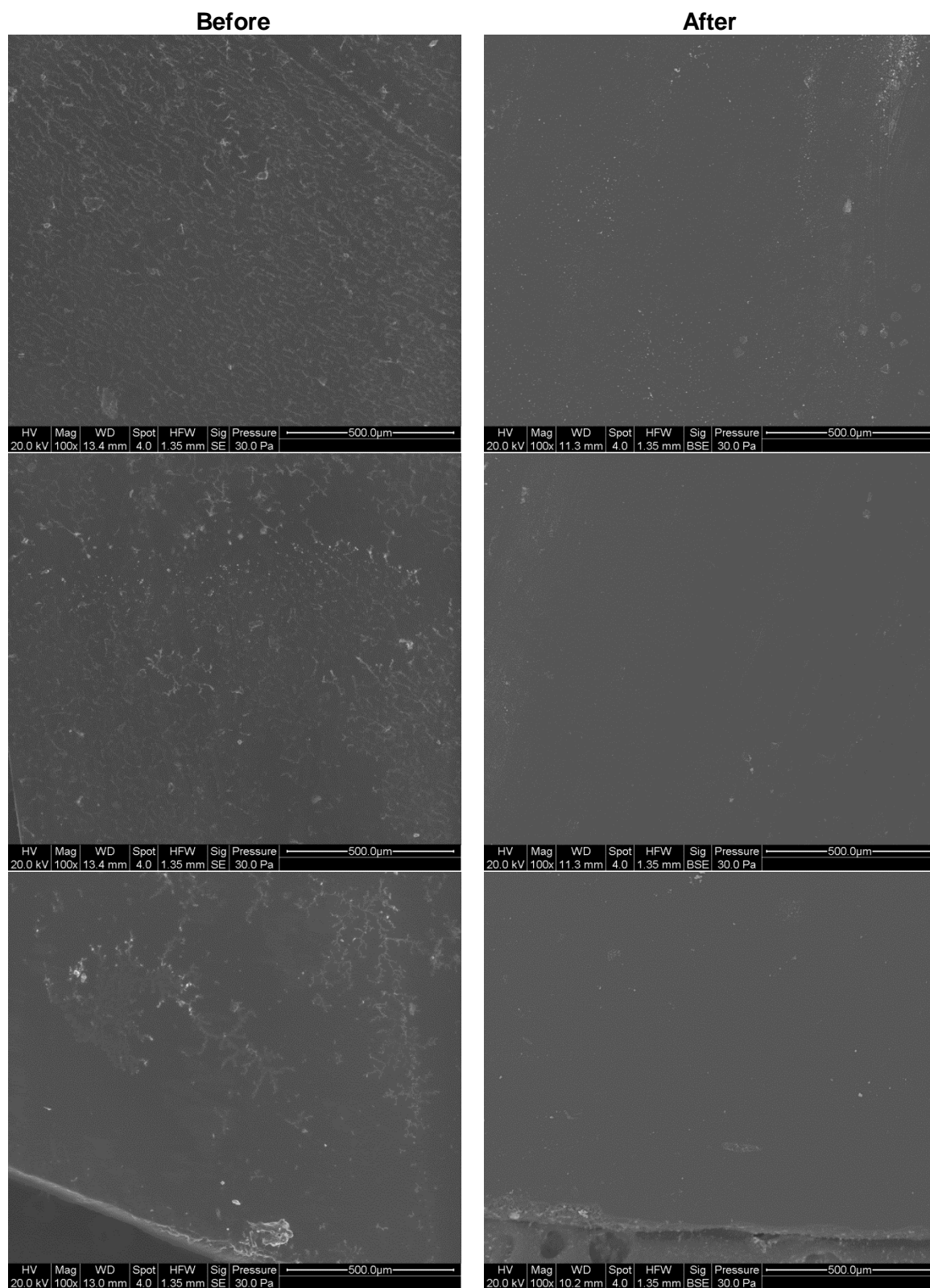
Before

After

Figure 4-43. Before and after pepsin degradation images for samples exposed to 5:1 pepsin:HCl for 3 hours.

Figures 4-40 to 4-43 shows that comparing the before and after images shows that the pepsin is indeed degrading the surface deposition. For some of the images, the surface is not completely clean after the degradation but it appears that the major depositions have been degraded, and the most likely explanation is that there is debris remaining on the surface from the degradation of the carbon tape as there was visible degradation of the tape and black particles in the pepsin solution after the incubation period. A rinse of the surface should remove any debris that is remaining on the surface.

4.5 Image Correlation

The purpose of the protocol is to view the same sample with confocal microscopy, environmental scanning electron microscopy, and optical profilometry. In order for this to be a useful analysis, the same regions of each sample should be viewed with all three microscopy techniques. While the technology exists for correlative microscopy to allow for the exact region of the same sample to be imaged with confocal and scanning electron microscopy, this technology is not available at the Millennium Science Complex, so a technique needed to be determined that allows for the same regions to be imaged. Different ways to accomplish this such as SEM grids underneath the samples were explored; however, the sac is too thick and opaque to see through when imaging. Another option was placing a grid on top of the sac samples, but this could disrupt the surface deposition and be difficult to place the grid in the same location. The most effective way to image the same regions was determined to be moving through the sample and take a specified number of images per sample starting at an origin. To

determine how many images to take per sample, the field of view of the different microscopy techniques was determined, and the results are summarized in Table 4-2.

Table 4-2. Summary of field of view dimensions for the different microscopy techniques and magnifications.

Microscope	Magnification	X (µm)	Y (µm)
Confocal	60x	176.295	176.295
ESEM	100x	1347.37	1240.79
	250x	553.51	509.73
	500x	273.80	252.14
Optical Profilometry	50x	336.24	336.24

4.6 Protocol Development

Even though a previous study with an established protocol was used to frame this project, developing the protocol to analyze the effects of surface roughness on thrombosis was a time-consuming process. This preliminary study involved framing the experiment, gathering the necessary materials, and setting up the protocol in such a way that it produces viable, meaningful data consistently. The challenges involved in framing the protocol included altering the existing protocol to study ovine blood components instead of bovine blood components and correlating the three microscopy techniques for the same sample.

The first step in the process was determining if irregularities existed at the surface instead of in the bulk material. The optical profilometry data clearly showed that there is

a significant difference in the sacs that do not contain visible surface features compared to the sacs containing scuffs or the visible features. While the scuffed sacs are not used in animal trials, the optical profilometry data shows that the average roughness for these sacs is on the order of a micron, which could induce thrombus formation. Upon closer examination of the smooth sacs that are used in the animal trials, there appears to be scratches and some pits in the sacs. Previous studies had suggested that pits may encourage platelet adhesion and thrombus formation. These pits were a result of a fabrication process that is no longer in use, but the new fabrication process still results in pits. However, these pits are smaller, which should not affect platelet adhesion. As a part of the new fabrication process, the polymer sacs are dipped in a steel mandrel that is finely polished to be as smooth as possible; however, the polishing results in scratches on the surface of the mandrel which can be seen in the sac surface as shown in the MetroPro output in Figure 4-4 and the ESEM image in Figure 4-11. The effects of the scratches and pits are unknown, which leads to the need for a protocol that allows for surface analysis of the explanted blood sacs.

Once the presence of surface irregularities was established, antibodies that could be used to label ovine platelets and fibrin needed to be identified. The antibodies available for an ovine model were limited, which led to the testing of three different antibodies. The protocol uses two primary antibodies, so in order to label platelets and fibrin with different colors, the primary antibodies needed to be from different host species or an antibody labeling kit needed to be used. These kits add an extra step to the labeling process and are an additional cost, so the anti- phospho-ITGB3 was investigated to label the platelets. While Figure 4-16 shows that the platelets were being labeled by

this antibody, the results could not be repeated using other positive controls. Johnson *et al.* showed that for some platelet markers the binding is dependent on the activation state, with markers having a higher propensity to bind to activated platelets[52]. The higher propensity for binding to activated platelets could be one possible explanation for why the PRP clot was the only control to result in fluorescence as most of the platelets in the clot would be activated by the addition of the calcium. Other controls such as a clot from a backward facing step model would contain both activated and inactivated platelets.

The same study stated that CAPP2A binds to platelets regardless of the activation state. This label had been previously used in the analysis of the sacs implanted in the bovine model, so it had been shown to be effective in labeling platelets for a similar application. Figures 4-17 and 4-18 show the platelets are successfully being labeled for an ovine model. However, CAPP2A is mouse derived similarly to the anti-fibrinogen antibody, which was the only antibody that could be found to label ovine fibrin, so a labeling kit needed to be used to label both platelets and fibrin. Testing of the labeling kit showed that both platelets and fibrin were successfully being labeled.

Focusing the microscope proved to be the most difficult step in imaging the samples with confocal microscopy and will be even more difficult when imaging the explanted sac samples due to the curvature of the samples requiring the microscope to have to be re-focused with every change in the x or y position along the sac. Another difficulty in imaging the samples will be mounting the samples on microscope slides because when the polymer samples are wet, they would not stick on the double sided tape that is used to mount the samples to the microscope slides. For imaging the explanted sac

samples, the best way to image the samples will be to place the samples on a cover slip so that the inside of the sacs is facing downwards.

Environmental scanning electron microscopy was a new microscopy technique to be used with the blood sac samples. To switch from confocal to ESEM, the samples need to be mounted onto an aluminum SEM stub with carbon tape. Even though there is beam damage, which did not have a significant effect on the surface roughness, imaging of the samples with ESEM proved to be an effective imaging technique for viewing the true surface of the samples without having to sputter coat the samples. The most difficult step in imaging the samples was setting the contrast level to obtain sufficient contrast. The contrast was routinely set to a level between 98 to 100 percent, but despite being set at the maximum level, sufficient contrast was obtained.

Another difficulty in imaging the samples with ESEM was removing the samples from the PBS solution that was used to rinse the samples before imaging. If the samples were placed into the low vacuum while still wet, the PBS solution would bubble and leave a fibrous residue as shown in Figure 4-44. A higher magnification image is shown in Figure 4-45. This fibrous residue is not a true deposition on the sac surface, so this should be avoided to prevent making a sample impossible to image.
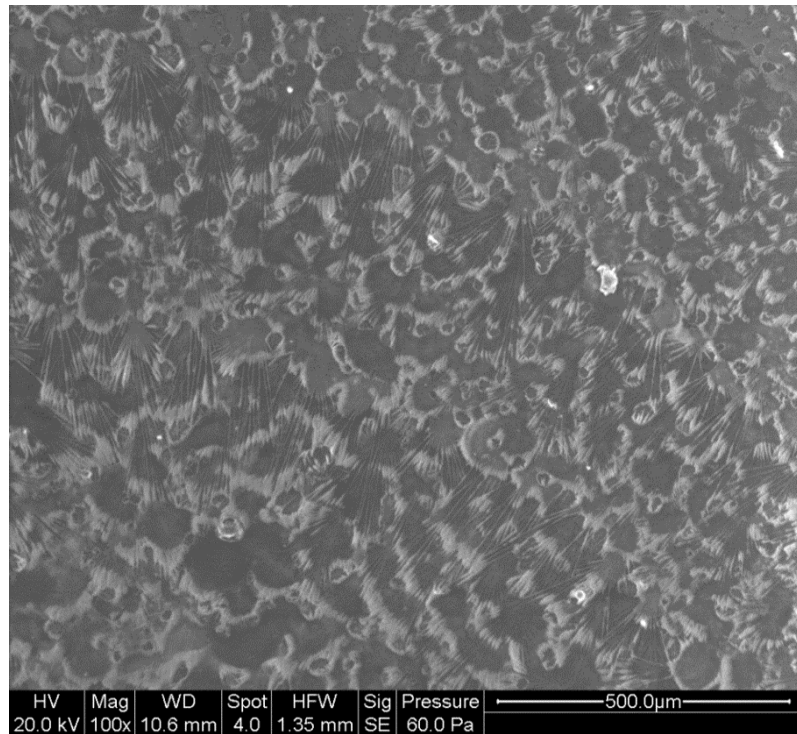
Figure 4-44. Fibrous residue from an explanted sac that was wet when placed in the ESEM.
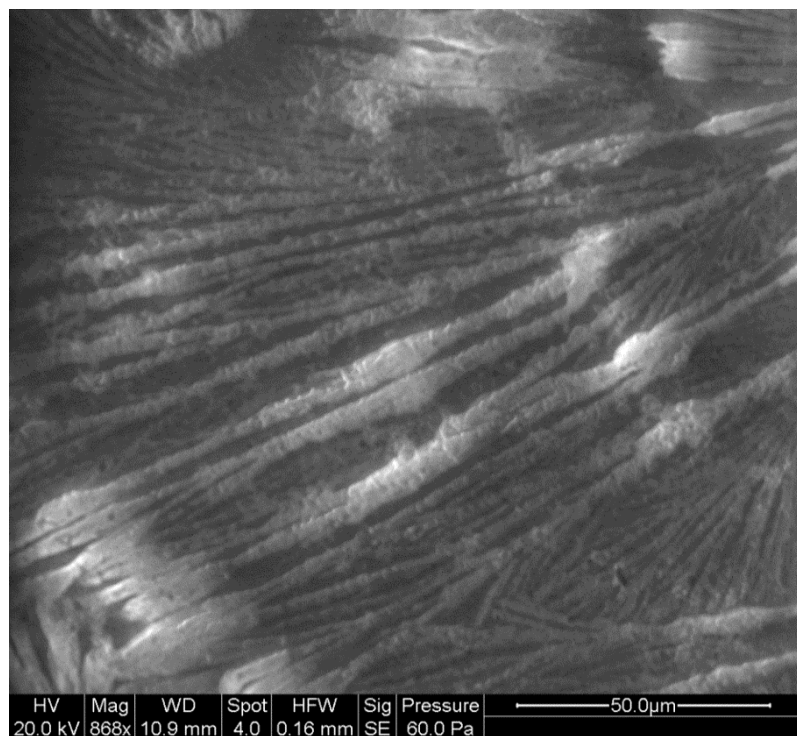
Figure 4-45. Higher magnification image of the fibrous residue.

On the other hand, if the sample is given time to dry before it is placed in the ESEM, the PBS dries, and salt crystals cover the surface of the sac samples as shown in Figure 4-46. Similar to the fibrous residue, this crystallization is to be avoided in order to effectively image any surface deposition. In the SEM protocol used for the bovine study, the crystallization was avoided by the dehydration step of the protocol. This step was necessary to sputter coat the surface but is not required for ESEM. In order to avoid the crystallization of the PBS, the samples need to be gently rinsed multiple times with DI water before being placed into the vacuum. If for some reason there are still salt crystals on the surface after the DI rinse, further DI rinsing was shown to rinse the crystals from the surface as shown in Figure 4-47.
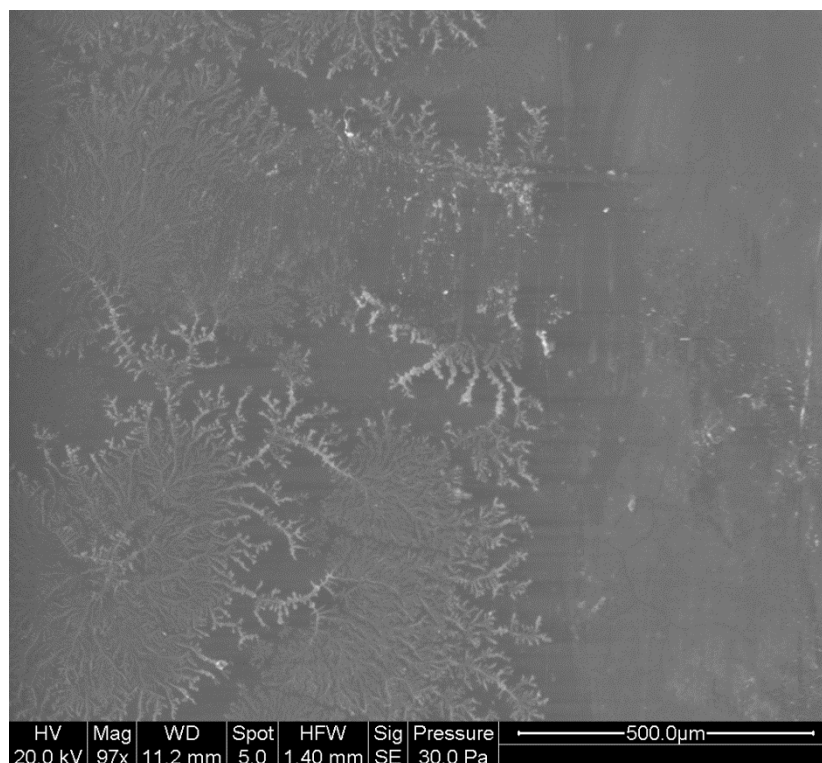
Figure 4-46. Dried PBS crystals on the sac surface
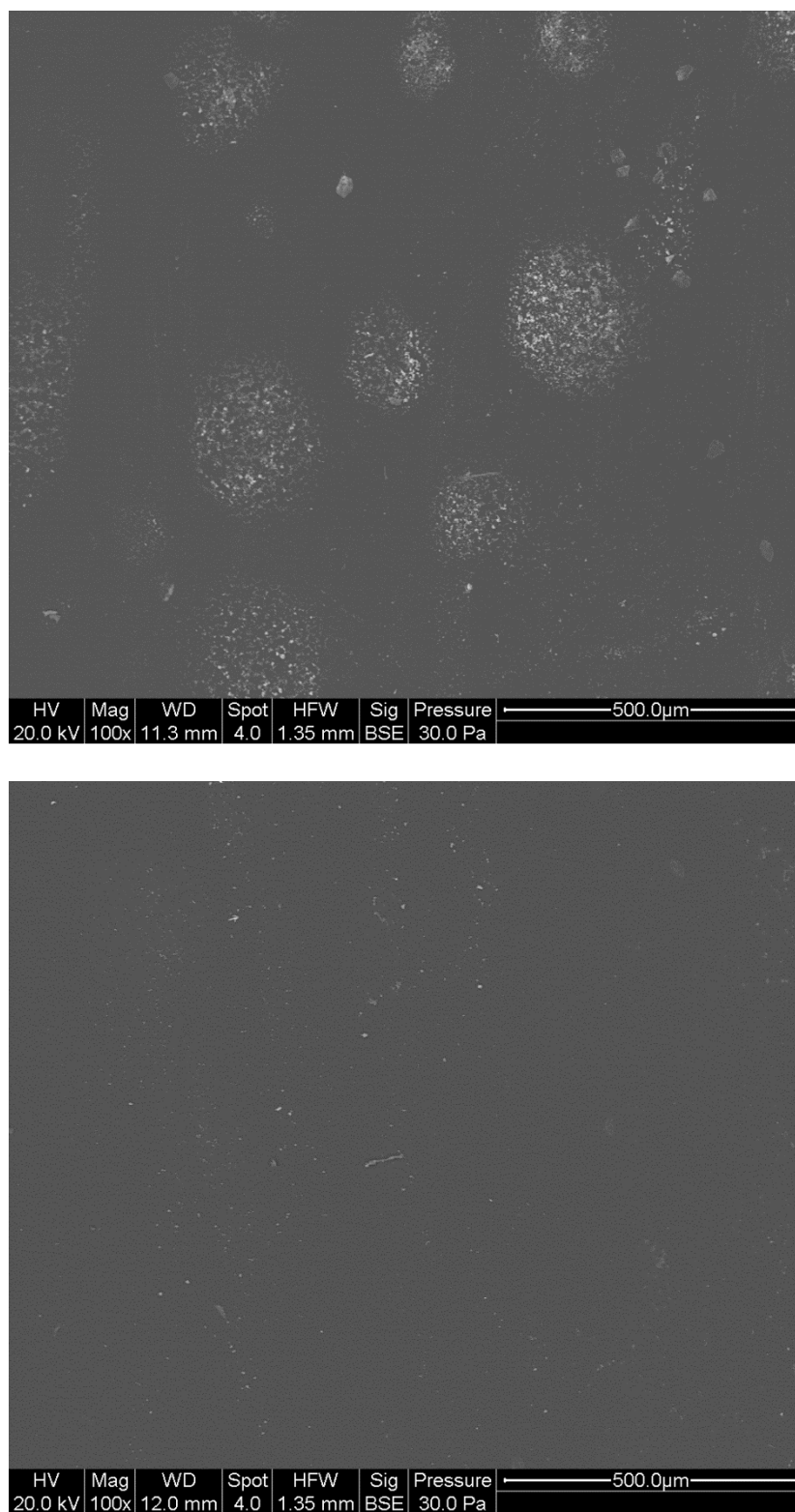
Figure 4-47. The top image shows some PBS crystals, while the bottom image shows the same region after a DI rinse. The PBS crystals were removed by the rinse.

In order to image the sac surface, the deposition needs to be degraded, and pepsin was identified as an enzyme to be used for this purpose. The effect of the pepsin on the SPEUU was unknown but was determined by comparison of optical profilometry before and after pepsin exposure. The results showed that there is no significant difference in the values for varying pepsin concentrations and exposure times, but upon closer examination of the surface profiles it appears that after pepsin exposure the surface has more waviness to it. However, these variations can be seen as noise because there is no difference in the surface roughness values and the variations are only on the order of magnitude of 0.1 microns, which is not large enough to cause a difference in platelet adhesion as previous studies have shown.

With it known that the pepsin was not affecting the polymer surface, the ability of the pepsin to degrade the deposition was tested. The before and after images in Figures 4-40 to 4-43 show that the majority of the deposition is being degraded. Some images contained salt crystals or residue from the pepsin degradation, so a DI rinse is needed before imaging the sac samples. During some of the testing of the pepsin, the samples were placed in the pepsin while they were still on the SEM stub and the carbon tape. This resulted in the pepsin reacting with the polish of the stubs and the carbon tape, which led to residue on the samples. A similar residue was not present when samples were removed from the carbon tape and then placed in the pepsin. For the future protocol, the samples will be removed from the carbon tape to not add extra debris that would alter the optical profilometry data significantly.

Because the literature for using pepsin to clean polymer surfaces only stated that the polymer was exposed to the pepsin at a pH of 1 for several hours, the optimal pepsin

to HCl concentration and duration needed to be determined. When comparing the concentrations there did not appear to be a significant difference between 3:1 and 5:1. In order to save money, as the pepsin is more expensive than HCL, a 3:1 concentration will be used in the protocol. The images appeared to show that the degradation is a function of time, with more complete degradation occurring as the length of the duration is increased. For this reason, a time of 3 hours will be used for the pepsin degradation.

Previous studies did not require exact correlation of the different microscopy techniques, so the same sample would not be viewed using the different techniques. Instead, different samples from the same region of the sac were imaged with the either confocal or SEM. However, ESEM allows for the same sample to be imaged with both confocal, ESEM, and optical profilometry. Therefore, the same region of a sample can be imaged with the different microscopy techniques as long as there is a method for imaging the same regions. While different options were explored, no method that guaranteed the same regions were being imaged was determined. Instead a similar technique that has been used before in the Artificial Heart Lab will be used, but with more images being taken to provide a better overlap between microscopy techniques. In this method the upper right-hand corner of the sample is cut at a diagonal, which serves two different purposes: to provide an origin for imaging and to orient the sample, so the inside of the sac is imaged. Then starting at the upper right-hand corner where the diagonal was cut images will be taken from right to left. Once the left edge of the sample is reached, the y position will be changed and then the sample will be imaged from left to right. The above method for imaging is repeated until all of the necessary images are obtained. To determine how many images should be taken per sample the field of view

of each of the microscopy techniques was determined as shown in Table 4-2. The different magnifications for ESEM were explored because this setting is simple to change on the microscope. The field of view of the 500x was the closest to the 60x of the confocal and the 50x of the optical profilometry, so 500x was decided upon as the magnification to be used for the ESEM. In addition to similar field of views, the 500x magnification should provide sufficient magnification to provide a large field of view to view a large area of either platelet or fibrin adhesion and still provide detail of the features to confirm their identity as either platelets or fibrin.

The first step in deciding how to image the samples is determining what size to cut each sample. Previous studies cut samples at the size of 4 mm by 2 mm. Based off of experiences from cutting the polymer sacs, the smaller the dimensions of the sample the more difficult it is to cut and handle. However, the larger the sample is the more images will need to be obtained in order to ensure that the same regions of the sample are being imaged. Based off of these observations a sample size of 4 mm by 3 mm would be best because the samples would be easy to cut and handle without requiring too many images. As shown in Figure 4-48, 16 images will be obtained from each sample. This number was chosen because 4 is an easy number to track which quarter of the sample is being imaged.
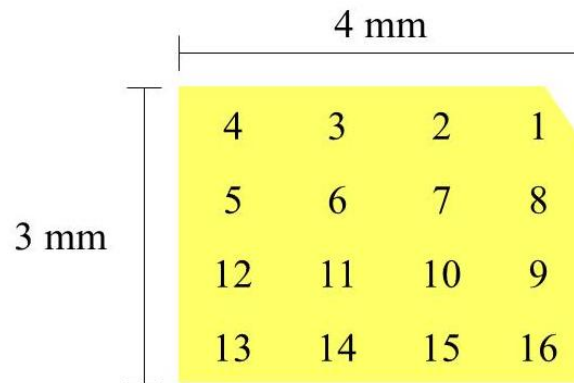
Figure 4-48. Imaging technique to obtain images from the same regions.

With all of these experiments carried out and observations made throughout the process, the following protocol has been established to analyze the surface of sacs explanted from ovine models at the Penn State College of Medicine:

Sample Prep:

1. Explanted sacs are received from Penn State Hershey in PBS.
2. 4 by 3 mm samples with the upper right hand corner of the inside of the sac removed are cut using a fine scalpel from the sac at the following 8 regions: inlet, outlet, center front, center back, top, bottom, inlet side and outlet side and any regions with a macroscopic deposition.
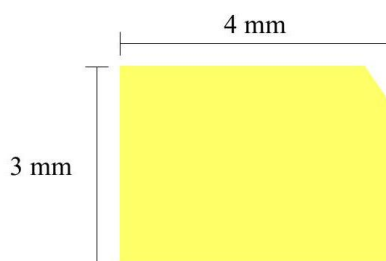
3. The samples are then placed in a 24 well tray and each sample is rinsed 5 times with 1 mL of PBS.

Confocal microscopy:

4. A primary solution of 1 mL of 6% goat serum (6 mL of normal goat serum and 94 mL of PBS), 10 μL of mix-n-stain CAPP2A (green), and 10 μL of mix-n-stain anti-fibrinogen (red) is added to each well containing a sample.
5. The samples are incubated overnight in the refrigerator.
6. Following completion of the incubation, the samples are gently rinsed 5 times with 1 mL of PBS.
7. The samples are placed on a cover slip with the inside portion of the sac facing downward.
8. To obtain images representative of the sac sample's surface 16 images are taken at 60x using the confocal microscope in numerical order based on the schematic below.
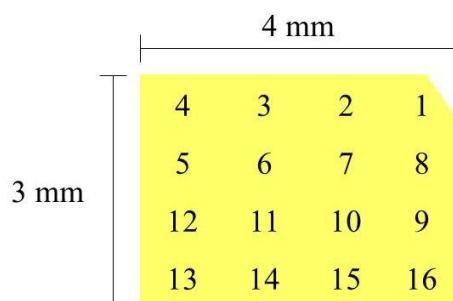
9. The samples are then returned to the 24 well tray and placed in DI water and stored in the refrigerator.

Environmental Scanning Electron Microscopy:

10. The samples are gently rinsed 3 times with DI water making sure that no large droplet of water is left remaining on the samples.
11. The samples are mounted to a SEM stub using carbon tape, which are found in the same room as the microscope.
12. To obtain images representative of the sac sample's surface 16 images in the same manner as confocal were taken at 500x using the low vacuum mode of the ESEM. A kv of 20 is used at a pressure of 30 Pa. Additional images at higher magnifications are to be taken as needed to examine specific features.
13. Following completion of the imaging, the samples are removed from the carbon tape and returned to DI water in the 24 well tray.

Pepsin Degradation:

14. The incubator is turned on and set to 37°C.
15. Pepsin is dissolved in DI water at 10 mg of pepsin for every 1 mL of DI water.
16. The pepsin and HCl solution is made by mixing 1.5 mL of the pepsin dissolved in DI water with 0.5 mL of 1 M HCl for every sample.
17. The DI water is removed from the 24 well tray and replaced with the pepsin and HCl solution.
18. The 24 well tray is placed in the incubator for 3 hours.
19. Following completion of the incubation, the samples are removed from the pepsin solution and rinsed 5 times with DI water.
20. The samples are then mounted onto a microscope slide using double sided poster tape. Attempt to dry the bottom of the samples to create better adhesion.

Optical Profilometry:

21. Before imaging the samples, rinse with DI water 3 times.
22. To obtain images representative of the sac sample's surface 16 images snaking from the upper right hand corner were taken using the 50x lens and the 0.5x zoom lens of the optical profilometer. The CSI measure mode with a z resolution of high is used. Use a scan length of 40 or 65 µm and adjust to include all data points.
23. Data is imported into MetroPro.
24. The surface roughness values of (rms, Ra, Rz, and H) are placed into an Excel spread sheet.

The above protocol will allow for analysis of the same sample with three different microscopy techniques to determine the effects of surface roughness on thrombus formation. The confocal and ESEM images for different sac regions will show whether or not platelets or fibrin is present. The surface roughness values for the same regions will allow for a comparison of the data for regions that do contain platelets or fibrin compared to regions that do not. This comparison along with a closer look at the ESEM images and surface profiles created in MetroPro should provide sufficient data to determine if surface roughness is playing a significant role in thrombus formation in the blood sacs of the Penn State PVAD.

4.7 Initial Sac Analysis

Initial sac assessment using the developed protocol was carried on sac 183, an explanted sac that had undergone previous analysis. The initial assessment was completed to confirm that all steps of the protocol could be seamlessly carried out and obtain useful data. For the sake of conserving the sac for future analysis only 8 images were obtained from a sample from region U5 of the sac taken that was half the size of the samples to be used in the protocol. The sample that was used was taken from a region near a macroscopic clot to increase the likelihood of biological deposition being present in the analysis. Figure 4-49 contains the confocal images taken from the 8 regions and Figure 4-50 contains the ESEM images.
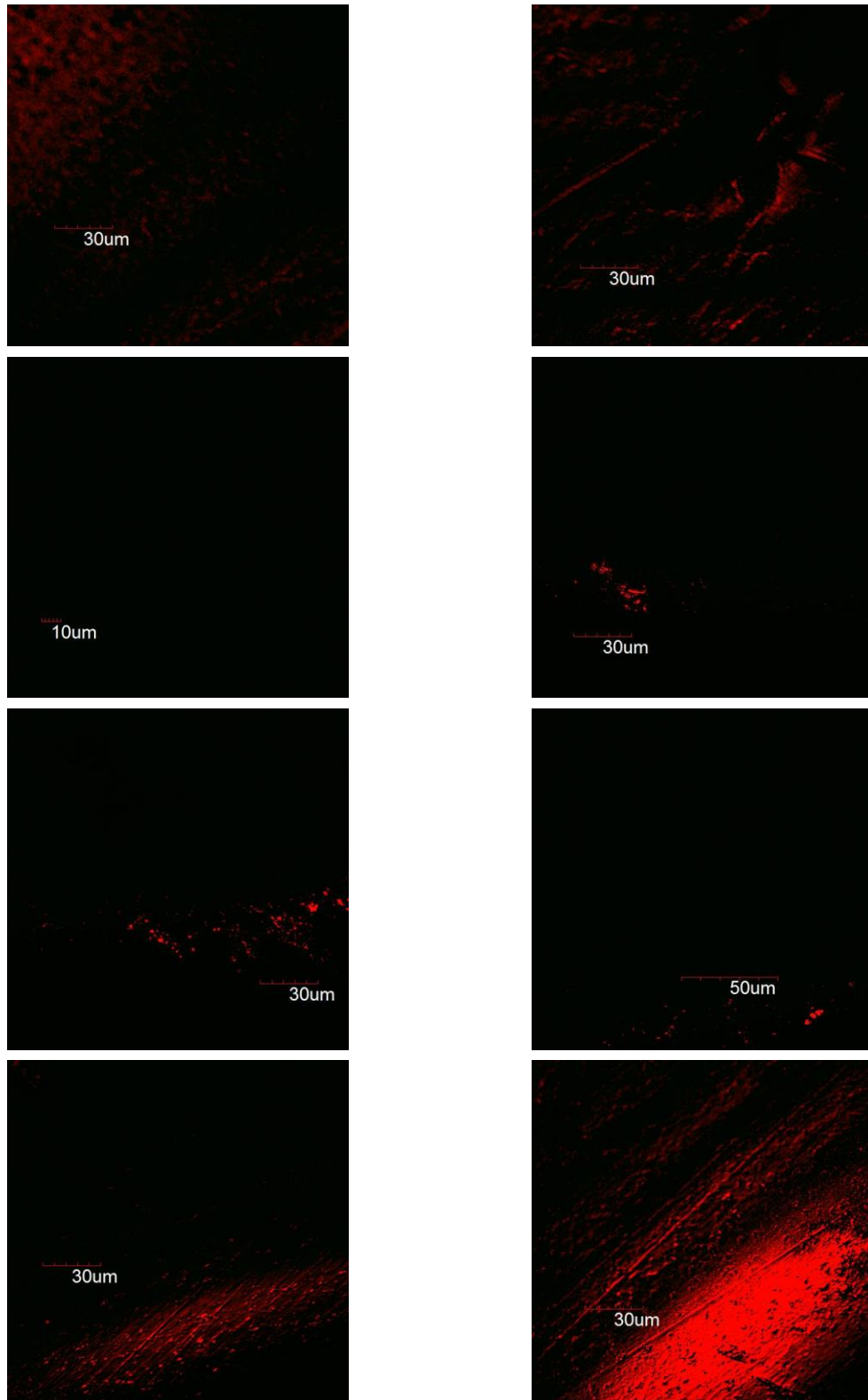
Figure 4-49. Confocal images of 8 different spots from an explanted sac. Platelets are labeled green and fibrin is labeled red.
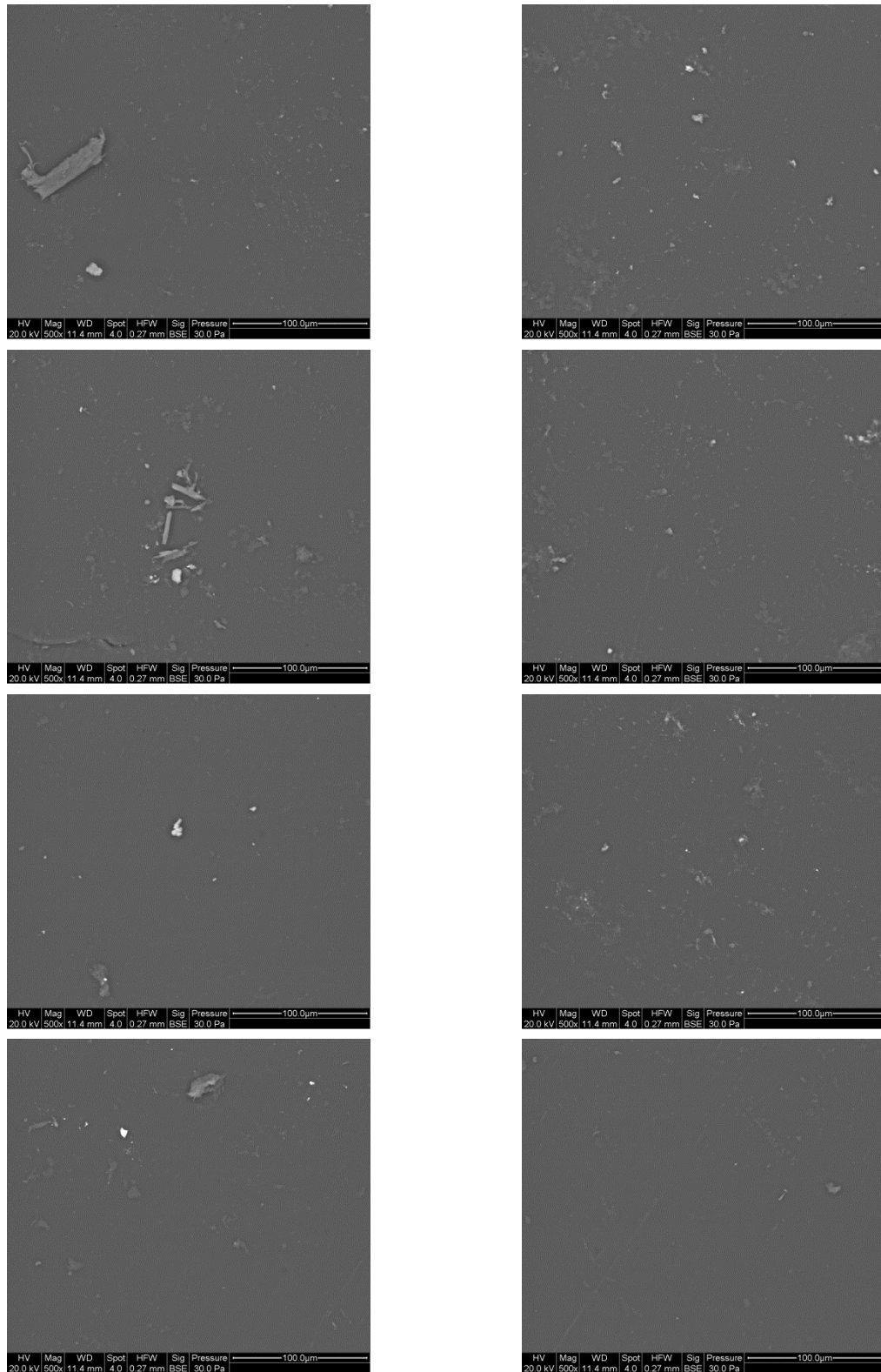
Figure 4-50. ESEM images of the same regions from the explanted sac imaged with confocal.

Comparison of the images taken with confocal and ESEM shows that there is overlap occurring between the two imaging techniques with the most evident overlap occurs in the eighth image in the bottom right hand corner because the scratches present in the surface are visible in both the confocal and ESEM image. The third ESEM image (2nd row, left hand column) has debris on the surface, which is verified by the lack of fluorescence in the corresponding confocal imaging. Despite both platelets and fibrin being fluorescently labeled, the only fluorescence in the confocal images is the red of the fibrin. In the third ESEM image of the left hand column, there is a structure that appears to be a small platelet aggregate. However, comparison to the confocal shows a similar sized structured that is fluorescing red, which could be the result of adsorbed fibrinogen on the platelet aggregate. Another possible explanation because green fluorescence was observed when testing the antibody labeling kit is that the CAPP2A expired. As a result, more explanted samples should be tested to verify that the labeling procedure is properly identifying platelets and fibrin. Based off of these images, the correlation of the images is possible using the developed technique. For best results, the surface must be thoroughly rinsed before imaging with ESEM to rinse any debris present on the surface.

Following the imaging with the ESEM, the samples were analyzed with optical profilometry, and the results are given in Table 4-3.

Table 4-3. Optical profilometry data of explanted sac.

Sample	rms (nm)	Ra (nm)	Rz (nm)	H (nm)
1	42.730	31.894	561.46	118.08
2	88.343	63.428	1517.31	252.26
3	78.851	39.828	2964.67	138.89
4	47.000	32.994	573.34	126.33
5	50.845	31.957	1474.80	117.64
6	45.892	33.732	629.09	124.94
7	48.634	28.724	1001.64	104.31
8	48.627	32.899	1071.04	121.96
Average	56.365	36.932	1224.17	138.05

Drawing any conclusions from the optical profilometry data is difficult due to the small sample size. The average value for each parameter is similar to what has been observed for the sac samples, which shows that the prior steps in the protocol are not altering the surface, so the entire protocol can be carried out on the same sample to provide correlation of the images and the surface roughness data. The need for the protocol is further shown by the optical profilometry data because the Rz value is greater than a micron, which is the threshold for surface roughness to effect thrombus formation. Analysis of the surface roughness data and correlation to the confocal and ESEM images will not be very telling with just a small sample of data. However, moving forward the data and images can be used to determine if surface roughness plays a role in the thrombosis.

Chapter 5

Conclusions

5.1 Summary of Findings

In this study, experiments were carried out to develop a protocol that allows for the correlation of the fibrin and platelet deposition on the SPEUU blood sac of an explanted Penn State pediatric ventricular device and surface roughness values obtained from optical profilometry. A requirement for the protocol had to first be established by identifying and observing surface features to show that there are variations in the sac surface. Then to develop this protocol, the individual microscopy techniques needed to be perfected for use with ovine blood and the polymer blood sac samples. The first of the three microscopy techniques used is confocal where samples are fluorescently labeled with antibodies to identify platelet and fibrin structures. To confirm these images and to view the true surface of the polymer blood sacs, environmental scanning electron microscopy is used. Finally, to determine the true surface roughness of the samples using optical profilometry, the biological depositions needed to be degraded from the surface without affecting the polymer in any way.

The surface evaluation using both a light microscope and ESEM showed that scuffs, scratches and pits are present in the blood sacs. The optical profilometry confirmed that these are indeed surface features and not features in the bulk material

showing that a protocol needed to be developed to study the effect of surface roughness on thrombus formation. Two antibodies to label platelets and only one fibrin antibody were identified; however, only one of the platelet antibodies effectively labeled the positive controls for platelets. Both the platelet and fibrin antibody are mouse derived, so an antibody labeling kit is needed to label both platelets and fibrin with different colors. ESEM had never been used with the polymer samples, but it was chosen as it allows imaging of the true surface of the samples. Imaging the controls showed that sufficient contrast can be achieved without sputter coating the samples, and despite there being apparent beam damage, there was no significant difference in the surface roughness values. Varying degrees of pepsin concentrations and exposure times were tested to ensure the surface of the polymer is not significantly altered and the optimal conditions for degrading the surface.

The observations and results from these experiments led to the development of a protocol that will allow for the same regions of the sacs to be viewed with the three different microscopy techniques. The protocol for each of the techniques was optimized for use with the polymer samples. Also an image mapping plan was developed to obtain multiple images from the samples that will allow for the correlation of the confocal and ESEM images with the optical profilometry data.

5.2 Future Studies

With the development of this protocol the sacs explanted from *in vivo* trials of the Penn State PVAD in ovine models can be analyzed to determine if the surface is playing

a role in thrombus formation. To date there are 6 sacs available for analysis with more animal trials planned for the future. The protocol will allow for the correlation of the surface roughness data with whether or not biological depositions are present to determine if the surface features present in the blood sacs play a role in thrombosis. Also, this could lead to a surface roughness parameter that is a true indicator of thrombus formation besides the four parameters that are currently being used in the analysis. In addition to correlating the surface roughness data with the confocal and ESEM images that are obtained from the developed protocol, the confocal and ESEM images can be correlated to *in vitro* fluid mechanics studies to determine the role of the fluid mechanics on thrombosis in the PVAD.

References

1. Lloyd-Jones, D. *et al.* Executive summary: Heart disease and stroke statistics-2010 update: A report from the american heart association. *Circulation* **121,** e46–e215 (2010).

2. Rossano, J. W., Kim, J. J., Decker, J. A. & Price, J. F. Increasing Prevalence and Hospital Charges in Pediatric Heart Failure Related Hospitalizations in the United States: A Population-Based Study. *Circ. (New York, N.Y.)* **122,** (2010).

3. Shreenivas, S. S., Rame, J. E. & Jessup, M. Mechanical circulatory support as a bridge to transplant or for destination therapy. *Curr. Heart Fail. Rep.* **7,** 159–66 (2010).

4. Walter, E. M. D. & Hetzer, R. Surgical treatment concepts for end-stage congenital heart diseases. **5,** 81–84 (2013).

5. Moazami, N. *et al.* Axial and centrifugal continuous-flow rotary pumps: a translation from pump mechanics to clinical practice. *J. Heart Lung Transplant.* **32,** 1–11 (2013).

6. Cassidy, J. *et al.* Changing patterns of bridging to heart transplantation in children. *J. Heart Lung Transplant.* **28,** 249–54 (2009).

7. Fraser, C. D. *et al.* Prospective trial of a pediatric ventricular assist device. *N. Engl. J. Med.* **367,** 532–41 (2012).

8. Rogers, J. G. *et al.* Continuous flow left ventricular assist device improves functional capacity and quality of life of advanced heart failure patients. *J. Am. Coll. Cardiol.* **55,** 1826–34 (2010).

9. Owens, W. R., Bryant, R., Dreyer, W. J., Price, J. F. & Morales, D. L. S. Initial clinical experience with the HeartMate II ventricular assist system in a pediatric institution. *Artif. Organs* **34,** 600–3 (2010).

10. Cabrera, A. G. *et al.* Outcomes of pediatric patients supported by the HeartMate II left ventricular assist device in the United States. *J. Heart Lung Transplant.* **32,** 1107–13 (2013).

11. Russell, H. M., Kulat, B., Zingle, N. & Backer, C. L. Successful Bridge to Transplant Using the TandemHeart(R) Left Ventricular Assist Device in a Pediatric Patient. *World J. Pediatr. Congenit. Heart Surg.* **3,** 249–50 (2012).

12. Fraser, C. D. & Jaquiss, R. D. B. The Berlin Heart EXCOR Pediatric ventricular assist device: history, North American experience, and future directions. *Ann. N. Y. Acad. Sci.* **1291,** 1–10 (2013).

13. Almond, C. S. *et al.* Berlin Heart EXCOR Pediatric Ventricular Assist Device for Bridge to Heart Transplantation in US Children. *Circulation* **127,** 1702–11 (2013).

14. Morales, D. L. S. *et al.* Bridging children of all sizes to cardiac transplantation: the initial multicenter North American experience with the Berlin Heart EXCOR ventricular assist device. *J. Heart Lung Transplant.* **30,** 1–8 (2011).

15. Rockett, S. R. *et al.* Preliminary single center North American experience with the Berlin Heart pediatric EXCOR device. *ASAIO J.* **54,** 479–82 (2008).

16. Etz, C. *et al.* Analysis of platelet function during left ventricular support with the Incor and Excor system. *Heart Surg. Forum* **7,** E423–7 (2004).

17. Stiller, B., Adachi, I. & Fraser, C. D. Pediatric ventricular assist devices. *Pediatr. Crit. Care Med.* **14,** S20–6 (2013).

18. Vogler, E. a & Siedlecki, C. a. Contact activation of blood-plasma coagulation. *Biomaterials* **30,** 1857–1869 (2009).

19. Gemmel, C., Black, J., Yeo, E. & Sefton, M. Material-induced up-regulation of leukocyte CD11b during whole blood contact: material differences and a role for complement. *J. Biomed. Mater. Res.* **32,** 29–65 (1996).

20. Colman, R. W. Mechanisms of thrombus formation and dissolution. *Cardiovasc. Pathol.* **2,** 23–31 (1993).

21. Jaquiss, R. D. B. & Lodge, A. J. Pediatric Ventricular Assist Devices: The Future (as of 2011). *World J. Pediatr. Congenit. Heart Surg.* **3,** 82–6 (2012).

22. Fan, Y. *et al.* Outcomes of ventricular assist device support in young patients with small body surface area. *Eur. J. Cardiothorac. Surg.* **39,** 699–704 (2011).

23. Young, G. New anticoagulants in children. *Hematology Am. Soc. Hematol. Educ. Program* 245–250 (2008).

24. Weiss, W. J. *et al.* Chronic in vivo testing of the Penn State infant ventricular assist device. *ASAIO J.* **58,** 65–72 (2012).

25. Weiss, W. J. Pulsatile Pediatric Ventricular Assist Devices. *ASAIO J.* **51,** 540–545 (2005).

26. Gorbet, M. B. & Sefton, M. V. Biomaterial-associated thrombosis: roles of coagulation factors, complement, platelets and leukocytes. *Biomaterials* **25,** 5681–703 (2004).

27. Hubbell, J. A. & Mcintire, L. V. Visualization and analysis of mural thrombogenesis on collagen, polyurethane, and nylon. *Biomaterials* **7,** 354–63 (1986).

28. Baldwin, J. T., Deutsch, S., Geselowitz, D. B. & Tarbell, J. M. LDA Measurements of lean Velocity and Reynolds Stress Fields Within an Artificial Heart Ventricle. *J. Biomech. Eng.* **116,** (1994).

29. Cooper, B. T., Roszelle, B. N., Long, T. C., Deutsch, S. & Manning, K. B. The 12 cc Penn State pulsatile pediatric ventricular assist device: fluid dynamics associated with valve selection. *J. Biomech. Eng.* **130,** 041019 (2008).

30. Roszelle, B. N., Deutsch, S., Weiss, W. J. & Manning, K. B. Flow visualization of a pediatric ventricular assist device during stroke volume reductions related to weaning. *Ann. Biomed. Eng.* **39,** 2046–58 (2011).

31. Yamanaka, H. Investigation of Thrombosis at the Biomaterial Surface in Left Ventricular Assist Systems. (2006).

32. Ikeda, Y. *et al.* The Role of von Willebrand Factor and Fibrinogen in Platelet Aggregation under Varying Shear Stress. **87,** 1234–1240 (1991).

33. Milner, K. R., Snyder, A. J. & Siedlecki, C. a. Sub-micron texturing for reducing platelet adhesion to polyurethane biomaterials. *J. Biomed. Mater. Res. A* **76,** 561–70 (2006).

34. Koh, L. B., Rodriguez, I. & Venkatraman, S. S. The effect of topography of polymer surfaces on platelet adhesion. *Biomaterials* **31,** 1533–45 (2010).

35. Koh, L. B., Rodriguez, I. & Zhou, J. Platelet adhesion studies on nanostructured poly(lactic-co-glycolic-acid)-carbon nanotube composite. *J. Biomed. Mater. Res. A* **86,** 394–401 (2008).

36. Linneweber, J. *et al.* The effect of surface roughness on activation of the coagulation system and platelet adhesion in rotary blood pumps. *Artif. Organs* **31,** 345–351 (2007).

37. Maruyama, O. *et al.* Hemolysis caused by surface roughness under shear flow. *J. Artif. Organs* **8,** 228–36 (2005).

38. Donald, A. M. The use of environmental scanning electron microscopy for imaging wet and insulating materials. *Nature* **2,** 511–516 (2003).

39. Danilatos, G. D. in *Adv. Electron. Electron Phys.* 110–248 (Acadmic Press, 1988).

40. Kimseng, K. & Meissel, M. *The ESEM- The Environmental Scanning Electron Microscope*. **1,** 1–12 (2001).

41. Evans Analytical Group. Optical Profilometry. (2015). at <http://www.eag.com/mc/optical-profilometry.html>

42. Zygo Corporation. Optical Profiler Basics. at <http://www.zygo.com/?/met/profilers/opticalprofilersabout.htm>

43. B.C. MacDonald & Co. Basic Components & Elements fo Surface Topography. (2004). at <http://www.bcmac.com/pdf_files/surface finish 101.pdf>

44. Zygo Corporation. MetroPro Surface Texture Parameters. (2005).

45. Grunenwald, L. E. The Effects of Hematocrit and Rotation Time on Platelet Adhesion to a Polyurethane Urea Surface. (2013).

46.	Navitsky, M. A. A COMPARISON OF THROMBUS SUSCEPTIBILITY FOR TWO PULSATILE 50 CC LEFT VENTRICULAR ASSIST DEVICES. (2012).

47.	Long, G. D. COMPUTATIONAL SIMULATIONS OF FLOW OVER THE SURFACE OF A FORMED. 1–159 (2009).

48.	Kinney, J. HISTOLOGICAL ANALYSIS OF IN VITRO THROMBUS FORMATION IN A BACKWARD FACING STEP FLOW DOMAIN USING CARSTAIRS ' STAIN. (2014).

49.	Division of Artificial Organs. *Pediatric Blood Sac Thickness*. 1 (2013).

50.	Rost, F. in *Fluoresc. Microsc.* 108–134 (Cambridge University Press, 1995).

51.	Szycher, M. & McArthrur, W. A. in *Corros. Degrad. Implant Mater.* 308–322 (American Society for Testing and Materials, 1985).

52.	Johnson, C. a, Snyder, T. a, Woolley, J. R. & Wagner, W. R. Flow cytometric assays for quantifying activated ovine platelets. *Artif. Organs* **32,** 136–45 (2008).